UNIVERSITY OF BELGRADE

FACULTY OF TECHNOLOGY AND METALLURGY

Amal Juma Habish

Influence of synthesis parameters on the properties of the composite adsorbents based on sepiolite and nano-zerovalent iron

Doctoral Dissertation

Belgrade, 2017

UNIVERZITET U BEOGRADU

TEHNOLOŠKO-METALURŠKI FAKULTET

Amal Juma Habish

Uticaj parametara sinteze na svojstva kompozitnih adsorbenata na bazisepiolita i nanočestica elementarnog gvožđa

doktorska disertacija

Beograd, 2017.

Supervisor

Dr Rada Petrović, Professor

University of Belgrade, Faculty of Technology and Metallurgy

Committee Members

Dr Đorđe Janaćković, Professor
University of Belgrade, Faculty of Technology and Metallurgy

Dr Snežana Grujić, Associate Professor
University of Belgrade, Faculty of Technology and Metallurgy

Dr Slavica Lazarević, Research Associate
University of Belgrade, Faculty of Technology and Metallurgy

Dr Ljiljana Živković, Research Professor
University of Belgrade, Vinča Institute of Nuclear Sciences

Date of Defense:

Acknowledgements

Alhamdulillah, all praises to Allah for the strengths and his blessing in completing this thesis. I would like to express my sincere gratitude to my advisor Prof. Dr. Rada Petrović for the continuous support of my PhD study and related research, for her patience, motivation, and immense knowledge. Her guidance helped me in all the time of research and writing of this thesis. I could not have imagined having a better advisor and mentor for my PhD study.

I wish to express my sincere thanks to all my Professors who taught me at this faculty.

I am also grateful to all members of the Department of Inorganic Chemical Technology.

I would like to express my thanks and gratitude to all my family, especially to my father and my mother for supporting and encouraging through all my studies. I like to convey many thanks to my sisters too.

I owe my loving thanks to my husband and my daughters and my sons, without whose love, encouragement and understanding, I would not have finished this thesis. Finally, thanks to all of my friends, and everyone for their contribution by supporting my work.

<div align="right">Amal Juma Habish</div>

List of figures

List of tables

Influence of synthesis parameters on the properties of the composite adsorbents based on sepiolite and nano-zerovalent iron

Abstract

Immobilizing nano-zerovalent iron particles (nZVI) on inert supporting materials of high surface area provides an easy operation for water contaminants removal and excellent adsorption/reduction ability of nZVI. In this dissertation, fibrous natural mineral sepiolite (SEP) with high specific surface area was used for nZVI immobilization, as well as partially acid-activated sepiolite (AAS) with even higher specific surface area. nZVI particles were loaded onto supports via Fe^{2+} reduction by sodium borohydride. Different support/nZVI ratios (10:1, 5:1, 2.5:1 and 2:1) were applied in order to obtain composites with good nZVI dispersibility and high efficiency for the removal of Cd^{2+}, CrO_4^{2-} and dye C.I. Reactive Orange 16 from water. Besides, during the synthesis, the SEP/AAS suspension was treated by ultrasound probe for different period of time (10 or 30 min) to achieve an efficient de-aggregation of the sepiolite particles. Effect of temperature and contact time on adsorption was also investigated.

Despite higher specific surface area of AAS than SEP, the dispersibility of nZVI particles was lower with AAS support, as acid activation created strong inter-fiber bonds, which could not be broken during ultrasound treatment. Prolonged ultrasound treatment improved de-aggregation of AAS, but caused shortening of the SEP fibers their re-aggregation. Good dispersibility of the spherical nZVI particles was achieved with SEP at the SEP:nZVI mass ratios $\geq$ 2.5:1 and with AAS only at the mass ratio AAS:nZVI = 10:1, for 10 min-ultrasound treatment.

The presence of Fe^0 in the composites was confirmed by X-ray diffraction (XRD) and differential-thermal/thermo-gravimetric (DTA/TGA) analyses. The results of DTA/TGA in air and nitrogen indicated that the composite with SEP contained more iron oxide formed by Fe^0 oxidation during synthesis than the composite with AAS, at the same support/nZVI ratio. Therefore, SEP used as a support provided better nZVI

dispersibility, but lower degree of oxidation during the synthesis was achieved using AAS.

High values of point of zero charge of all the composites indicate the high basicity of the surface due to the presence of basic Fe–OH groups, as proven by infrared spectroscopy (FTIR analysis). X-Ray photoelectron spectroscopy (XPS) confirmed that the surface of nZVI was composed of oxidized iron species. Metallic iron was detected after sputtering, at a depth of 40 nm beneath the original surface. The content of Fe^0 decreased after Cd^{2+} adsorption as a result of iron oxidation during adsorption process. The XPS depth profile showed that cadmium was present at the surface and in subsurface region of the composite, whereas its concentration was higher on the surface.

The adsorption capacities of the composites for Cd^{2+} ions increased as the quantity of nZVI increased, regardless of the decrease in the specific surface area. The adsorption isotherms confirmed that the presence of SEP and AAS lowered the degree of agglomeration in comparison to pure nZVI, which provided higher adsorption capacities of nZVI in the composites than of pure nZVI. The results also showed that the prevention of both aggregation and oxidation during the synthesis was necessary for obtaining SEP/AAS–nZVI composite with high adsorption capacity. However, oxidation during adsorption was proven beneficial for Cd^{2+} removal. Prolonged ultrasound treatment of the support suspension provided higher adsorption capacity for the SEP-based composite, regardless of worse textural and morphological properties while the opposite was found for AAS-based composite. According to the modeling of the adsorption data, the establishment of strong bonds between Cd^{2+} and adsorbents sites of different energy and monolayer formation were proposed. Adsorption capacity of the composites obtained at support/nZVI ratio = 2.5:1 increased with temperature increase from 25 to 40 ºC and then decreased with further temperature increase to 50 ºC.

The efficiency of CrO_4^{2-} removal from water by the investigated composites was determined by the content of hosted nZVI. The efficiency of AAS–nZVI composites were higher than of SEP-nZVI, which shows that the degree of nZVI oxidation during synthesis is the factor that determines the adsorption capacity more than nZVI particles dispersivity. Possible mechanisms of CrO_4^{2-} removal by the composites involve CrO_4^{2-} reduction to Cr^{3+}, followed by Cr^{3+} adsorption or $Cr(OH)_3$ and $Fe(OH)_3$ co-

precipitation, and electrostatic attraction between CrO_4^{2-} and protonated functional groups of the composite.

The efficiency of the composites with small content of nZVI for the removal of anionic dye C.I. Reactive Orange 16 was increased significantly when H_2O_2 was used to form Fenton reagens. On the other hand, the efficiency of composites with higher content of nZVI was much higher without H_2O_2, when reductive mechanism was dominant, especially at higher temperatures.

The results showed that the *in situ* formed porous oxide layer on the nZVI surface was beneficial for the removal of Cd^{2+}, while the detachment of the oxide layer from the nZVI particles was desirable for the reductive mechanism of the pollutant removal.

Key words: Nano-zerovalent iron (nZVI), Sepiolite, Acid-activated sepiolite, Composite, Dispersibility, Cd^{2+}, CrO_4^{2-}, C.I. Reactive Orange 16, Adsorption, Efficiency of water pollutants removal, Influence of temperature

Scientific field: Technical engineering

Major in: Chemical engineering

UDC number: 544.723.21:549.623.8:546.72

Uticaj parametara sinteze na svojstva kompozitnih adsorbenata na bazi sepiolita i nanočestica elementarnog gvožđa

Izvod

Imobilizacijom nanočestica elementarnog gvožđa (nZVI) na inertne materijale velike specifične površine dobijaju se efikasni kompozitni materijali za adsorpciono/redukciono uklanjanje zagađujućih materija iz vode. U ovoj disertaciji, za imobilizaciju nZVI korišćen je sepiolit (SEP), prirodni vlaknasti mineral velike specifične površine, kao i kiselinski aktivirani sepiolit, veće specifične površine u odnosu na SEP. Nanočestice elementarnog gvožđa su deponovane na nosače redukcijom Fe^{2+} natrijum-borhidridom, pri čemu je korišćen različit maseni odnos nosač/nZVI (10:1, 5:1, 2.5:1 i 2:1) u cilju dobijanja kompozita sa dobro dispergovanim česticama nZVI i velikom efikasnošću uklanjanja Cd^{2+}, CrO_4^{2-} i anjonske boje C.I. Reactive Orange 16 iz vode. Pored toga, tokom sinteze, suspenzija SEP/AAS je tretirana ultrazvučnom sondom u toku 10 ili 30 minuta da bi se ispitao uticaj dužine trajanja ultrazvučnog tretmana na efikasnost deagregacije vlakana sepiolita. Takođe, ispitivan je i uticaj temperature i vremena kontakta na proces adsorpcije.

Uprkos većoj specifičnoj površini AAS, disperznost nZVI čestica je bila manja kada je kao nosač korišćen AAS, zbog jačih veza između vlakana AAS, nastalih kao posledica kiselinske aktivacije, koje se nisu mogle raskinuti ultrazvučnim tretmanom tokom sinteze kompozita. Produženi tretman ultrazvučnom sondom je obezbedio bolju deaglomeraciju AAS, ali je doveo do skraćivanja vlakana SEP i njihove re-agregacije. Dobra disperznost sfernih čestica nZVI je postignuta pri masenim odnosima SEP:nZVI $\geq$ 2.5:1, a u slučaju AAS do aglomeracije nZVI čestica nije došlo jedino pri odnosu AAS:nZVI = 10:1, pri 10-minutnom tretmanu ultrazvučnom sondom.

Prisustvo Fe^0 u kompozitima je potvrđeno rendgenskom difrakcionom analizom (XRD) i diferencijalno-termijskom i termo-gravimetrijskom (DTA/TGA) analizom. Rezultati DTA/TGA u vazduhu i azotu su ukazali da kompoziti na bazi SEP sadrže više gvožđe-oksihidroksida, formiranog oksidacijom Fe^0 tokom sinteze, nego kompoziti na bazi AAS, pri istom odnosu nosač/nZVI. Prema tome, bolja disperznost nZVI je

postignuta korišćenjem SEP kao nosača, ali je manji stepen oksidacije tokom sinteze postignut korišćenjem AAS.

Visoke vrednosti tačke nultog naelektrisanja svih kompozita ukazuju na veliku baznost površine usled prisustva baznih Fe–OH grupa, što je potvrđeno FTIR spektroskopijom. Fotoelektronska spektroskopija X-zraka (XPS) je takođe potvrdila da se na površini nZVI nalaze oksidne vrste gvožđa. Metalno gvožđe je detektovano nakon raspršivanja (spaterovanja), na dubini od 40 nm ispod površine. Sadržaj Fe^0 je smanjen nakon adsorpcije Cd^{2+} usled oksidacije koja se odigrava tokom procesa adsorpcije. Dubinski XPS profil je pokazao da se Cd^{2+} nalazi i kako na površini, tako i u oblasti ispod površine, pri čemu je koncentracija na površini veća.

Adsorpcioni kapacitet kompozita za Cd^{2+} jone raste sa povećanjem sadržaja nZVI, bez obzira na smanjenje specifične površine. Rezltati određivanja adsorpcionih izotermi su potvrdili da prisustvo SEP i AAS smanjuje aglomeraciju čestica nZVI, što obezbeđuje veći adsorpcioni kapacitet imobilisanih u poređenju sa neimobilisanim česticama nZVI. Rezultati su pokazali da je potrebno sprečiti kako aglomeraciju, tako i oksidaciju nZVI tokom sinteze da bi se dobili kompoziti SEP/AAS–nZVI velikog adsorpcionog kapaciteta za Cd^{2+} jone, ali je oksidacija tokom procesa adsorpcije poželjna. Produženi tretman suspenzije nosača ultrazvučnom sondom je obezbedio veći adsorpcioni kapacitet kompozita na bazi SEP, bez obzira na lošije teksturalne karakteristike, zahvaljujući manjem stepenu oksidacije nZVI. U slučaju kompozita na bazi AAS, adsorpcioni kapacitet je smanjen. Na osnovu rezultata modelovanja adsorpcije, pretpostavljeno je uspostavljanje jakih veza između Cd^{2+} i površinskih mesta različite energije, kao i formiranje monosloja. Ispitivanje uticaja temperature na adsorpcioni kapaciteti kompozita dobijenih pri odnosu nosač/nZVI = 2.5:1 je pokazalo da se kapacitet prvo povećava pri povišenju temperature od 25 do 40 ºC, a zatim smanjuje sa daljim povišenjem temperature do 50 ºC.

Efikasnost kompozita u procesu uklanjanja CrO_4^{2-} iz vode raste sa povećanjem sadržaja nZVI. Efikasnost kompozita AAS–nZVI je veća u odnosu na SEP-nZVI, što je pokazalo da stepen oksidacije tokom sinteze u većoj meri utiče na adsorpcioni kapacitet od stepena aglomerisanosti nZVI čestica. Mogući mehanizmi uklanjanja CrO_4^{2-} jona korišćenjem ispitivanih kompozita je redukcija CrO_4^{2-} do Cr^{3+} uz naknadnu adsorpciju

Cr^{3+} jona ili koprecipitacija Cr(OH)$_3$ i Fe(OH)$_3$, kao i elektrostatičko privlačenje između CrO$_4^{2-}$ i protonovanih funkcionalnih grupa kompozita.

Efikasnost kompozita sa malim sadržajem nZVI za uklanjanje anjonske boje C.I. Reactive Orange 16 se znatno povećava dodatkom H$_2$O$_2$, čime se formira Fentonov reagens. S druge strane, efikasnost kompozita sa većim sadržajem nZVI je značajno veća bez dodatka H$_2$O$_2$, kada je redukcioni mehanizam dominantan, posebno na visokim temperaturama.

Rezultati su pokazali da je *in situ* formiranje poroznog oksidnog sloja na površini nZVI čestica poželjno u slučaju uklanjanja Cd^{2+} jona, dok je za redukcioni mehanizam poželjno da se taj oksidni sloj ukloni sa površine nZVI čestica.

Ključne reči: Nanočestice elementarnog gvožđa (nZVI), sepiolit, kiselinski aktiviran sepiolit, kompozit, disperznost, Cd^{2+}, CrO$_4^{2-}$, C.I. Reactive Orange 16, adsorpcija, efikasnost uklanjanja zagađujućih supstanci iz vode, uticaj temperature

Naučna oblast: Tehnološko inženjerstvo
Uža naučna oblast: Hemijsko inženjerstvo
UDK broj: 544.723.21:549.623.8:546.72

Content

1. Introduction

Nanoscale zerovalent iron (nZVI) has been extensively applied for removal of a variety of pollutants from wastewater because of small particle size, large surface area, high *in situ* reactivity and magnetic properties that facilitate its rapid separation from water via a magnetic field. The mechanism of contaminants removal from water by nZVI is rather complex since oxidation/reduction, surface complexation, surface precipitation, and co-precipitation may be involved. However, the removal efficiency of nZVI particles is decreased due to aggregation and oxidation in ambient conditions, causing the specific surface area reduction and producing a less negative oxidation–reduction potential. To resolve these issues, various stabilization methods have already been developed to facilitate the use of nZVI in a wide range of environmental remediation scenarios.

Recently, research interest has increased in terms of the use of porous materials including carbon materials, resins, and different natural minerals and materials for the support of nZVI particles to enhance their dispersibility and stability. Natural minerals as abundant resources are suitable supporting materials because of the cheapness, availability, environmental stability, and high surface area. Various natural minerals, including montmorillonite, bentonite, kaolinite, zeolite, palygorskite and sepiolite, have been used for the preparation of composites with nZVI for the removal of different heavy metals and organic compounds from water.

Sepiolite, a hydrated magnesium silicate clay mineral, $Mg_8Si_{12}O_{30}(OH)_4(OH_2)_4 \cdot 8H_2O$, is a promising dispersing agent for nZVI owing to its high specific surface area and fibrous morphology. It was already shown that nZVI was more effective in Cr(VI) removal from aqueous solutions when sepiolite was introduced as a support material, owing to improvement of the colloidal stability of nZVI particles and to providing high surface area to interact with Cr(VI). Moreover, nZVI was stabilized by using an acid activated sepiolite and the obtained composite was shown to be more efficient in the removal of Cr(VI) and Pb^{2+} ions from water than the pure nZVI. However, there has been no systematic study of the influence of acid-activation of the

sepiolite or some other synthesis parameters on the properties and the removal efficiency of the sepioite/nZVI composites.

It is known that an acid activation increases the specific surface area of sepiolite due to to removal of mineral impurities and structural Mg^{2+} ions. Variable amounts of structural Mg^{2+} ions can be removed, depending on the intensity of the acid treatment. If the treatment is aggressive enough, the octahedral Mg^{2+} cations are completely dissolved, while the tetrahedral sheets form a free amorphous silica gel, insoluble in the acid solution. However, by the partial acid treatment, the crystal lattice of sepiolite is not entirely disrupted.

In this research, both natural and partially acid-activated sepiolites were used as supports for nZVI in order to investigate whether nZVI dispersibility on sepiolite could be improved by its acid activation. The composites were prepared by Fe^{2+} reduction in the presence of the support, at different support/nZVI ratios, in order to achieve the best nZVI dispersibility and the highest removal efficiency of the composites. In addition, duration of the ultrasonic treatment of the sepiolite suspension was also varied aimed at providing an efficient de-aggregation of the sepiolite fibers.

The scientific goals of the research in this dissertation were:
• Synthesis of the composites sepiolite/nZVI with large removal efficiency for cationic and anionic water pollutants
• Investigation of the influence of acid activation of sepiolite on the nZVI dispersibility in the composites and the removal efficiency
• Investigation of the influence of the ratio nZVI:sepiolite/acid-activated sepiolite on the nZVI dispersibility and the properties of the composites
• Study of the removal of Cd^{2+} and CrO_4^{2-} ions from water by the composites, at different temperatures and contact times
• Determination of the dominant mechanism of ions removal from water;
• Study the processes of reductive degradation of dye in the presence of investigated composites and oxidative degradation in the presence of composites and hydrogen peroxide.

THEORETICAL PART

2. Adsorption as a process for the removal of water polutants

Adsorption is a process in which a gas, liquid or solid adheres to the surface of a solid or, less frequently, a liquid, but does not penetrate it. The process of adsorption arises due to presence of unbalanced or residual forces at the surface of solid or liquid phase. These unbalanced residual forces have tendency to attract and retain the species which are in contact with the surface [1].

Adsorption process involves two substances. One is the substance on the surface of which adsorption takes place and it is called an adsorbent. The second is the adsorbate, the substance that is being adsorbed on the surface of adsorbent [2].

Adsorption is different from absorption. In absorption, the molecules of one substance are removed by dissolution in another (typically a liquid). A more general term is sorption, which covers absorption, adsorption, and ion exchange.

2.1. Adsorption on a solid surface

Although adsorption can occur on liquid–liquid interfaces, adsorption is commonly known to occur on solid surfaces. Adsorption on solid surfaces is widely applied in separation, clarification and purification of matter [3]. In water treatment, adsorption has been proved as an efficient process for the removal of a multiplicity of solutes. Solid surfaces are characterized by active, energy-rich sites that are able to interact with solutes in the adjacent aqueous phase due to their specific electronic and spatial properties. Typically, the active sites have different energies, or – in other words – the surface is energetically heterogeneous [4].

Adsorption process is spontaneous and therefore the free energy of adsorption is always negative. In addition, during adsorption, randomness of the adsorbate species decreases and entropy change is negative [2]. As a result, changes in enthalpy of adsorption, which is determined by these parameters, must also be negative. Therefore, adsorption is an exothermic process.

The most important properties of a solid adsorbent are chemical composition, structure, specific surface area and porosity. According to the chemical nature,

adsorbents can be organic or inorganic, natural or synthetic. The structure of adsorbent can be crystalline, amorphous or mixed. Since adsorption is a surface process, the surface area is a key quality parameter of adsorbents. Engineered adsorbents are typically highly porous materials with surface area in the range between 10^2 and 10^3 m^2/g. Their porosity allows realizing such large surfaces as internal surfaces constituted by the pore walls [4]. The most commonly used adsorbents are carbon materials (activated carbon), silicate and alumino silicate minerals, natural or synthetic organic polymers, as well as hardly soluble sulfates, phosphates and carbonates.

2.2. Mechanisms of adsorption

Adsorption process can be classified as either physical adsorption (physisorption) or chemical adsorption (chemisorption) [2], depending on the nature of forces between adsorbate species and adsorbent.

In physical adsorption, the forces of attraction between adsorbate and adsorbent are weak Van der Waals forces and hydrogen bonds. The heat of adsorption is low *i.e.* about 20 – 40 kJ/mol. The activation energy for physisorption is also very low and hence it is practically a reversible process. Physical adsorption is not specific with respect to adsorbent and the individuality of adsorbate and adsorbent is preserved. The adsorption occurs quickly and may be of monolayer or multilayer character [1, 2]. This type of adsorption decreases with increase of temperature.

In chemical adsorption, there is a transfer or sharing of electrons between adsorbate and adsorbent, which tends to form chemical bonds. Due to the strong bonds, chemical adsorption is difficult to reverse. Enthalpy change of chemical adsorption is between 200 and 400 kJ/mol. The activation energy for chemisorption is high and it occurs slowly. Hence, it is also called activated adsorption. It is highly selective and occurs only between certain adsorbate and adsorbent species and only if the chemically active surface is cleaned of previously adsorbed molecules [1]. Chemisorption proceeds as long as the adsorbate can make direct contact with the surface; it is therefore a monolayer process [5].

Adsorption from solutions differs significantly from adsorption from the gaseous phase. For a dilute solution, adsorption of one type of adsorbate species involves replacement of the other from the surface. Thus, adsorption from solution is essentially an exchange process, and hence the adsorbate species adsorb not only because they are attracted by solids but also because the solution may reject them. A typical illustration is that the attachment of hydrophobic molecules on hydrophobic adsorbents from aqueous solutions is mainly driven by their dislike of water and not by their attraction to the surface. In addition, multilayer adsorption from solution is less common than from the gas phase, because of the stronger screening interaction forces in condensed fluids [6].

In the case of adsorption from solutions, there is a wide range of energies contributing to the free energy of adsorption, which can be grouped into non-electrostatic and electrostatic. Although at atomic level all ionic and molecular interactions can be interpreted as "electric", this term is restricted to coulombic interactions and all other interactions are termed non-electrostatic, whatever their origin. Electrostatic interactions appear when the adsorptive is an electrolyte that is dissociated or protonated in aqueous solutions under the experimental conditions. These interactions, that can be either attractive or repulsive, strongly depend on the charge densities for both the adsorbent surface and the adsorptive species and on the ionic strength of the solution. The non-electrostatic interactions are always attractive, and can include van der Waals forces, hydrophobic interactions and hydrogen bonding [6].

In order to describe the adsorption in the electrolyte solution, the formation of specific and non-specific complexes (inner-sphere and outer-sphere complexes, respectively) between the surface functional groups and the ions, was proposed [7]. Outer sphere complexes occur if at least one solvent (water) molecule is interposed between the surface functional group and the bound ion. They involve electrostatic bonding. Inner-sphere complexes are more stable and occur when no molecule of the aqueous solution is interposed and the adsorbing ion forms a direct coordinate covalent bond with surface functional groups on the variable charge surface. Inner sphere complexes can either form with a 1:1 stoichiometry, forming monodentate complexes, or with a 1:2 stoichiometry, forming bidentate complexes (Fig. 2.1) [8].
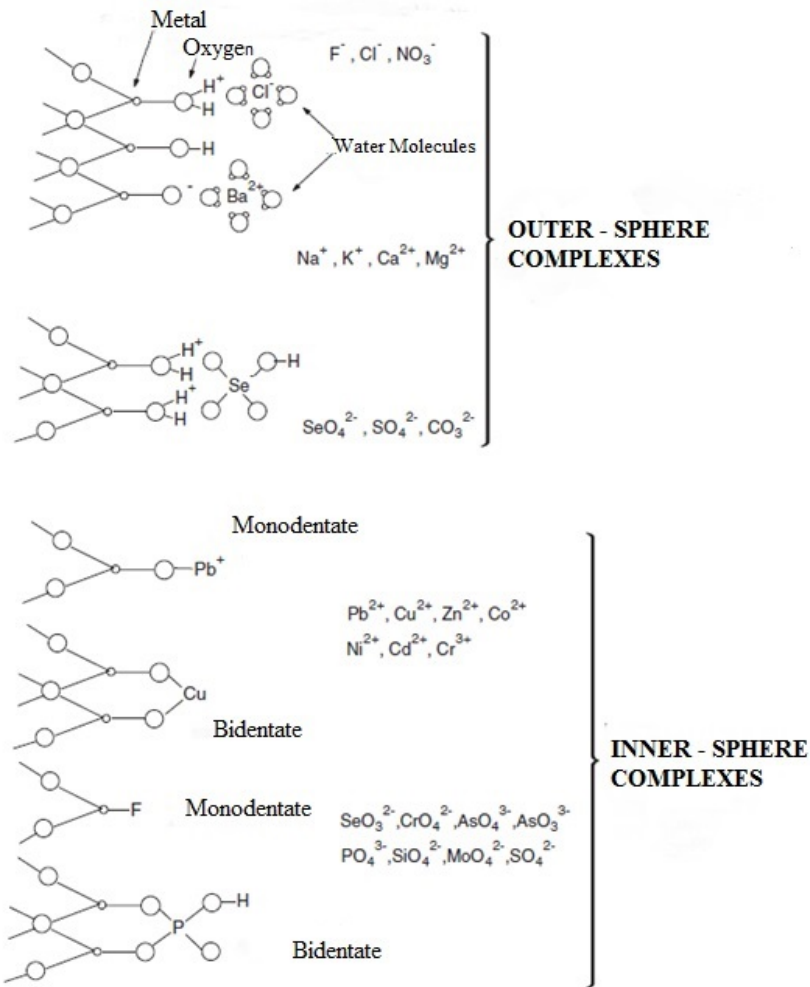
Fig. 2.1. Schematic representation of the different types of adsorption complexes that can occur on solid surfaces [8].

The distribution of ions in the proximity of the charged surface is described as an "electrical double layer". The adsorption process can be visualized in three planes: charged surface of the adsorbent, specific adsorbing plane, and outside plane of balancing indifferent ions in the water layers near the surface. Specifically, adsorbed (inner sphere) ions plus potential determining ions confer charge on the surface. Electroneutrality at the charged surface is maintained by indifferent counter ions with a charge equal in magnitude and opposite in sign to the surface charge [8].

2.3. Factors affecting adsorption on a solid surface

Adsorption on a solid is influenced by a number of factors, which can be classified in three groups: characteristics of the adsorbent, characteristics of the adsorbate and the parameters of the adsorption process.

2.3.1. Influence of adsorbent characteristics

Many characteristics of an adsorbent influence the adsorption: particle size and shape, particle-size distribution, crystallinity, chemical composition, surface area, porosity, and numbers and types of surface functional groups.

Adsorption is a surface phenomenon and as such, the extent of adsorption is proportional to specific surface area of the adsorbent, which increases with the porosity increasing and particle size and pore size decreasing. However, the pores should be large enough to allow the adsorbate to enter them. According to dimensions, pores are divided into [9, 10]:

- Macropores, dimensions > 50 nm, which are transport channels, and adsorption in them is negligible

- Mesopores, dimensions from 2 to 50 nm

- Micropores, dimensions <2 nm; the main factor affecting the adsorption at micropores is the geometric volume rather than surface of micropores.

The particle size has no influence on the adsorption capacity, but the rate of adsorption is faster if the particle diameter is smaller. Smaller particle sizes reduce internal diffusional and mass transfer limitation to the penetration of the adsorbate inside the adsorbent.

Different solids would adsorb different amounts of the same adsorbate even under similar conditions.The physiochemical nature of adsorbent and the nature of the surface functional groups have profound effects on both adsorption rate and capacity.

2.3.2. The influence of the adsorbate characteristics

Among the characteristics of the adsorbate that mainly influence the adsorption process are its size, solubility and acidity constant, pKa. The size of adsorbate species controls the accessibility to the pores of the adsorbent, while the solubility determines the hydrophobic interactions. In general, as solubility increases, the extent of adsorption decreases. A polar solute is strongly adsorbed from a non-polar solvent by a polar adsorbent, but it prefers a polar solvent to a non-polar adsorbent. The acidity constant controls the dissociation of the adsorbate and this parameter is closely related to the solution pH [1, 2].

In the case of metal ions, the relative affinities for adsorption sites depend on a wide range of metal properties. Important properties include polarizability, ionization potential, electronegativity, electron affinity, enthalpy and entropy of hydration, hydrolysis constants, andionic radius (or radius of the hydrated ion) [8]. Generally, increases in ion charge and metal electronegativity and decreases in hydrated cation radii and hydration energy lead to a growing tendency of the ion for the adsorption [11].

2.3.3. The influence of the adsorption parameters

pH value of the solution is known to play an important role in the binding of adsorbate to the surface functional groups of adsorbents. The solution pH affects the surface charge of the adsorbent, and hence the interactions between adsorbate and adsorbent surfaces [2]. Important characteristic of the solid adsorbent, which is particularly expressed in the adsorption from electrolyte solution, is the point of zero charge, pH_{pzc}. The solution pH value at which the surface charge density of the solid phase, σ_o, is equal to zero is called the point of zero charge (pH_{pzc}) [12]. If the pH value of the electrolyte solution is equal to pH_{pzc}, the number of positively charged centers is equal to the number of negatively charged centers at the surface. The most common method used to determine the point of zero charge is potentiometric titration and balancing the sample with electrolyte solutions of different concentrations [12, 13].

The point of zero charge is frequently taken to be equal to isoelectric point (pH_{pzc}), which is the pH value at which the electrokinetic potential is equal to zero. The point of zero charge, however, will be equal to the isoelectric point only if there is no specific adsorption of ions at the surface of the solid phase. The specific adsorption shifts the point of zero charge to lower pH values in the case of adsorption of cations, and to higher pH values in the case of specific adsorption of anions [12]. Specific adsorption of cations lowers the number of sites available for the adsorption of H^+ ions; hence, a larger number of H^+ ions remain in the solution, which leads to lower pH_{pzc} value [11, 12]. If the pH of the electrolyte solution is below the pH_{pzc}, the surface of solid phase is positively charged due to the sorption of H^+ ions from the solution. If the solution pH value is above the pH_{pzc}, the surface is negatively charged due to dissociation of surface hydroxyl groups or adsorption of OH^- ions from the solution [11, 13]. In either case, created charge is compensated by the counter-ions in the electric double layer.

Besides the influence on adsorbent charge, solution pH value affects the solution chemistry of adsorbate. The degree of ionization of a species is affected by the pH (e.g., a weak acid or a weak basis).This, in turn, affects adsorption. In the case of metal ions, hydrolysis, complexation by organic and/or inorganic ligands, redox reactions, precipitation and availability of heavy metals are all influenced by pH. The different metal species dominating in the solution at various pHs differ in their charge and ability to adsorb on the adsorbent.

The solvent molecules compete with the adsorbate species in adsorption process for limited number of sites; therefore reduce the extent of adsorption of the adsorbate. This competition depends on the type and strength of adsorbate-solid surface binding, solid-solvent attraction, and adsorbate-solvent binding [2].

Temperature is an important parameter influencing the adsorption process because of the exothermic nature of the process. Thus, the extent of adsorption generally increases with decreasing temperature. Physical adsorption always occurs more readily at lower temperatures and decreases with increase in temperature (Le-Chatelier's principle). Even though chemical adsorption is an exothermic process, it occurs slowly at lower temperature due to high kinetic energy barrier. Hence, like most

chemical changes, the extent of chemisorption increases with increase in temperature up to certain limit and then after that it starts decreasing.

The influence of temperature on the adsorption of metal ions is different for cations and anions. Usually, cations adsorption increases with the temperature, while the adsorption of anions decreases. The increasing of cation adsorption with temperature is explained by the fact that ions are well hydrated and have to be denuded of their hydration sheath to some extent in order to be adsorbed [14]. With increasing temperature, more hydrate water could be shedded and ion adsorption increased. In addition, the temperature also affects the solubility of the components in solution and thus influences and the adsorption capacity: If the solubility increases with increasing temperature, the degree of adsorption decreases and vice versa.

The contact or residence time: Sufficient contact time is required to reach adsorption equilibrium and to maximize adsorption efficiency.

2.4. Adsorption isotherms

In adsorption, dynamic phase equilibrium is established for the distribution of adsorbate between the fluid (gas, vapour or liquid) and the solid surface. The equilibrium is usually expressed in terms of the adsorbate loading on the adsorbent, q_e, and the concentration of adsorbate in the fluid, c_e.

Unlike vapour-liquid and liquid-liquid equilibria, where theory is often applied to estimate phase distribution, no acceptable theory has been developed to estimate fluid-solid adsorption equilibria. Thus, it is necessary to obtain experimental equilibrium data for a particular adsorbate and the solid adsorbent of interest. If the data are taken over a range of concentrations at a constant temperature, a plotof adsorbate loading on the adsorbent versus concentration in the fluid can be made. Such a plot is called the adsorption isotherm:

$$q_e = f(c_e) \tag{2.1}$$

A variety of different isotherm equations have been proposed for predicting the equilibrium distribution, some of which have a theoretical foundation and some being of a more empirical nature. Many of these equations are valid over small ranges of

adsorbate concentrations, but do not fit experimental data when tested over the wide range of the concentrations.Most commonly observed isotherm models are Langmuir and Freundlich models, as well as the combination of these two models, so called Sips model [15].

2.4.1. Langmuir adsorption isotherm

Langmuir adsorption isotherm is based on the following assumptions [16]:

• Fixed number of adsorption sites is available on the surface of adsorbent.
• Each site can hold maximum one adsorbate species and a constant amount of heat energy is released during this process.
• Dynamic equilibrium exists between adsorbed and the free species.
• Adsorption is monolayer process.
• Adsorbed spacies do not move on the surface of adsorbent (although, they can be lost back to the solution).
• Enthalpy of adsorption is the same for all species independently of how many of them have been adsorbed.

The Langmuir isotherm model can be represented by the equation [16]:

$$q_e = \frac{q_m K_L c_e}{1 + k_L c_e} \tag{2.2}$$

where: c_e is the equilibrium concentration of adsorbate in the fluid, q_e is the maximum adsorption capacity, and K_L is the equilibrium constant related to the energy or net enthalpy of adsorption.

The Langmuir isotherm can be rearranged to give:

$$\frac{c_e}{q_e} = \frac{1}{K_L q_m} + \frac{c_e}{q_m} \tag{2.3}$$

A plot of $\frac{c_e}{q_e}$ versus c_e should give a straight line with intercept $\frac{1}{K_L q_m}$ and slope $\frac{1}{q_m}$.

The characteristics of the Langmuir isotherm can be used to predict the affinity between the adsorbate and adsorbent using the separation factor or dimensionless equilibrium parameter, R_L expressed as [17]:

$$R_L = \frac{1}{1 + K_L c_o} \qquad (2.4)$$

where: c_o is the initial concentration of adsorbate, R_L is a dimensionless separation factor which indicates the type of isotherm to be either unfavorable ($R_L > 1$), linear ($R_L = 1$), favorable ($0 < R_L < 1$), or irreversible ($R_L = 0$).

2.4.2. Freundlich adsorption isotherm

The Freundlich isotherm is empirical equation, which can be applied to adsorption on heterogeneous surfaces as well as multilayer adsorption [18]:

$$q_e = K_f c_e^{\frac{1}{n}} \qquad (2.5)$$

where: K_f and $1/n$ are Freundich constants (indicators of adsorption capacity and intensity, respectively). The value of $1/n > 1$ indicates a "normal" Langmuir isotherm (concurrent adsorption), while $1/n < 1$ is indication of cooperative adsorption. For $n = 1$, isotherm is linear, which indicates that adsorbed species do not influence further adsorption.

The Freundlich isotherm can be rearranged to give:

$$\log q_e = \log K_f + \frac{1}{n} \log c_e \qquad (2.6)$$

Accordingly, the plot of $\log q_e$ versus $\log c_e$ gives straight line with a slope $1/n$ and an intercept $\log K_f$.

2.4.3. Sips adsorption isotherm

Sips isotherm [19] is a combined form of Langmuir and Freundlich expressions, deduced for predicting the heterogeneous adsorption systems [20] and circumventing the limitation of the rising adsorbate concentration associated with Freundlich isotherm model. At low concentrations, when the adsorbate content is muchlower than the adsorbent capacity, the Sips model reduces to the Freundlich isotherm, while at higher concentrations, when the adsorbate content is higher than the adsorbent capacity, it predicts a monolayer adsorption capacity characteristic of the Langmuir isotherm [21]. The Sips model takes the following form:

$$q_e = \frac{q_m K_a (c_e)^{n_s}}{1 + K_a (c_e)^{n_s}} \tag{2.7}$$

where: q_m is the theoretical maximum adsorption capacity, K_a and n_s are the Sips parameters. It is convenient to remark that n_s was considered as an empirical adjustable parameter (i.e., no restrictions were imposed for its value during data fitting) given that this isotherm is empirical and n_s has no clearly defined physical meaning [22]

2.5. Adsorption kinetics

When adsorption is concerned, thermodynamic and kinetic aspects should be involved to know more details about its performance and mechanisms. Except for adsorption capacity, kinetic performance of a given adsorbent is also of great significance for the application. From the kinetic analysis, the solute uptake rate, which determines the residence time required for completion of an adsorption process, may be established. In addition, one can know the scale of an adsorption apparatus based on the kinetics information. Adsorption kinetics is the base for determination of the performance of fixed-bed or any other flow-through systems [23].

Several mathematical models have been proposed to analyze the adsorption data, which can be generally classified as adsorption reaction models and adsorption

diffusion models. Both types of models are applied to describe the kinetics of adsorption; however, they are quite different in nature.

Adsorption diffusion models are always constructed based on three consecutive steps:

- Diffusion across the liquid film surrounding the adsorbent particles, *i.e.*, external diffusion or film diffusion

- Diffusion in the liquid contained in the pores and or along the pore walls, which is so-called internal diffusion or intra-particle diffusion

- Adsorption and desorption between adsorbate and active sites, *i.e.*, mass action

Adsorption reaction models originating from chemical reaction kinetics are based on the whole process of adsorption without considering the steps mentioned above [23, 24].

At present, both adsorption reaction models (mainly pseudo-first order and pseudo-second ordermodels) and adsorption diffusion models (mainly intraparticle diffusion model) are widely employed for fitting kinetic data.

2.5.1. Pseudo-first order kinetic model

The pseudo-first order equation [24, 25] is generally expressed as follows:

$$\frac{dq_t}{dt} = k_1(q_e - q_t) \tag{2.8}$$

where: q_e and q_t are the adsorption capacities at equilibrium and at time t, respectively, and k_1 is the pseudo-first order constant of adsorption.

Integrating Eq. (2.8) with the boundary conditions of $q_t = 0$ at $t = 0$ and $q_t = q_t$ at $t = t$, yields:

$$\log(q_e - q_t) = \log q_e - \frac{k_1}{2.303}t \tag{2.9}$$

The plot of log $(q_e$-$q_t)$ *vs.* t should give a linear relationship from which k_1 and q_e can be determined from the slope and intercept of the plot, respectively.

2.5.2. Pseudo-second order kinetic model

The pseudo-second order adsorption kinetic equation [24, 25] is expressed as:

$$\frac{dq_t}{dt} = k_2(q_e - q_t)^2 \tag{2.10}$$

where: k_2 is the pseudo-second order constant of adsorption. For the boundary conditions: $t = 0$ to $t = t$ and $q_t = 0$ to $q_t = q_t$, the integrated form of Eq. (2.10) becomes:

$$\frac{1}{(q_e - q_t)} = \frac{1}{q_e} + k_2 t \tag{2.11}$$

Eq. (2.11) can be rearranged to obtain linear form:

$$\frac{t}{q_t} = \frac{1}{k_2 q_e^2} + \frac{1}{q_e} t \tag{2.12}$$

If the initial adsorption rate, h, is:

$$h = k_2 q_e^2 \tag{2.13}$$

then Eq. (2.12) and (2.13) become:

$$\frac{t}{q_t} = \frac{1}{h} + \frac{1}{q_e} t \tag{2.14}$$

According to Eq. (2.12), the plot of (t/q_t) vs. t should give a linear relationship from which q_e and k_2 can be determined from the slope and intercept of the plot, respectively.

2.5.3. Inraparticle diffusion model

The intraparticle diffusion model or Weber-Morris model is of major interest because the internal diffusion determines the adsorption rate in most of the liquid systems. Weber and Morris found that in many cases, solute uptake varies almost proportionally with $t^{1/2}$ rather than with the contact time t. The model [24, 25] is expressed as:

$$q_t = k_{id} t^{1/2} + c \tag{2.15}$$

15

where: k_{id} is the intraparticle diffusion rate constant and c is a constant related to the mass transfer (diffusion) across the boundary layer.

According to Eq. (2.15), a plot of $q_t \sim t^{1/2}$ should be a straight line with a slope k_{id} when the intraparticle diffusion is a rate-limiting step. It is essential for the $q_t \sim t^{1/2}$ plot to go through the origin if the intraparticle diffusion is the sole rate-limiting step. However, it is not always the case and adsorption kinetics may be controlled by film diffusion (dufusion across the boundary layer) and intraparticle diffusion simultaneously. Thus, the intercept, which is equal to constant c, is not equal to zero.

2.6. Thermodynamics parameters of adsorption

Thermodynamic studies are basic tool in adsorption–adsorbate systems, to provide information on the feasibility (spontaneity), exo- orendo-thermicity of the adsorption and explain whether or not the randomness increases or decreases at the solid–solution interface.

The Gibbs free energy change (ΔG^{o}) is an indication of spontaneity of an adsorption and therefore is one of the most importantcriteria. It is calculated as follows:

$$\Delta G^{\circ} = - RT \ln K_a \qquad (2.16)$$

where: R is the universal gas constant (8.314 J/mol·K) and K_a is the equilibrium constant.

Negative or positive values of ΔG^{o} indicate the spontaneity or no-spontaneity of adsorption process, respectively. Enthalpy change, ΔH^{o}, provides information about the energy release (exothermic process) or consumption (endothermic process) during adsorption process. Another thermodynamic parameter namely ΔS^{o} (entropy change) depending on the sign, indicates if the randomness increases (positive values) ordecreases (negative values), during adsorption procedure. Therefore, the correct estimation of the thermodynamic parameters is essential in describing the adsorption process [26, 27].

For ΔG^{o} determination, it is necessary to estimate equilibrium constant K_a. There are conflicting approaches regarding the appropriate calculation of K_a. According to Liu [28], Langmuir conatant K_L expressed in unit dm^3/mol can be used as equilibrium

constant. On the other hand, ΔG^o is wrongly estimated leading to misunderstandings by using other units (such as dm^3/mg). In addition, the authors [29] concluded that the calculation of ΔG^o by using K_L in dm^3/mol is feasible for (i) neutral adsorbates or adsorbates with very weak charge, and (ii) dilute solutions of charged adsorbate; whereas for charged adsorbate solution at high concentration the effect of the activity coefficient needs to receive the appropriate attention. On the contrary, Milonjic [30] supports that the equilibrium constant K_a is wrongly presented with units in many works due to the fact that ΔG^o unit is J/mol and RT is also J/mol. As a result, the K_a variable must be dimensionless. Milonjic recommended to recalculate the K_a as dimensionless by multiplying it by 55.5 (number of moles per litre of solution). If K_a is given in units dm^3/g, it can be easily recalculatedto become dimensionless by multiplying it with 1000 (1 dm^3 = 1000 cm^3).

Generally, for an adsorption process, which can be depicted as follows [29]:

$$A_{\text{(free adsorptive species)}} + B_{\text{(adsorption sites on the adsorbent)}} \leftrightarrow AB_{\text{(the occupied sites)}} \tag{2.17}$$
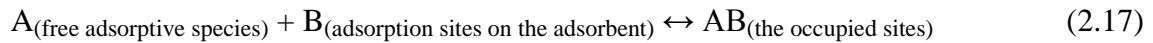
the thermodynamic equilibrium constant (K_a) can be written as follows:

$$K_a = \frac{a_{AB}}{a_A \cdot a_B} \tag{2.18}$$

in which a_A, a_B, and a_{AB} are the respective activities of species A, B, and AB adsorbed at equilibrium. In an extreme case where the adsorption capacity of the adsorbent is much higher than the amount of adsorbate to be removed, the adsorbent B in Eq. (2.17) would be regarded as a pure solid; that is, the activity of which would be close to unity. Consequently, Eq. (2.18) reduces to:

$$K_a \approx \frac{a_{AB}}{a_A} \tag{2.19}$$

For a dilute solution, the activity coefficient is very close to unity, and thus reducing Eq. (2.19) to the following form:

$$K_a \approx \frac{c_{AB}}{c_A} = \frac{q_e}{c_e} = K_c \tag{2.20}$$

where K_c is the distribution constant. Eq. (2.20) suggests that only at very low adsorbate concentrations, K_c is equal to the thermodynamic equilibrium constant K_a, and only

inthis case can it be used for the calculation of ΔG^o according to the Eq. (2.16). Value of K_c for the dilute solution can be obtained by plotting q_e/c_eversus c_e and extrapolating c_e to zero [31].

The determination of ΔH^o and ΔS^o has been performed by using van't Hoff equation as follows [29]:

$$\ln K_a = \frac{\Delta H^o}{RT} + \frac{\Delta S^o}{R}$$

(2.21)

In order to calculate ΔH^o and ΔS^o, adsorption data from two or more temperatures are bare necessities, $i.e.$, the values of K_a for different temperatures should be determined. The values of ΔH^o and ΔS^o are determined from the slop and intercept of the linear plot of $\ln K_a$ vs. $1/T$ [32].

3. Structure, properties and modification of sepiolite

3.1. Origin and structure of sepiolite

Sepiolite is a naturally occurring, non-swelling, lightweight clay mineral. Chemically, it is a hydrated magnesium silicate $Mg_8Si_{12}O_{30}(OH)_4(OH_2)_4 \cdot 8H_2O$, which individual particles have fibrousor needle-like morphology.

There are very few commercial sepiolite deposits in the world. Over 90% of sepiolitic clays are produced in Spain. Other small operations are in Nevada (USA), Turkey and China [5]. Sepiolite occurs in the form of lumps, sedimentary beds, matted plates (so-called mountain leather), or fibers, all of which are based on single crystal fibers. The felting in one, two, or three dimensions of these extremely thin single crystal fibers leads to their aggregation into these various forms. Generally, several single crystal fibers (laths) are grouped in a rod and several rods are aggregated approximatelyparallel to the c axis of the fibre to form bundles. Each deposit has its own characteristics that vary greatly from one locality to another, explaining why each deposit has different physical and chemical properties.

Sepiolite fibers vary considerably in shape and size from one deposit to another, and even among samples from the same deposit [33]. Fibres can show lengths of less than 1 μm (Fig. 3.1.), like thesepiolite obtained from Nevada (USA), to centimetres (sepiolites from China and Finland). However, sepiolites from some of the Spanish or Turkish deposits consist of intermediate fibres (between 1and 10 μm of length).
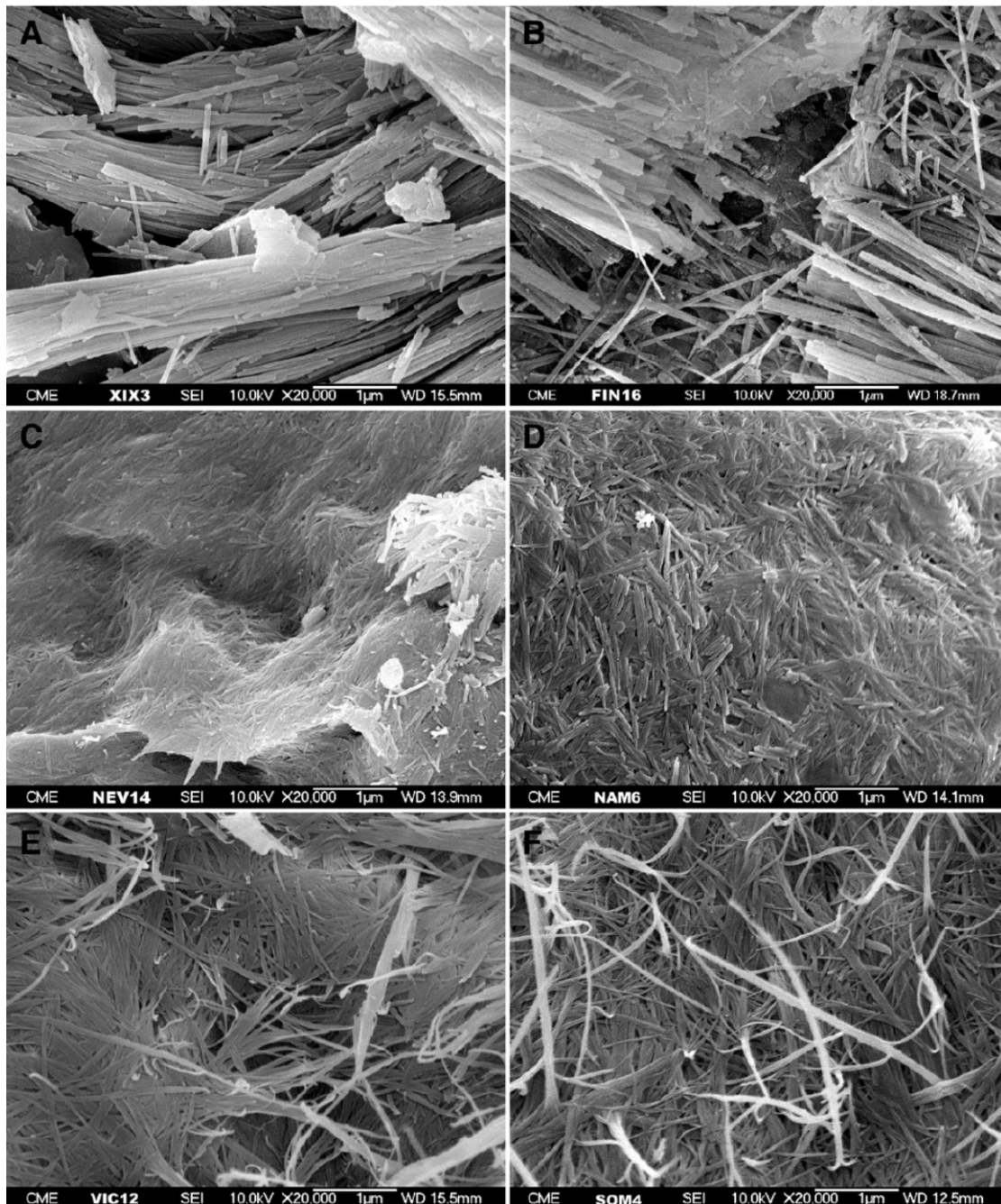
Fig. 3.1. Scaning electron micrographs of sepiolites from different localities: A) China, B) Finland, C) Nevada (USA), D) Namibia, E) Spain, and F) Somalia [35].

Regardless of the fibre length, there are remarkable variations intheir bend or curl. The fibres can be completely straight with rigid aspects, or they can be very curled. Similar to the length, all intermediate possibilities can be found. Based on their degree of bend or curl, the samples of different deposits have beengrouped into three types:

i) straight and rigid fibres, which include fibres of different sizes, from the smallest to the macroscopic fibres; they grow in different arrangements similar to a mass of sticks and often look rigid and fragile

ii) curved fibres, which include fibres that are softly curled

iii) curly type, which is extreme, and only a few of the samples belong to this type; these types of fibres are commonly randomly oriented and are intricately intertwined, forming planes or mats of fibres [34].

The final characteristics of the samples depend not only on the fibre morphology but also on the way that these fibres are arranged. Therefore, textures and porosities of the samples can vary greatly.

The fibrous structure of sepiolite comes from structural ribbons and channels in the direction of c-axis of fibers. Each ribbon is 2:1 type and consists of two tetrahedral silica layers and a central magnesium octahedral layer [36]. Arrangement of the structural units and channels is shown in Fig. 3.2. This chain-like structure produces fibrous or needle-like particles instead of plate-like particles like other clays.
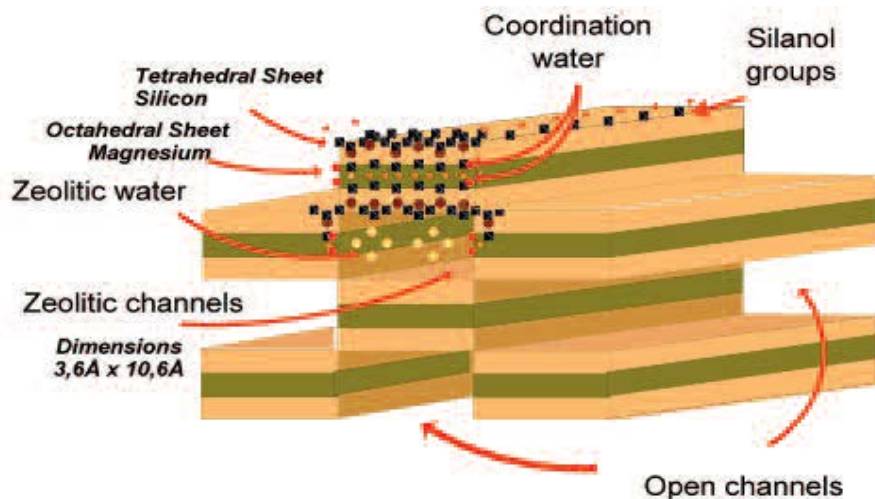
Fig. 3.2. Structure of sepiolite [36].

The sepiolite structure was first deduced by Brauner and Preisinger [37] according to X-ray diffraction analysis. According to this model (Fig. 3.2), sepiolite unit cell is orthorhombic, with cell parameters: $a = 1.35$ nm, $b = 2.70$ nm and $c = 0.526$ nm.

Four oxygen atoms surround every silicon atom in the tetrahedron, three at a distance of 0.156 nm and one at 0.166 nm. Tetrahedral silica layers are continuous, but after each six tetrahedrons, an inversion of the direction of the edge tetrahedron occurs. In that way, structural channels were formed [38]. In the inner ribbons, all corners of the silica tetrahedral are connected to adjacent ribbons, but in the outer ribbonss, some of the corners are Si atoms bound to hydroxyls (Si–OH). The channels are filled by zeolitic water, which forms hydrogen bonds with the oxygen ions on the tetrahedral sheet or with other water molecules. In the same way, the terminal Mg^{2+}, which are located at the edges of the octahedral sheet, complete their octahedral coordination creating bounds with other water molecules, named coordination (bound) water.

The investigationof thermal properties of sepiolite confirmed the presence of three types of water: zeolitic, coordinated and constitutional (OH groups bonded the Mg atoms) water [39]. Dehydration of sepiolite takes place in several stages:

1. zeolitic water is released at about 100 °C:

$$Mg_8Si_{12}O_{30}(OH)_4 \cdot 4H_2O \cdot 8H_2O \rightarrow Mg_8Si_{12}O_{30}(OH)_4 \cdot 4H_2O + 8H_2O \qquad (3.1)$$
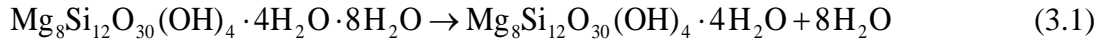
2. half of the coordination water is released at about 300 °C:

$$Mg_8Si_{12}O_{30}(OH)_4 . 4H_2O \rightarrow Mg_8 Si_{12}O_{30}(OH)_4 . 2H_2O + 2H_2O \qquad (3.2)$$

3. second half of coordinated water is released at about 550 °C:

$$Mg_8Si_{12}O_{30}(OH)_4 . 2H_2 O \rightarrow Mg_8 Si_{12}O_{30}(OH)_4 + 2H_2O \qquad (3.3)$$

4. constitutional water is released at about 800 °C, which leads to sepiolite transformation to enstatite ($MgSiO_3$):

$$Mg_8Si_{12}O_{30}(OH)_4 \rightarrow 8MgSiO_3 + 4SiO_2 + 2H_2O \qquad (3.4)$$
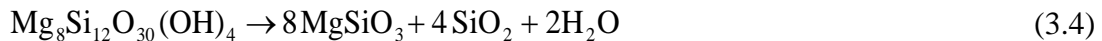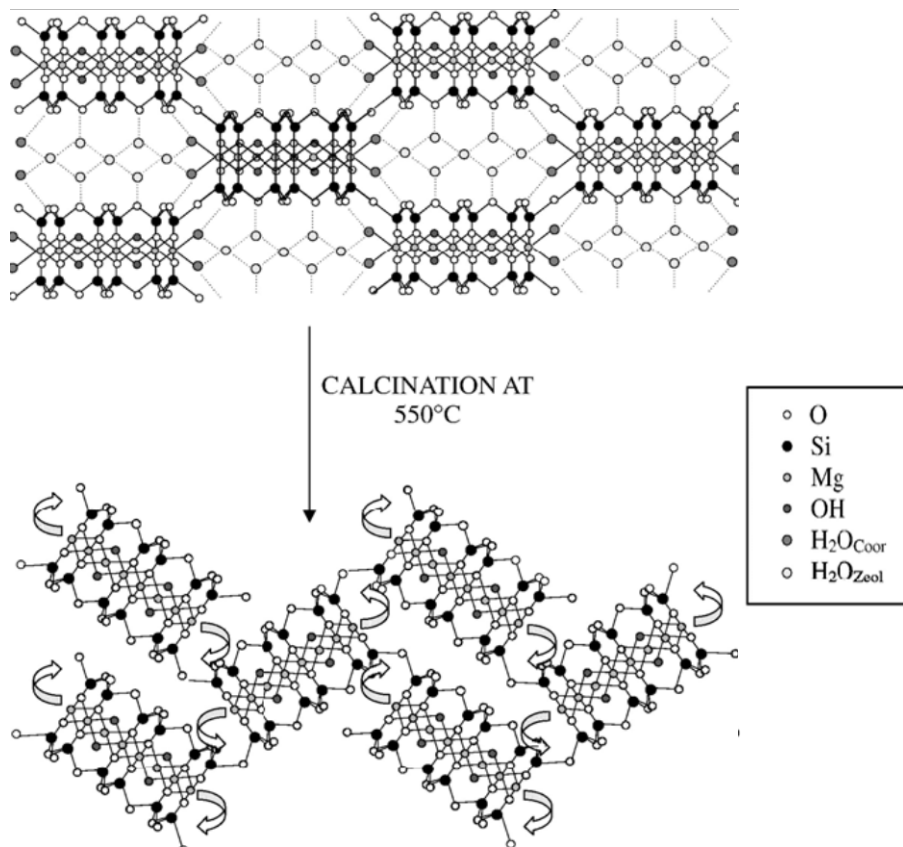
Fig. 3.3. Brauner-Preisinger model of sepiolite structure (up) and structure of folded sepiolite (down) [40].

The loss of the coordinated H_2O causes the structure folding due to the rotation of the structural ribbons about an axis through the Si-O-Si corner bonds that link the ribbons (Fig. 3.3.). In the structure of sepiolite (Fig. 3.3), coordinated water forms the hydrogen bridges with oxygen of the neighboring silica surface, which stabilizes the structure. When coordinated water molecules are eliminated, the bridge effect is lost and the structure is folded in order to satisfy the coordination of the octahedral magnesium by the oxygen of the neighboring silica surface (Fig. 3.3) [40].

3.2. Adsorption properties of sepiolite

The high surface area and porosity account for the remarkable adsorptive and absorptive properties of sepiolite [41, 42]. It is used as industrial absorbent for liquid spills andleaks, for decoloration and deodorization of edible and mineral oils, drying and purification of transformer oils [36], as a carrier for chemicals, for moisture and odor control, for toxic and hazardous wastes stabilization or inertisation; as cat and pet litter, for the pollutants removal from water, etc.

Sepiolite has high specific surface area not only due to the small size of its particles and fibrous morphology, but also because of its intra-crystalline channels, *i.e.* micropores. Both the external surface and the surface of the micropores influence the specific surface area of this mineral. Sepiolite has the highest surface area of all the clay minerals (200-350 m^2/g, depending on origin and presence of impurities [38]), with a high density of silanol groups, which explains the marked hydrophilicity of this clay. The silicate lattice doe not have a significant negative charge and therefore the cation exchange capacity of this clay is very low.

The structure of sepiolite includes three types of active adsorption sites: (a) oxygen ions on thetetrahedral sheet of the ribbons, (b) water molecules coordinated to Mg^{2+} ions at the edges of structural ribbons (two H_2O moleculesper Mg^{2+} ion), and (c) SiOH groups along the fibre axis [5]. In addition, a small amount of exchangeable cations (4 to 40 mEq/100 g) and Mg^{2+} ions from the structure give a contribution to the adsorption capacity of sepiolite.

Adsorption onto sepiolite is influenced by the size, shape and polarity of the adsorbate. Neither large molecules nor those of low polarity can penetrate the channels though they can be adsorbed on the external surface. Barrer and Mackenzie [42] suggested that the accessibility of sepiolite channels might depend more on the polarity of a substance than on the dimensions of molecules. Both polar and non-polar molecules can enter the channels, with a negative value of free energy change for polar molecules and a positive one for non-polar molecules. If the adsorbed cations or water molecules are distributed within the sepiolite channels, the diffusion of non-polar molecules is suppressed.

Recently, sepiolite hasbeen investigated for water purification on the basis of its adsorptive properties. It was shown that sepiolite has high affinity for heavy metal cations, such as Pb^{2+}, Cd^{2+}, Cu^{2+}, Co^{2+}, Ni^{2+} etc. Lazarevic et al. [11, 12, 43] showed that the retention of Pb^{2+}, Cd^{2+}, Cu^{2+}, Co^{2+}, Ni^{2+} occurs dominantly by specific adsorption, *i.e.* surface complexation, and ion exchange with Mg^{2+} ions from the sepiolite structure. High efficiency of sepiolite to remove cationic dyes from water has been demonstrated [11, 44-46] although these studies have been mostly focused on methylene blue and crystal violet dyes, which are not typically used in textile industry.

On the other hand, adsorption capacity of sepiolite for anions is very low due to the negative surface charge of sepiolite in a wide range of pH values of the solution. Marjanovic et al. [47] showed that the removal of Cr(VI) anion species by sepiolite was negligible because there were only very weak electrostatic interactions between the Cr(VI) anion species and surface of the sepiolite, owing to the nature of surface and because there was no complex formation of the chromium species with the surface of the mineral. Regarding anionic dyes, natural sepiolite provided relatively low adsorbed amounts of an azo acid dye [48]. In its untreated form, sepiolite was neither able to remove reactive dyes, requiring a chemical modification to create a positive surface charge and provide suitable adsorption [49].

Generally, sepiolite is an efficient adsorbent for cationic pollutants, while the modifications are necessary to provide effective removal of anionic pollutants from water.

3.3. Modifications of sepiolite

It was shown in recent studies that adsorption capacity and general physical and chemical properties of sepiolite could be highly improved by various modifications [50]. Sepiolite can be modified in various ways to increase the specific surface area or to alter the nature of the surface. In addition, nanocomposites with iron compounds have been synthesized in order to increase the adsorption capacity or provide some useful properties for the practical applications. Sepiolites obtained by acid activation or by

surface modification, as well as nanocomposites with iron compounds have been applied for the removal of differrent pollutants from water.

3.3.1. Modification by acid activation

Acid treatments have been used to increase the specific surface area and to obtain solids with high porosity and a high number of acidic centers on the surface [11].There are many publications which describe the modification of sepiolite by acid treatment, using H_2SO_4, HNO_3 or HCl. Depending on the duration and intensity of the treatment, the reported results of the acid attack are protonization of exchangeable cations and edge Mg^{2+}, followed by dissolution of the octahedral sheet with release of Mg^{2+} cations and creation of silanol groups from the broken surface siloxane ones (Si-O-Si). With stronger treatment, the presence of free silica has been reported [51]. The properties of partially acid activated sepiolite depend on the nature and concentration of the acid used, temperature and duration of the attack, but fibrous structure of the original sepiolite is generally preserved. The correlation between the quantity of Mg^{2+} ions released from sepiolite and its properties, mainly an increase of the surface area and enhanced ability for adsorption on acid-activated sepiolite, have been reported in several studies [52- 56].

Hernandez et al. [57] have proposed a possible two steps reaction for the process of acid treatment of sepiolite. In the first step, the octahedral layers are eliminated by dissolution in the acid, leading to the formation of two new surfaces facing each other. These surfaces are very reactive and contain a large number of silanol groups. The second step involves condensation of silanol groups, resulting in a closure of pores.

Aznar et al. [58] analyzed the activation of sepiolite by acid and obtaining of amorphous SiO_2. The results showed that the process was affected by the type of acid, acid concentration, the ratio of solid/liquid, temperature and duration of activation. They found that activation of sepiolite by acid of higher concentrations (2 M HNO_3 or 4 – 6 M H_2SO_4) led to complete removal of Mg^{2+} ions from the structure. In addition, the temperature increasing led more rapidly to full activation. Increasing amounts of

leached Mg reduced the crystallinity of the solid phase and simultaneously increased the specific surface area and mesoporosity.

Balci [59] examined the effect of heat treatment on sepiolite structure with and without acid pre-treatment. He found that specific surface area increased by heating to 100°C, but further increase in temperature caused channel plugging and crystal structure deformation. As a result, the specific surface area decreased with temperature. On the other hand, acid pre-treatment caused a change in pore size distribution by increasing the surface area 2.5 times. The surface area of the original mineral, which was heated up to 900 °C, was 60 m^2/g, while the corresponding value of the acid pretreated sepiolite was 360 m^2/g.

Valentine et al. [60] examined changes in structure of acid activated sepiolite during heating until 550 °C. The presence of both structures after treatment, sepiolite and free silica, caused changes in the structural behavior of the sepiolite at elevated temperatures. The structure of untreated sepiolite was folded by the elimination of the coordinated water molecules, but acid pre-treated sepiolite remained unfolded after the heat treatment at 550 °C.

Franco et al. [61] examined the influence of the microwave-assisted acid treatment on the structure and texture of sepiolite samples with different compositions and crystalline ordering. Using this type of treatment it is possible to obtain, in just a few minutes, materials whose specific surface areas are similar to those materials activated by traditional methods in two days,despite employing acid solutions of very low concentrations.This treatment caused a progressive amorphization of the starting sepiolite giving rise to the formation of sepiolite with partially disrupted structures and an increasing amount of amorphous silica, which was accompanied by a huge mass loss, due to the Mg^{2+} depletion of the octahedral sheet. The characteristic fibrous morphology of natural sepiolite remained in acid-activated materials with partially dissolved structures. However, when Mg^{2+} was completely released, the fibrous shape disappeared, generating particles of amorphous silica with globular-like irregular morphologies.The microwave-acid treatment effectiveness depended also on the starting sepiolite's own characteristics. The lower crystalline sepiolite tended to lose easily its structure completely with these treatments, but the presence of Al^{3+} in octahedral sheets seemed to have a negative influence on the rate of dissolution. Factors such as the

presence of mineralogical impurities did not affect the effectiveness of this acid activation.

Lazarević et al. [11] investigated adsorption of Pb^{2+}, Sr^{2+} and Cd^{2+} on acid activated and natural sepiolite from polluted waters. These divalent cations were retained on sepiolites in the following order $Pb^{2+}>Cd^{2+}>Sr^{2+}$. The retention of Pb^{2+} and Cd^{2+} occured dominantly by specific adsorption and exchange of Mg^{2+} ions from the sepiolite structure. Concentration in the external outer sphere of the Stern layer by electrostatic forces was the dominant mechanism for the retention of Sr^{2+} ions onto the surface of sepiolites. During partial acid treatment, the crystal lattice of sepiolite was maintained, albeit with some decrease in crystallinity. The specific surface area, total pore volume, mesopore volume and mean pore radius were increased. Despite increases in the surface areas upon acid activation, improvements in the adsorption were not observed, as a result of the decreasing number of Mg^{2+} ions available for ion exchange with Pb^{2+} and Cd^{2+}. This clearly showed that the untreated form of sepiolite is more effective for the adsorption of Pb^{2+}, Cd^{2+} and Sr^{2+} ions from wastewater.

Marjanović et al. [47] examined the adsorption of Cr(VI) onto natural and acid-activatedsepiolites. The results indicated that the amount of Cr (VI) ions adsorbed onto acid-activated sepiolite increased with decreasing pH of the solution. As the pH of the Cr (VI) solutions became lower than the pH_{pzc} of the sepiolites, the more protonated hydroxyl groups on the surfaces would be favorable for the adsorption of $HCrO_4^-$ species, as Coulombic interaction forces can readily exist. The adsorption capacity of the acid-activated sepiolite was slightly higher than of sepiolite, but in both cases, the adsorption capacity was very low.

3.3.2. Surface modification by organic functional groups

The properties of sepiolite can be tailored for specific applications through surface functionalization [62, 63]. Two different functionalization processes are possible: (i) adsorption of quaternary ammonium salts or amines, and (ii) surface modification through reaction of surface silanol groups with organosilane reagents.

Sepiolite may be modified by quaternary ammonium salt or neutral amines in a manner that significantly enhances its capability to remove hydrophobic contaminants from aqueous solution.The exchangeable cations from the sepiolite structure are replaced by quaternary ammonium salt or neutral amines, which have cationic head groups with long chain hydrocarbon molecule forming the surfactant tail, thus it can be effectively used to remove hydrophobic nonionic organic compounds from aqueous solutions [64]. The amount of these types of modifiers is usually quite high, to compensate possible migration of the modifier in the polymer matrix owing to instability of the link between the modifier and the sepiolite surface [65].

Sepiolite surface could be functionalized with silanes in order to remove anions from water. Very high density (2.2 groups per 100 Å^2) of silanol groups on the sepiolite surface allows an adequate functionalization with silane reagents [65]. Silane coupling agents are a family of organosilicon monomers, which are characterized by the general structure R–SiX$_3$, in which R is an organo-functional group attached to silicon in a hydrolytically stable manner. X designates hydrolysable alkoxy groups (usually methoxy, –OCH$_3$, or ethoxy, –OC$_2$H$_5$), which are converted to silanol groups by hydrolysis. Most commonly, R is composed of a reactive group R′ separated by a propylene group from silicon, R′–(CH$_2$)$_3$–SiX$_3$. The reactive group can, for example, be vinyl (–HC$=$CH$_2$), amino (–NH$_2$), or mercapto (–SH) or can contain several chemical functional groups [66].

Marjanović et al. [67] examined chromium(VI) adsorption onto amine-functionalized sepiolites from aqueous at initial pH values of 4.5, 3.0, and 2.0. Natural and acid-activated sepiolites were functionalized by covalent grafting of [3-(2-aminoethylamino)propyl]trimethoxy-silane to the silanol groups at the sepiolite surface. The maximum chromium(VI) removal was achieved at an initial pH of 2.0: approximately 60 mg/g of functionalized acid-activated sepiolite and about 37 mg/g of functionalized natural sepiolite. Adsorption capacities of amine-functionalized sepiolites for chromium(VI) were the highest at pH of 2.0, which can be explained by the remarkable protonation of the amine groups and the electrostatic attraction of Cr(VI) anionic species. At higher initial pH, the solution pH increased drastically during Cr(VI) adsorption due to the high value of pH$_{pzc}$ and large buffer capacity of the amine-

functionalized sepiolites, which caused low adsorption capacities of these adsorbents for Cr(VI).

Marjanović et al. [47] investigated the adsorption of Cr(VI) onto sepiolite samples obtained by functionalization of natural and acid-activated sepiolite with 3-mercaptopropyltrimethoxysilane. The efficiency of functionalized acid-activated sepiolite was higher than of functionalized natural sepiolite. As the number of silanol groups on the sepiolite surface increased during the acid activation, the silane functionalization increased and this led to an increase in Cr(VI) adsorption. The adsorption capacity strongly depended on the pH of the solution from which the adsorption occurred. Liang et al. [68, 69] prepared also mercapto-functionalized sepiolite by surface grafting with mercaptopropyltrimethoxysilane. The chemical bonding takes place between the surface hydroxyl group of sepiolite and the methoxy group of mercaptopropyltrimethoxysilane. The surface modification increased the adsorption capacities for Pb^{2+} and Cd^{2+}.

3.3.3. Formation of nanocomposites with iron compounds

Although sepiolite is an adsorbent with high adsorption capacity, especially for cations, researchers have tried to modify this substrate in order to synthesize an adsorbent with even higher retention ability than that of the parent material. Having in mind that iron oxides are active adsorbents and play an important role in the reaction behavior of many ions in environmental sediments [70, 71], the formation of an iron-oxide phase onto sepiolite increases the number of active sites of the adsorbent due to the presence of the Fe–OH groups in external and internal surface positions. In addition, composites of sepiolite with magnetite (Fe_3O_4) are magnetically separable adsorbents, which improves the performance of the adsorption process.

Generally, sepiolite - iron oxide systems were synthesized by precipitation of iron hydroxide from iron salt solution by strong base, in the presence of sepiolite [70, 72]. These systems were applied mainly for the adsorption of heavy metals from water.

Lazarević et al. [12, 73] examined the characteristics of the sepiolite-iron oxyhydroxide system (Fe-sepiolite) and effectiveness of the obtained adsorbent in the

removal of Ni^{2+}, Co^{2+} and Cu^{2+} from aqueous solutions. Fe-sepiolite maintained the basic structure of sepiolite. The presence of new crystalline Fe phases was not observed, indicating that an amorphous Fe species was formed. Results showed that Fe-sepiolite had higher adsorption capacity than the natural sepiolite owing to a higher specific adsorption and higher ion exchange with Mg^{2+} ions from sepiolite. In addition, it was shown that this material was effective adsorbent for As(III) and As(V) [74].

Eren et al. [70, 72] examined the effectiveness of iron oxide coated sepiolite in Cu^{2+} and Pb^{2+} removing from aqueous solutions. Results showed that Mg^{2+} cations were removed loosing water and hydroxyl group coordinated to them during the oxide coating process. The decreasing intensity of the hydroxyl vibration of the zeolitic water indicated the replacement of part of the zeolitic water with iron oxide particles. Adsorption experiment showed higher capacity of the composite material in comparison to unmodified sepiolite.

Yu et al. [75] prepared the magnetite/sepiolite (M/SEP) composite by co-precipitation method, by adding base in deoxygenated suspension of the support with Fe^{2+} and Fe^{3+} ions. The characterization results showed that M/SEP was composed of magnetite and sepiolite and had a superparamagnetic property, which means that in the absence of an external magnetic field, the magnetization appears to be in average zero, but an external magnetic field is able to magnetize the material. The composite was used as anadsorbent for the removal of Co^{2+} and Cd^{2+} from aqueous solutions. After adsorption, the Co^{2+} and Cd^{2+}-loaded adsorbent were quickly separated and recovered from the aqueous solutions by easy magnetic separation.

In order to obtain sepiolite-based magnetic nanocomposites (MNCs) with a high adsorptioncapacity for Cd^{2+} and good magnetic properties, Ahribesh et al. [76] varied the conditions of the co-precipitation synthesis. Both untreated natural (SEP) and partially acidactivated (ASEP) sepiolites were used as supports. The synthesis conditions differed as follows: NaOH or NH_3 was added in the SEP or the ASEP suspensionbefore or after the addition of Fe^{3+} and Fe^{2+}. The SEP-based MNCs prepared using NaOH had a lowermagnetization, but higher adsorption capacities than the MNCs synthesized using NH_3. The order of the mixingof the reagents had a small influence on the properties of SEP-based MNCs, especially when NaOH was used forthe synthesis. Due to acidity of the surface functional groups of the ASEP, the magnetic composite

could be synthesizedonly when NH_3 was added in the suspension of ASEP having Fe^{3+} and Fe^{2+} ions. Despite of the worsedispersibility of the magnetic particles, the adsorption capacity of the ASEP-based composite was higher than oftheMNCwith SEP prepared by the same procedure. All theMNCs showed a superparamagnetic behavior at roomtemperature, while the adsorption capacities were higher than of pure compounds (SEP, ASEP and Fe_3O_4).

4. Synthesis, properties and application of nano-zero valent iron (nZVI) and nZVI-based composites

In recent years, the use of nano zero-valent iron (nZVI) for the treatment of toxic contaminants in ground water and wastewater has received wide attention. Due to its nanometer size (1–100 nm) and hence its large specific surface area, nZVI has higher reducing ability and activity, stronger adsorption properties and better mobility than bulk or microscale iron particles [77]. These characteristics allow nZVI to work as an effective remediating agent for a wide range of contaminants: chlorinated organic compounds (RCl), nitroaromatic compounds (NACs), arsenic, heavy metals, nitrate, dyes and phenol (Fig. 4.1.) [78]. Mechanisms of contaminants removal from water by nZVI varies with different contaminants and may involve oxidation/reduction, surface complexation, surface precipitation, and co-precipitation.
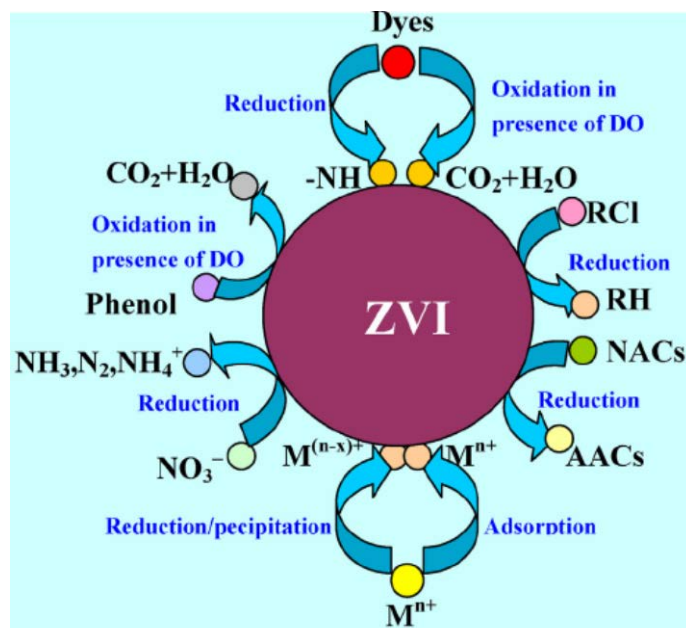
Fig. 4.1. Schematic model of reaction mechanism of nZVI with different contaminants (RCl - chlorinated organic compounds, RH – reduced organic compounds, NACs - nitroaromatic compounds, AACs – aromatic amine compounds, DO – dissolved oxygen, M^{n+} - heavy metal ion) [78].

There are some disadvantages in the use of nZVI particles,such as high tendency to agglomerate, lack of stability, secondaryiron pollution, separation and recovery of the fine nZVIparticles after utilization [79]. To resolve these issues,various stabilization methods have already been developed tofacilitate the use of nZVI in a wide range of environmentalremediation scenarios.

4.1. Synthesis of nZVI particles

There are many methods for the synthesis of iron nanoparticles, which are divided into two categories [80, 81]: top-down and bottom-up methods (Fig. 4.2).
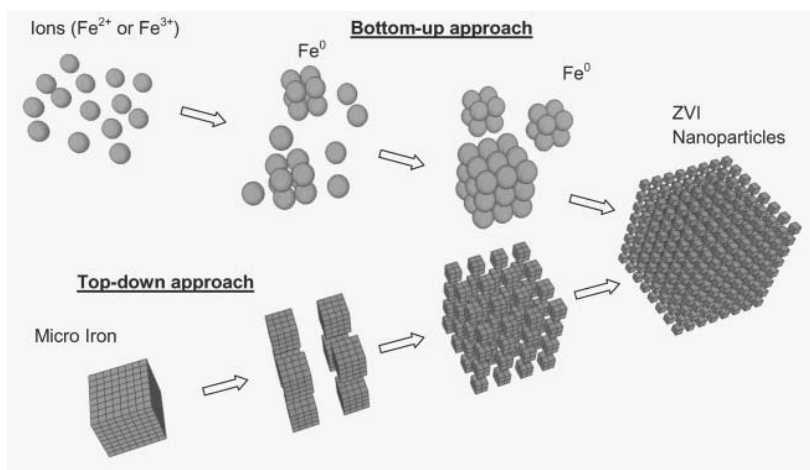
Fig. 4.2. Conceptual models of bottom-up and top-down approaches for nanoparticle preparations [80].

Bottom-up approach entails piecing together individual atoms or molecules to form nanosized structures. The top-down approach, on the other hand, is the process where large size materials are converted to nZVI with the aid of mechanical and chemical processes such as milling, etching, and/or machining.

The synthesis methods can be also divided into two principal groups: physical methods and chemical methods. Generally, physical methods, such as gas condensation processing and ball milling, possess the advantages of simple operation and easy separation of products over chemical methods. However, chemical methods are thought to be potentially advantageous for nZVI manufacture and have been the focus of recent research studies, resulting in the development of a diverse range of chemical synthesis techniques of nZVI.

4.1.1. Physical methods of nZVI synthesis

Mechanical milling has rarely been applied for nanoparticle production, partly due to the limitation of the conventional equipment to achieve size reduction down to the nanometre scale. In addition, mechanical forces during milling introduce considerable dislocations, vacancies and strain to the products. However, precision ball milling [80] in a high-speed rotary chamber with steel shot, using microiron particles as raw materials, could effectively produce zerovalent iron nanoparticles of uniform size

and a high specific surface area. The method is nontoxic, free of secondarypollution and suitable for industrial scale supply. But, this method is energy-intensive and requires specialized equipment to achieve size reduction down to the nanometer scale. In addition, the product homogeneity of this method is not satisfactory [77].

In gas condensation processing, nano iron particles are obtained by condensingthe vapour of iron atoms under an inert gas atmosphere viacooling with liquid nitrogen. This method enables good control of particle size, but highly restricted process conditions are required: high temperature, high pressure and substantialcoolant. In addition, energy consumption is very high, while the yield is extremely low.

4.1.2. Chemical methods of nZVI synthesis

Among various chemical synthesis methods, chemical reduction is the most common for nZVI synthesis in both laboratories and large-scale applications due to its simplicity, productivity and chemical homogeneity of the product [82-84]. Most of other techniques for synthesizing nZVI are not feasible or cost-effective for industrial large-scale production.

Borohydride reduction method. The synthesis of nZVI can be achieved by reduction of ferrous or ferric ions in aqueous solutions using sodium borohydride ($NaBH_4$) under inert conditions. The method includes four steps: (1) preparation of supersaturated solution (ferric or ferrous salts), (2) nucleation of the nZVI cluster (reduction of Fe(II) or Fe(III) by reducing agent), (3) growth of nZVI nuclei, and (4) agglomeration of nZVI. Investigation showed that the last two steps have the most significant effects on shape and properties of nano particles [85-87]. Therefore, it is important to control the growth and agglomeration time by controlling the reductant delivery rate, reductant concentration and other synthesis parameters [85, 87]. Excess of borohydride is needed to speed up the synthesis reaction and to provide the uniform growth of nZVI particles.

The reactions of the ferrous and ferric ions reduction in aqueous solutions using sodium borohydride can be represented by equations [88, 89]:

$$4Fe^{3+} + 3BH_4^- + 9H_2O \rightarrow 4Fe^0\downarrow + 3B(OH)_3 + 9H^+ + 6H_2 \qquad (4.1)$$

$$2Fe^{2+} + BH_4^- + 3H_2O \rightarrow 2Fe^0(s) + B(OH)_3 + 3H^+ + 2H_2(g) \qquad (4.2)$$
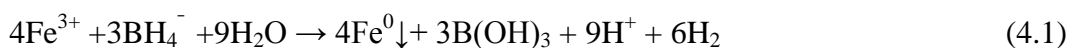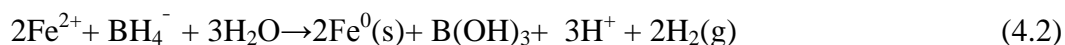
In borohydride reduction, washing and drying processesare required in order to rinse out excess chemicals on nZVI surfaces and to prevent gradual oxidation and aging of nZVI by residual water on the surfaces, respectively [90]. Deionized water is the most typical washing solution used in nZVI preparation, while some researchers have applied volatile solvents like ethanol and acetone [90]. For drying, several methods have been employed to minimize nZVI oxidation during the process, including vacuum oven drying and freeze drying [90].

Recent studies have reported alterations in the surface properties of nZVIs experiencing different washing and drying conditions. This implies possible variations in the reactivity of nZVIs prepared under different conditions since nZVI reactivity is primarily surface-mediated. Nurmi et al. [91] found that fast removal of adsorbed water on nZVI surfaces using acetone washing and vacuum filtration drying protect nZVI surface from deposition of salts, etching, and cementation. Yaacob et al. [92] reported that washing solutions and drying methods affect color, particle size, and texture shape of nZVI.

Volatile solvent washing and anaerobic drying could maximize nZVI reactivity toward reducible contaminants by decreasing thickness of Fe-oxide shell layer on nZVI and increasing content of Fe^{2+}-containing oxide forms in the shell layer [90].

Many attempts have been made to combine reduction methodwith some supplementary means to improve thequality of nZVI. For example, nZVI with high reductive activityhas been prepared by the borohydride reduction method in anaqueous solution of ionic liquids, which can control theformation and stabilization of nanoparticles. The obtained particles are smaller, more uniform and easier to separate [77].

Ultrasound assisted method. It was found that ultrasound affects the growth and coalescence of iron nanoparticles. The nZVI synthesized in this manner has a smaller particle size, a larger specific surface area and higher crystallinity than that synthesized by the conventional borohydride reduction method. It was also observed that under ultrasound, the morphology of nZVI particles was changed from spherical to plate and needle types by increasing the ultrasonic power [81].

Carbothermal reduction. Generally, in carbothermal reduction, C or CO is used to reduce iron oxide (natural iron ores, such as goethite), ferrous or ferric ions at elevated temperatures (Eqs. 4.3 and 4.4). Raw materials are inexpensive andwidely available, leading to low production cost. However, thegeneration of carbon monoxide (CO), a flammable and toxic gas, is an unavoidable drawback of this method.

$$Fe(C_2H_3O_2)_2 + C \rightarrow Fe^0 + 2CH_2CO + CO + H_2O \qquad (4.3)$$

$$Fe_2O_3 + 2C \rightarrow 2Fe^0 + CO + CO_2 \qquad (4.4)$$
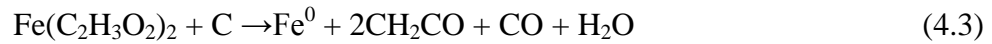
Thermal decomposition method. High quality nZVI particles can be produced by thermal decomposition of an iron precursor.Organometallic molecules containing iron, especially $Fe(CO)_5$, can be used as a starting material. Spherical nano iron particles can be generated by adding $Fe(CO)_5$ into trioctylphosphineoxide (TOPO) at 320 °C under an argon atmosphere:

$$Fe(CO)_5 \quad \rightarrow \quad Fe^0 + 5CO \qquad (4.5)$$

The product from this method has an extremelysmall size (2 nm) and good homogeneity. Nevertheless, this method also has some drawbacks: $Fe(CO)_5$ is highly toxic and unstable, the process is energy-intensive, and a considerable amount of carbon monoxide is generated as a by-product.

Thermal reduction method. Nano zero-valent particles can be produced by the reduction of goethite (α-FeOOH) or hematite (α-Fe_2O_3) at elevated temperature, by H_2. Depending on hydrogen reduction conditions, the complete reduction can be accomplished even at low temperature up to 380 °C in pure hydrogen. The reduction behaviour is strongly influenced by the particle size, crystallinity and the conditions of the temperature–time– pressure dependent reduction [93].

4.1.3. Electrochemical method

In this method, cathodes are used toattract Fe^{2+}/Fe^{3+} ions from solution by help of electric current [94]. The method is extremely simple, cheap, and fast [95] in comparison to chemical reduction [96]. Produced Fe^0 is gradually deposited on the

cathode, but they often display a strong tendency towards aggregation and the formation of clusters. To counteract that phenomenon, cationic surfactants are used [80], act as a stabilizing agent, and ultrasonic waves, which constitute a source of energy necessary for fast removal of iron nanoparticles from the cathode.

The nZVI particles produced with the use of ultrasonication can be between 1 and 20 nm and have a specific surface area of 25 m^2/g [94]. This method has the advantages of simplicityand low cost, though the as-prepared product has shown a tendencyto aggregate.

4.1.4. Green synthesis

Recently, a green method that uses natural, plant extracts in which the active substances are highly reductivecompounds, such as polyphenol, has been developed [97]. Green synthesis is not only environmentally friendly, but also inexpensive. Because there is no need to use high temperatures, pressure, or additional energy inputs, it is easy to implement on a large scale [97, 98].The method included the preparation of a polyphenolic solution by heating plant extracts (coffee, green tea, black tea, lemon, balm, sorghum, bran, grape etc.) in water to a temperature close to the boiling point. Structural characterization of polyphenol-reduced nanoparticles revealed that they contain large amounts of α-Fe_2O_3 or iron oxyhydroxide with only a less component of amorphous Fe^0, which explains their low reactivity in reduction applications and more applicability towards oxidative reactions with H_2O_2. In addition, presence of hydroxyl and phenol groups in these compounds affords them as good capping agents to stabilize the reactive surfaces of the nanoparticles and decreases their biotoxicity. These extracts have high reductive capacities and assure the reduction of iron(III)/(II) producing nZVI particles [99]. One of the major drawbacks of using plant resources for nanoparticle synthesis is the destruction of plants and plant parts. A possible way to avoid this is to employ agrowaste e.g. waste of eucalyptus leaf [100] or extracts from various residues (skin, albedo, flesh) of such fruits as lemons, mandarins, limes, oranges or vine pomace [97, 101]. Depending upon plant type and concentration of phytochemicals, nanoparticles are synthesized within a few minutes or hours.

In spite of the numerous advantages of using this method, green synthesis is still not commonly accepted. These results from insufficient knowledge of the reactivity, physicochemical properties, and agglomeration of the nanoparticles produced [101]. The information available in the literature indicates that depending on the kind of plant extract used for the production of nZVI, we obtain nanoparticles with various sizes and values of specific surface area. Green synthesis can also be limited by the incomplete reduction of iron to nZVI by plant extracts [102], resulting in of the formation of other forms of iron, e.g. iron oxides of hydroxides, in the course of the process [103].

4.2. Structure and properties of nZVI particles

The properties of nZVI are usually different from the bulk Fe particles and this difference is mainly caused by factors such as the history of the sample, its handling and processing which would affect the size, structure and even composition of the nanoparticle.

Nanozero-valent particles, synthesized at both laboratory and industrial scale [104], exhibit a typical core shell structure where the core consists of zero valent or metallic iron and a shell is largely iron oxides/hydroxides formed from the oxidation of the surface of zero-valent iron (Fig. 4.3). Fresh nZVI particles are mainly composed of Fe^0, with a thin layer of oxides which increases in time. Ageing processes were observed over a wide period, from few days to years. Oxidation is extremely fast in the first few days after synthesis. After the formation of the oxide shell, the Fe^0 core is partly protected from undesired reactions, and corrosion is slower [104].

The core shell structure has important implications on the chemical properties of nZVI: the core provides the reducing power (the electron source) for the reactions, whereas the shell provides the site for chemical complex reactions (chemisorptions) and electrostatic interactions.The oxide layer is amorphousand disordered, owing to the extremely small radii of the nanoparticles, which hinders crystalline formation.The defective and disordered nature of the oxide shell renders it potentially more reactive compared to a simple passive oxide layer formed on bulk iron material. Therefore, the presence of thin and defective oxide layer does not hinder iron reactivity, allowing the

transfer of electrons from the Fe^0 core to the particle surface, where reactions with contaminants adsorbed on the oxide shell or in the close vicinity of the particle can take place [105]. The mixed valence oxide shell is largely insoluble in water underneutral pH and thereby protects the core from rapid oxidation.

The size distribution of nZVI primary particles obtained through the different methods is typically in the range of 10-100 nm, with a corresponding specific surface area in the order of 10-50 m^2/g [107]. Nevertheless, dendritic aggregates, tens or hundreds of times larger than primary particles, are usually observed in aqueous dispersions of nZVI [108], due to the strong particle-particle attractive interactions.When the nanoparticles agglomerate,they have a continuous oxide shell and the metallic cores are separatedby a thinner interfacial oxide layer.
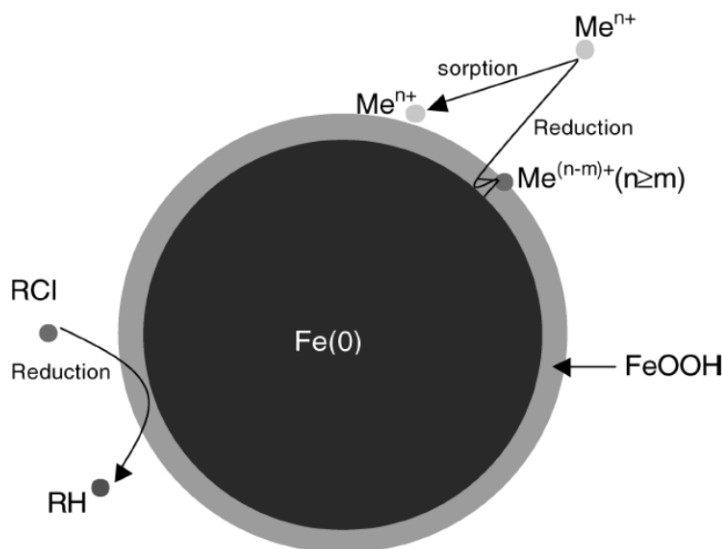
Fig. 4.3. The core-shell model of zero-valent iron nanoparticles, where reduction of environmental contaminants (RCl) and chemical complex formation (Me^{n+}) are shown [106].

Size, shape and composition of the particles are significantly affected by the synthesis process. nZVI obtained by borohydride reduction method are smaller (few tens of nanometers), more regular and smoothed in shape and the Fe^0 structure in the core is amorphous [109], while particles obtained by reduction of goethite and hematite are, as a general rule, larger (up to 100 nm), more irregularly shaped, and the core has a

crystalline structure [110]. Larger particles (50 nm-1 mm approximately) are found in some other commercial products, with nominal specific surface of 20-25 m^2/g [111]. Differences in size and shape also have an impact on nZVI reactivity and ageing [112].

nZVI has shown to possess some magnetic properties, although this properties largely vary on history(preparation method and storage), size, shape, chemicalcomposition, surface oxidation and dimension of the nanoparticles.In fact, magnetic properties result in the barenanoparticles forming chain like structure and resulting inagglomeration (Fig. 4.4.).
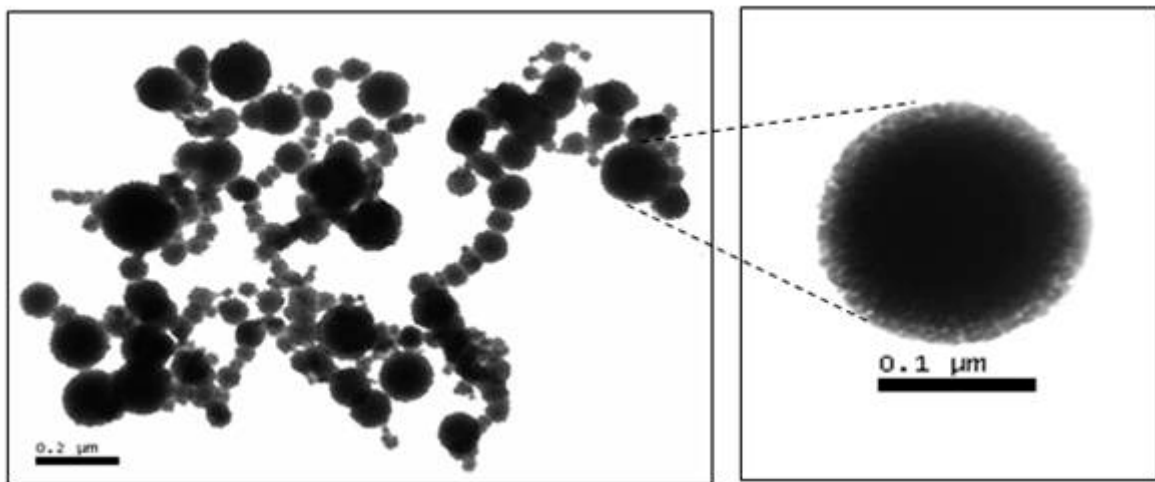
Fig. 4.4. Chain-like structure of nZVI agglomerates [113].

In spite of their effectiveness in the removal of contaminants, nZVI have weaknesses including a lack of stability, difficult separation from the medium being purified, rapid passivation of the material, and limited mobility of the particles due to the formationof agglomerates. To counteract the negatives accompanying the use of nZVI and to increase effectiveness, nZVI are being modified more and more frequently. The most frequent methods of modification of nZVI include admixtures of other metals to nZVI, coating the surfaceof nZVI, emulsification of nZVI, deposition of nZVI on a carrier, or trapping of nZVI in a matrix [114].

4.3. Mechanisms of water pollutants removal by nZVI

Over the past decades, extensive studies have demonstratedthat ZVI nanoparticles are effective for the treatment of manypollutants in water, including chlorinated and nitroaromatic organic compounds, phenol, dyes, arsenic, nitrate, heavy metals, etc. The reaction processes and pathways occurring at the iron surface are strongly influenced by a number of factors, namely the nZVI chemical properties and structure, the presence of more than one contaminant species, and, more in general, the hydrochemistry of the aqueous environment (pH, redox, natural dissolved species, etc.).

The oxidation reaction of metallic iron Fe^0 to dissolved aqueous ferrous iron Fe^{2+} has a standard reduction potential E^0 of 0.440 V, indicating that Fe^0 is a moderately strong reducing agent, capable of reducing a widerange of contaminants. The large surface area of nZVI allows quick release of the electrons. The thin and distorted oxide layer allows electron transfer from the metal directly through defects such as pits or pinholes, indirectly via the oxide conduction band, impurity or localized band, and from adsorbed or structural Fe^{2+}. On the other hand, this (hydr)oxide layer may act as an efficient adsorbent for various contaminants [105].

In aqueous media, nZVI is highly susceptible to corrosion, being oxidized to Fe^{2+} (fast process) and Fe^{3+} (slower process). In natural waters, the preferred oxidant is the dissolved oxygen, whose presence results in a rapid corrosion according to equation (4.6.). Fe^{2+} could be furthermore oxidated to Fe^{3+} by dissolved oxygen (Eq. 4.7) with the precipitation of the less soluble ferric hydroxides (rust). Moreover, corrosion could occur also under anaerobic conditions by using water as the oxidant (Eq. 4.8) and producing molecular hydrogen.

$$2Fe^0(s) + 4H^+(aq) + O_2(aq) \rightarrow 2Fe^{2+}(aq) + 2H_2O(l) \tag{4.6}$$

$$4Fe^{2+}(aq) + 4H^+(aq) + O_2(aq) \rightarrow 4Fe^{3+}(aq) + 2H_2O(l) \tag{4.7}$$

$$Fe^0(s) + 2H_2O(l) \rightarrow Fe^{2+}(aq) + H_2(g) + 2OH^- \tag{4.8}$$
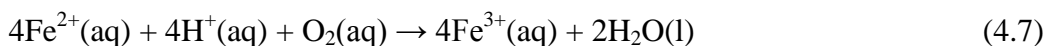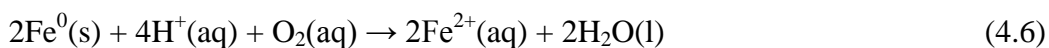
The products of corrosion in anaerobic conditions (Fe^{2+} and H_2) are also reducing agents and give contributions to the nZVI reactivity. On the other hand, it was generally anticipated that oxygen would result in a thicker layer of iron oxides with higher oxidation states and thereby, decreasing the reactivity of ZVI. However, the precipitated

amorphous and crystalline iron oxyhydroxides (Fe_3O_4, Fe_2O_3, $FeOOH$, $Fe(OH)_2$, $Fe(OH)_3$, etc.) in the vicinity of the ZVI surface are well known for their adsorptive properties of organic and inorganic contaminants. Iron oxide precipitation is a dynamic process and thus some contaminants will be adsorbed onto aged iron oxyhydroxides (adsorption), others will be adsorbed on to nascent iron oxyhydroxides and will be entrapped in their structure while aging (co-precipitation). Furthermore, local supersaturation of the inflowing water can cause contaminant precipitation.

In addition to the removal processes discussed above, oxidation of contaminants by the reactive oxygen species (including $^{\bullet}OH$, $O_2^{\bullet-}$) are possible in the $Fe^0/H_2O/O_2$ system [115]. The reactive oxygen substancescan be generated under acidic conditions through the two-electron oxidation of Fe^0 followed by the Fenton reaction [116, 117], as shown by Eqs. (4.9) and (4.10):

$$Fe^0 + O_2 + 2H^+ \rightarrow Fe^{2+} + H_2O_2 \qquad (4.9)$$

$$Fe^{2+} + H_2O_2 \rightarrow Fe^{3+} + {}^{\bullet}OH + OH^- \qquad (4.10)$$

The mechanisms of contaminants removal by nZVI are schematically illustrated in Fig. 4.5. Obviously, the corrosion of nZVI governs the rate of contaminants removal by nZVI. Consequently, the methods, which can accelerate ZVI corrosion, can enhance contaminant sequestration by nZVI.
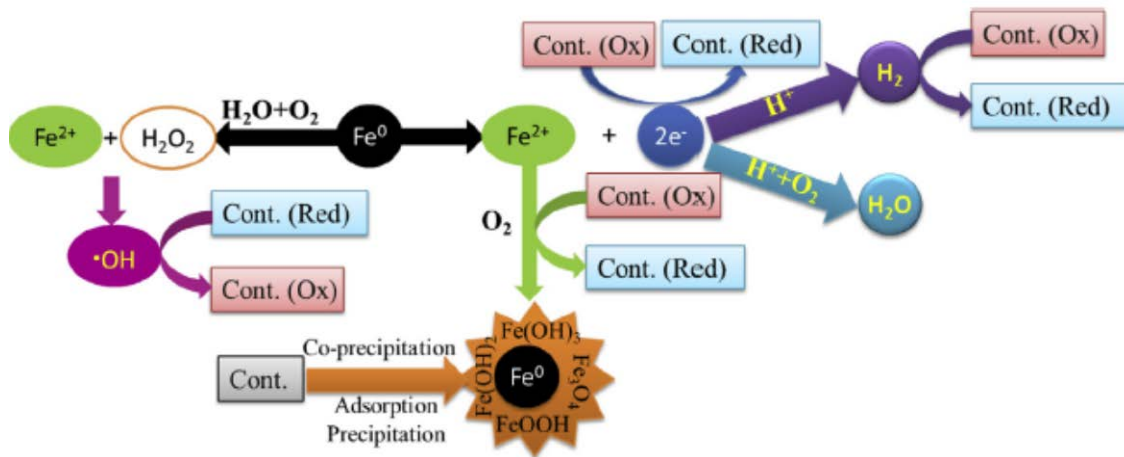
Fig. 4.5. Illustration of the major reactions occurred in the Fe^0/H_2O system and the mechanisms of contaminants (Cont.) removal [115].

The process of contaminants removal by nZVI usually involves the transfer of electrons between nZVI and the oxidizing species (O_2, H^+, and contaminants that can accept electrons). Due to the interfacial nature of the electron transfer, the process involves typically a series of steps, including the transport of the oxidizing species from the bulk solution to the nZVI surface, the reaction between nZVI and the oxidizing species, as well as the transport of products (Fe^{2+}, OH^-) away from the nZVI surface to the bulk solution (Fig. 4.6). If the rate constant of the reaction between nZVI and the oxidizing species is large, any reactant (O_2, H^+, and contaminants that can accept electrons) close to the nZVI surface is immediately consumed. Under this circumstance, the whole process will be controlled both by the continuous supply of O_2, H^+, the oxidized contaminants, and by the rapid escape of Fe^{2+} and OH^- from the Fe^0 surface. The concentration gradients will lead to molecular diffusion of the species (across the oxide film) toward or away from the nZVI surface [115].
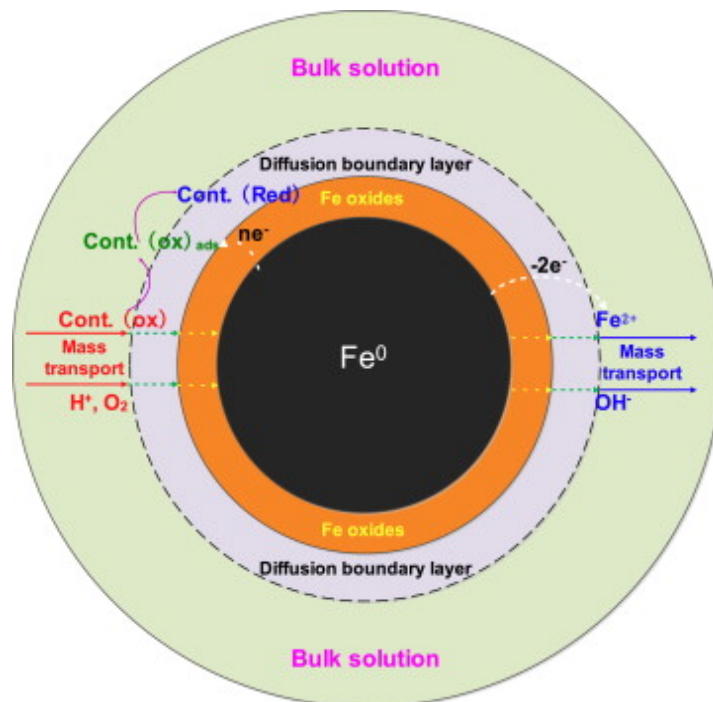
Fig. 4.6. Illustration of the process of contaminants (cont.) sequestration by ZVI [115].

The structure of the oxide film (e.g. composition, porosity, thickness, surface groups) and the nature of the contaminant (size, chemical nature, affinity to oxide film) can influence the resistance of the iron oxides film on mass transport of the solutes

towards or away from the nZVI surface. For example, the process of aging of oxyhydroxides is usually accompanied by dehydration and conversion to a less porous structure. Therefore, the passive layer on the surface of pristine nZVI particles, as well as the deposition of Fe^{2+}/Fe^{3+} (oxy)hydroxideson nZVI surface in the process of contaminants removal by nZVI, can act as a diffusion barrier for Fe^{2+}, O_2, H^+ and the oxidized contaminants and thus can result in a drop in the corrosion rate. In addition, the diffusion boundary layer (Fig. 4.6.) plays an important role in the mass transfer and consequently in the process of contaminants removal by nZVI.

The specific removal mechanisms involved in the nZVI-treatment of water polluted by heavy metals depend on the standard redox potential (E^0) of the metal contaminant. Metals that have an E^0 that is more negative than, or similar to, that of Fe^0 (e.g. Cd and Zn) are removed purely by adsorption to the iron (hydr)oxide shell. Metals with E^0 much more positive than Fe^0 (e.g. Cr, As, Cu, U, and Se) are preferentially removed by reduction and subsequent precipitation or co-precipitation. Metals with slightly more positive E^0 than Fe^0 (e.g. Pb and Ni) can be removed by both reduction and adsorption [105].

The metal-nZVI interactions for various metals can be categorized as:
- Reduction: Cr, As, Cu, U, Pb, Ni, Se, Co, Pd, Pt,Hg, Ag
- Adsorption: Cr, As, U, Pb, Ni, Se, Co, Cd, Zn, Ba
- Oxidation/reoxidation: As, U, Se, Pb
- Co-precipitation: Cr, As, Ni, Se
- Precipitation: Cu, Pb, Cd, Co, Zn

As it can be seen, most metals can react with nZVI by more than one mechanism. For example, the carcinogenic, soluble and mobile Cr(VI) may be reduced to less toxic Cr(III) by nZVI and immobilized by precipitation as $Cr(OH)_3$ (Eq. 4.11) or by incorporation into the iron (hydr)oxide shell forming alloy-like Cr^{3+}–Fe^{3+} hydroxides (Eqs. 4.12 and 4.13). Cr (VI) can also be directly adsorbed on the surface of nZVI (Eq. 4.14).

➢ Reduction Cr (VI) to Cr (III):

$$3Fe^0 + Cr_2O_7^{2-} + 7H_2O \rightarrow 3Fe^{2+} + 2Cr(OH)_3 + 8OH^- \qquad (4.11)$$

➤ Co-precipitation:

$$xCr^{3+} + (1-x)Fe^{3+} + 3H_2O \rightarrow Cr_xFe_{(1-x)}(OH)_3 + 3H^+ \qquad (4.12)$$

$$xCr^{3+} + (1-x)Fe^{3+} + 2H_2O \rightarrow Cr_xFe_{(1-x)}OOH + 3H^+ \qquad (4.13)$$

➤ Adsorption Cr (VI):

$$nZVI\text{-}FeOH + CrO_4^{2-} \rightarrow nZVI\text{-}Fe\text{-}CrO_4^- + OH^- \qquad (4.14)$$
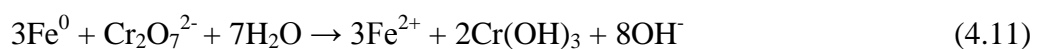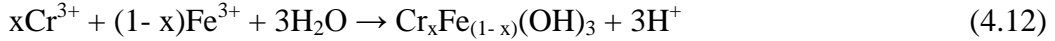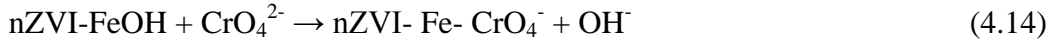
The formation of mixed Cr^{3+}–Fe^{3+} hydroxides on the oxidized nZVI surface layer may inhibit further electron transfer from the Fe^0 core to Cr(VI) at later reaction times, favoring adsorption of Cr(VI) on the nZVI surface, especially at high Cr(VI) concentrations.

On the other hand, cadmium ($E^0 = -0.40$ V) has a standard potential very close to that of nZVI, thus the likelihood of Cd(II) being reduced to Cd(0) on nZVI is low. Therefore, the adsorption or surface complex formation on the surface ferri oxyhydroxide layer is the most likely mechanism of cadmium removal by nZVI [118].

The surface reactions of cadmium removal by nZVI may be described by the following equations:

$$FeO^- + Cd^{2+} \rightarrow FeOCd^+ \qquad (4.15)$$

$$FeOH + Cd^{2+} + H_2O \rightarrow FeOCdOH + 2H^+ \qquad (4.16)$$

4.4. Synthesis of supported nZVI

Similar to other nanoscale materials, nZVI has a strong tendency to agglomerate into larger particles resulting in diminishing reactivity in application conditions. Difficulty in preparing stable, well-dispersed aqueous nZVI suspensions has remained an obstacle that hinders practical applications of nZVI in various environmental systems. Another problem related to its small size is the difficult separation of nano iron from the purified matrix. The remaining nZVI in the treatment system makes the technology uneconomical and even generates secondary iron pollution.

Several strategies have been explored to overcome these disadvantages, including coating the nanoparticle surface with polyelectrolytes or nonionic surfactants and conjugating with a solid support, like activated carbon [119], zeolite [120], resin

[121], chitosan/silica [122], polyelectrolyte multilayers [123], clays [124], starch and carboxymethyl cellulose [125]. Apart from immobilizing nZVI, the support can affect its physicochemical properties. The immobilizationof nZVI by above-mentioned carriers can be achieved through the fixing of nZVI on their surface or trapping inside their pores. Ex situ and in situ methods of synthesis have been applied, while the in situ methods gain popularity for their technological advantages over the ex situ methods [126].

Natural minerals as abundant resources are suitable supporting materials because of the cheapness, availability, environmental stability, and high surface area.Various natural minerals, including montmorillonite [127], bentonite [128], kaolinite [129, 130], zeolite [131], palygorskite [132] and sepiolite [133, 134], have been used for the preparation of composite adsorbents with nZVI for the removal of different pollutants from water. It was shown that nZVI is more effective in Cr(VI) removal from aqueous solutions when bentonite had been introduced as a support material due to reduction of aggregation and increasing of specific surface area [128]. Similarly, in the case of montmorillonite as a support, the dispersibility of nZVI was found to be increased with decreasing tendency to agglomerate into larger particles, which provided good adsorption properties for As(III) and As(V) [127]. The presence of kaolinite during the nZVI synthesis provided higher uptake capacities toward Cu^{2+}, Co^{2+}, Ni^{2+} and Pb^{2+} ions than in the case of pure kaolinite [129, 130]. Zeolite is also an effective dispersant and stabilizer of nZVI, and the composite was superior to pure zeolite in removing Pb(II) from the aqueous solutions [131]. The presence of zero-valent iron nanoparticles on the surface of fibrous palygorskite mineral strongly increased the decolourization capacity for methylene blue in comparison to pure nZVI and palygorskite [132].

Recently, sepiolite has also been used for nZVI stabilization in order to enhance the efficiency of Cr(VI) removal from water [133]. The composite was synthesized using borohydride reduction method at a ratio sepiolite/Fe^{2+} ~ 2.8:1. Batch experiments showed that the removal efficiency of the composite was higher than of bare nZVI. The acidic and neutral pH values were appropriate for Cr(VI) removal. The enhancement was observed in Cr(VI) removal by increasing concentration of chloride, as one of the most common ions in groundwater. Sepiolite was proven as an efficient and cost-

effective stabilizer to enhance the colloidal stability of nZVI as well as to increase their reactivity with contaminants.

Moreover, nZVI has been stabilized by using an acid activated sepiolite [134] and the obtained composite with a sepiolite/iron mass ratio of 9:1 was used for the removal of Cr(VI) and Pb^{2+} ions from water. The removal mechanism was proposed as a two-step interaction including both the physical adsorption of Cr(VI) and Pb(II) on the surface or inner layers of the sepiolite-supported nZVI particles and the subsequent reduction of Cr(VI) to Cr(III) and Pb(II) to Pb(0) by nZVI. The removal efficiency of Cr(VI) and Pb(II) by S-nZVI was not affected to any considerable extent by the presence of co-existing ions, such as $H_2PO_4^-$, SiO_3^{2-}, Ca^{2+} and HCO_3^-. The results suggested that supporting nZVI on sepiolite had the potential to become a promising technique for in situ heavy metal-contaminated groundwater remediation.

EXPERIMENTAL PART

5. Experimental procedure

5.1. Materials and chemicals

The natural sepiolite used in the experiments (SEP) was obtained from Andrići (Serbia). The fraction < 250 μm was used in the experiments. The acid-activated sample (AAS) was prepared according to a previous study [11]: 10 g of sepiolite was stirred with 100 cm^3 of 4 mol/dm^3 HCl solution for 10 h, at room temperature. The solid was separated from liquid by vacuum filtration and washed with distilled water until Cl$^-$ ion free. The obtained sample was dried at 110 °C for 2 h. The physico-chemical properties of the sepiolite samples were reported previously [11].

All chemical reagents used in this work, FeSO$_4$·7H$_2$O, NaBH$_4$, absolute ethanol, HNO$_3$, NaCl, HCl, NaOH, H$_2$O$_2$, Cd(NO$_3$)$_2$·4H$_2$O, K$_2$Cr$_2$O$_7$ and dye C.I. Reactive Orange 16 were of analytical grade. The Cd^{2+}, Cr(VI) and dye solutions were prepared by dissolving Cd(NO$_3$)$_2$·4H$_2$O, K$_2$Cr$_2$O$_7$ and C.I. Reactive Orange 16, respectively, in deionized water (Millipore Milli-Q 18 MΩ).

5.2. Synthesis of SEP/AAS supported and pure nZVI

The pure nano zero-valent iron, nZVI, was synthesized using the conventional chemical reduction procedure [126]. In brief, 100 cm^3 of 1 mol/dm^3 NaBH$_4$ solution, prepared in degassed water, was added drop by drop to a magnetically stirred solution of 5 g of FeSO$_4$ .7H$_2$O in 500 cm^3 of a mixture of ethanol and water (v/v = 1:4), at ambient temperature, under a N$_2$ atmosphere. The mixed liquid was used in order to decrease the nZVI oxidation [90, 135]. After complete addition of the NaBH$_4$ solution, the mixture was left under stirring for 20 min. The reduction of ferrous ions (Fe^{2+}) by NaBH$_4$ is represented by Eq. (4.2). The black precipitate (*i.e.* nZVI) was separated from the liquid phase via vacuum filtration and washed three times with pure ethanol, under a N$_2$ atmosphere. The nZVI was dried under vacuum for 12 h at 60 °C.

In order to synthesize SEP/AAS supported nZVI, a suspension of 5 g of SEP or AAS in 500 cm^3 of ethanol/water solution mixture (1:4 v/v) was first ultrasonicated for

10 min, using a Sonics ultrasonic processor of 750W output with a 20 kHz converter and a solid titanium probe of 19 mm diameter to provide de-aggregation of the SEP/AAS. The pH of the suspension was adjusted to 4 by the addition of 0.1 mol/dm^3 HNO$_3$ solution and then 2.5, 5.0, 10.0 or 12.5 g of FeSO$_4$·7H$_2$O was added (the SEP/AAS:Fe mass ratio was 10:1, 5:1, 2.5:1 or 2:1, respectively) in order to prepare samples with different nZVI loads. The ultrasonic treatment was repeated for a further 10 min. The suspension was transferred to a flask and stirred for 30 min under a nitrogen flow, followed by the dropwise addition of 100 cm^3 of a freshly prepared 0.5 or 1.0 or 2.0 or 2.5 mol/dm^3 solution of NaBH$_4$, respectively, depending on the quantity of FeSO$_4$·7H$_2$O. Molar ratio NaBH$_4$:Fe^{2+} was approximately 5:1, which is much higher than the stechiometric ratio (Eq. (4.2.)) in order to speed up the synthesis reaction and to provide the uniform growth of nZVNI particles. The suspension was left in the flask with stirring under a nitrogen atmosphere for 15 min. As in the case of pure nZVI, the solid material was separated from the liquid phase via vacuum filtration, washed three times with pure ethanol, under a N$_2$ atmosphere, and dried under vacuum for 12 h at 60 °C.

In order to investigate the influence of the duration of the ultrasonic treatment on the nZVI dispersibility and the composite properties, the samples with mass ratio SEP/AAS:Fe = 2.5:1 were also prepared with prolonged ultrasound treatment of the sepiolite suspension (30 min).

The experimental conditions of the composites preparation are systematized in Table 5.1.

Table 5.1. The experimental conditions of the composites preparation

Sample	Support (m = 5 g)	$m(FeSO_4 \cdot 7H_2O)$ (g)	$c(NaBH_4)$ (mol/dm^3) (V = 100 cm^3)	Mass ratio support/Fe^{2+}
SEP–nZVI(10:1)	SEP	2.5	0.5	10:1
AAS-nZVI(10:1)	AAS	2.5	0.5	10:1
SEP–nZVI(5:1)	SEP	5.0	1.0	5:1
AAS-nZVI(5:1)	AAS	5.0	1.0	5:1
SEP–nZVI(2.5:1)	SEP	10.0	2.0	2.5:1
AAS-nZVI(2.5:1)	AAS	10.0	2.0	2.5:1
SEP–nZVI(2.5:1)*	SEP	10.0	2.0	2.5:1
AAS-nZVI(2.5:1)*	AAS	10.0	2.0	2.5:1
SEP–nZVI(2:1)	SEP	12.5	2.5	2:1
AAS-nZVI(2:1)	AAS	12.5	2.5	2:1

*Samples synthesized with the prolonged ultrasound treatment of the sepiolite suspension (30 min instead of 10 min for the other samples)

5.3. Characterization and measurement

5.3.1. XRD analysis

The diffraction patterns of the samples were determined using a conventional powder diffractometer (Ital Structures APD 2000) with Bragg–Brentano geometry and CuKα1,2 radiation (Ni filter). The XRD plots were recorded at room temperature in the 2θ range 4–60° with a 0.02^o 2θ step and 2 s counting time per data point. A 1/2° source slit and 0.1 mm receiving slit were used.

5.3.2. FTIR spectroscopy

The FTIR analysis was performed on a MB BOMAN HARTMANN 100 instrument in the wave number range from 4000 to 400 cm^{-1}. The samples were prepared by the KBr disc method, at a sample to KBr mass ratio of 1:150.

5.3.3. Thermal analysis

The differential-thermal and thermo-gravimetric analyses were conducted on an SDT Q600 TGA/DSC instrument (TA Instruments), at a heating rate of 20 °C/min, in a flow of either air or nitrogen, at a flow rate of 100 cm^3/min. The sample mass was less than 10 mg.

5.3.4. Scanning and transmission electron microscopy (SEM and TEM)

The morphological analysis of the samples was performed using a Tescan MIRA3 field emission gun scanning electron microscope (FESEM), with electron energies of 20 kV under high vacuum. The samples were sputter-coated with an Au–Pd alloy to ensure conductivity.

The TEM analysis of some samples was performed on a JEOL T-100 instrument. The samples were ultrasonically dispersed in ethanol to form a dilute suspension. A drop of the suspension was applied onto a holy carbon film supported by a copper-mesh TEM grid and air-dried at room temperature.

5.3.5. Textural properties

The N_2 adsorption–desorption isotherms were measured at -196 °C on a Micrometrics ASAP 2020 instrument. Before the measurements, the samples were out-gassed at 150 °C for 10 h under reduced pressure (<1 torr). The specific surface area (S_{BET}) was calculated according to the Brunauer, Emmett, Teller (BET) method from the linear part of the nitrogen adsorption isotherm [136]. The total pore volume (V_{total}) was given at $p/p_0 = 0.998$. The volume of the mesopores ($V_{mesopore}$) and the mesopore size distribution were analyzed according to the Barrett, Joyner and Halenda method from the desorption isotherms [137]. The volume of the micropores ($V_{micropore}$) was calculated according to α-plot analysis [138].

5.3.6. Point of zero charge

The point of zero charge, pH_{pzc}, of the samples was determined by a batch equilibration technique [139]. The three sets of measurements included samples with 20 cm^3 of NaCl solution (concentration 0.1 mol/dm^3 in one set, 0.01 mol/dm^3 in the second set and 0.001 mol/dm^3 in the third set) in PVC vessels. The initial pH values (pH_i), in the pH range from 2 to 8, were adjusted by the addition of a 0.1 mol/dm^3 solution of HCl or NaOH to the electrolyte solutions. Then, 0.020 g of the sample was added to each vessel. Equilibration was realized by shaking in a thermostatic bath for 24 h at 25 °C. The dispersions were then filtered and the final pH of the solutions (pH_f) was measured. The point of zero charge was determined as a pH value of the plateau on the pH_f *vs*. pH_i dependence.

5.3.7. X-Ray photoelectron spectroscopy (XPS)

The XPS analyses of the sample SEP–nZVI(2.5:1), before and after exposure to Cd^{2+} ions were realized using a PHI-TFA XPS spectrometer exciting a sample surface with X-ray radiation from an Al monochromatic anode. The samples were in the form of 1mm-thick pressed pellets. The analyzed area was 0.4 mm in diameter and the analyzed depth was 3–5 nm. The XPS survey and narrow scan spectra of the emitted photoelectrons were taken with 187 and 23 eV, respectively. In order to follow the distribution of the elements in the subsurface region, XPS depth profiling was performed by alternating cycles of ion sputtering to remove surface layers and acquisition of photoelectron spectra. The ion sputtering was performed with 1 keV Ar^+ beam rastering over a $3 \cdot 3$ mm^2 area. In this way, the depth distributions of the elements were obtained. The total sputtering time was 20 min with a sputtering rate of 2 nm/min, measured on a Ni/Cr reference multilayer structure. The base pressure in the XPS analysis chamber was $3 \cdot 10^{-9}$ mbar when the samples were loaded, whereas during the sputtering with Ar^+ ions the pressure in the analysis chamber was $3 \cdot 10^{-8}$ mbar. The binding energy 284.8 eV for the C 1s peak (characteristic for C–C bonds) was used as the reference energy for spectra alignment. The relative sensitivity factors (RSF), provided by the instrument producer, was used to calculate the concentrations.

5.4. Adsorption experiments

5.4.1. The adsorption of Cd^{2+} and Cr(VI)

The Cd^{2+} and Cr(VI) solutions were prepared by dissolving Cd(NO$_3$)$_2 \cdot$4H$_2$O and K$_2$Cr$_2$O$_7$, respectively, in deionized water (Millipore Milli-Q 18 MΩ).

The batch technique was used for the adsorption experiments. The adsorbents and ion solutions were equilibrated in a thermostated water bath with shaker. The initial pH value (pH$_i$) of the solutions was adjusted by using HNO$_3$ or KOH solutions. The adsorption of Cd^{2+} ions was investigated at initial pH$_i$ = 7.0 ± 0.1, while the adsorption of Cr(VI) investigated at pH$_i$ = 2.0 ± 0.1 and pH$_i$ = 3.0 ± 0.1. After equilibration, the adsorbents were separated from the solutions and the pH values of the solutions were determined using a pH meter (Ino Lab WTW series pH 720). The initial concentrations of Cd^{2+} and Cr(VI), as well as the concentrations after the adsorption, were determined using the atomic absorption spectrometer (AAS) (Perkin Elmer 730). All the adsorption experiments were repeated twice; the reported values are the average of two measurements.

The amount of cadmium or chromium adsorbed per unit mass of an adsorbent at equilibrium, q_e (mg/g), was calculated using the equation:

$$q_e = \frac{c_i - c_e}{m} V \qquad (5.1)$$

where: c_i and c_e are the initial and the equilibrium concentrations (mg/dm^3), m is the mass of an adsorbent (g), and V is the volume of a solution (dm^3).

The adsorption of Cd^{2+} ions was investigated first at different rations adsorbent/solution (S/L). For S/L = 0.02 g/20 cm^3, an initial concentration of Cd^{2+} ions was c_i = 130 mg/dm^3, while for S/L = 0.02 g/100 cm^3, an initial concentration of Cd^{2+} ions was c_i = 34.0 mg/dm^3. The dispersions were equilibrated at 25 ± 1 °C for 24 h.

The adsorption isotherms were determined at 25 °C for the pure compounds and the composites with the ratio nZVI:SEP/AAS = 2.5:1, at S/L = 0.02 g/100 cm^3. In addition, the adsorption isotherm for the composite Fe(III)-sepiolite, synthesized

previously [12], was determined at the same initial pH value and temperature, at a ratio S/L = 0.04 g/20 cm^3.

The adsorption isotherms for the composites with the ratio nZVI:SEP/AAS = 2.5:1 were also determined at temperatures 40 and 50 °C in order to investigate the influence of temperature on the Cd^{2+} adsorption.

The influence of contact time on the Cd^{2+} adsorption at 25 °C was investigated for the samples SEP-nZVI(2.5:1) and AAS-nZVI(2.5:1), at a ratio S/L = 0.02 g/100 cm^3 and initial concentration of 100 mg/dm^3. The quantity of Cd^{2+} ions adsorbed after contact time (t) of 0.5, 1, 2, 4, 8, 16 and 24 h (q_t) was calculated according to equation:

$$q_t = \frac{c_o - c_t}{m} V \tag{5.2}$$

where: c_t is the concentration of Cd^{2+} after contact time t.

The Cr(VI) adsorption was investigated at different initial concentrations in order to determine adsorption isotherms and compare the maximal adsorption capacities of the composite synthesized with different ration SEP/AAS:nZVI, at initial pH 2.0 ± 0.1 and 3.0 ± 0.1.

5.4.2. The removal of dye C.I. Reactive Orange 16

The removal of anionic dye C.I. Reactive Orange 16 was analyzed by using the solution of concentration 74.0 mg/dm^3, with no pH adjustment (pH$_i$ of the solution was ~ 5.8). The solid/liquid ratio was 0.02 g/20 cm^3. The experiments were performed in two ways: 1) with H$_2$O$_2$ at concentration 4, 8 or 12 mM and 2) without H$_2$O$_2$. The suspensions of the composites and dye solution with or without H$_2$O$_2$ were equilibrated in a thermostated water bath with shaker for 24 h at 25 ± 1 °C. Following this, the solutions were centrifuged and the residual dye concentration and the pH$_f$ were determined.

The influence of temperature on the process of dye removal without H$_2$O$_2$ was investigated at different initial concentrations, at pH$_i$ = 5.0 ± 0.1, for the samples SEP-nZVI(2.5:1) and AAS-nZVI(2.5:1). After centrifugation, the dye concentration and pH$_f$ values were determined. The dye concentration was determined according to

absorbance measurements at 493 nm, using a UV/Vis spectrophotometer Shimadzu UV-1800 instrument. The amount of dye removed per unit mass of the adsorbent, q_e (mg/g), was calculated using the Eq. (5.1).

6. Results and discussion

6.1. Samples characterization

6.1.1. XRD analysis

The XRD patterns of nZVI, SEP, AAS and the SEP/AAS–nZVI composites are shown in Fig. 6.1. In the pattern for the pure nZVI, the characteristic peak for Fe^0 at 2θ = 44.6 ^{o} is broad and of the very low intensity, indicating poor crystallinity. In fact, when the crystallites are smaller than 5 nm, the diffraction peaks are significantly broadened and the intensities are very low [140]. In the case of composites with SEP (Fig. 6.1a), the diffraction peak characteristic for Fe^0 is hardly noticeable, indicating an almost amorphous phase of iron, i.e. the presence of very small crystallites, smaller than in pure nZVI. On the other hand, in the patterns for the AAS–nZVI composites (Fig. 6.1b), the characteristic peak at $2\theta = 44.6$ ^{o} increased with increasing nZVI quantity: the peak is invisible in the pattern of AAS–nZVI(10:1) composite, while in the case of AAS–nZVI(2.5:1) and AAS–nZVI(2:1) composites, this peak is even more intensive than for pure nZVI. For the sample AAS-nZVI(2.5:1)*, obtained with the prolonged ultrasound treatment of the sepiolite suspension, the XRD pattern indicates much smaller crystallites then in the sample AAS–nZVI(2.5:1).

The signals of iron oxides (hematite, Fe_2O_3, or magnetite, Fe_3O_4) were detected neither in the XRD patterns of the composites nor in that of pure nZVI, which indicates that iron was present mainly in its zero-valent state or that the iron-oxide compounds, if present, were amorphous.

The intensities of SEP/AAS diffraction peaks gradually decreased as the quantity of the nZVI in the composites increased. This is due to the decreasing quantity of SEP/AAS and the increased background noise from the fluoresced X-rays induced by the presence of iron.
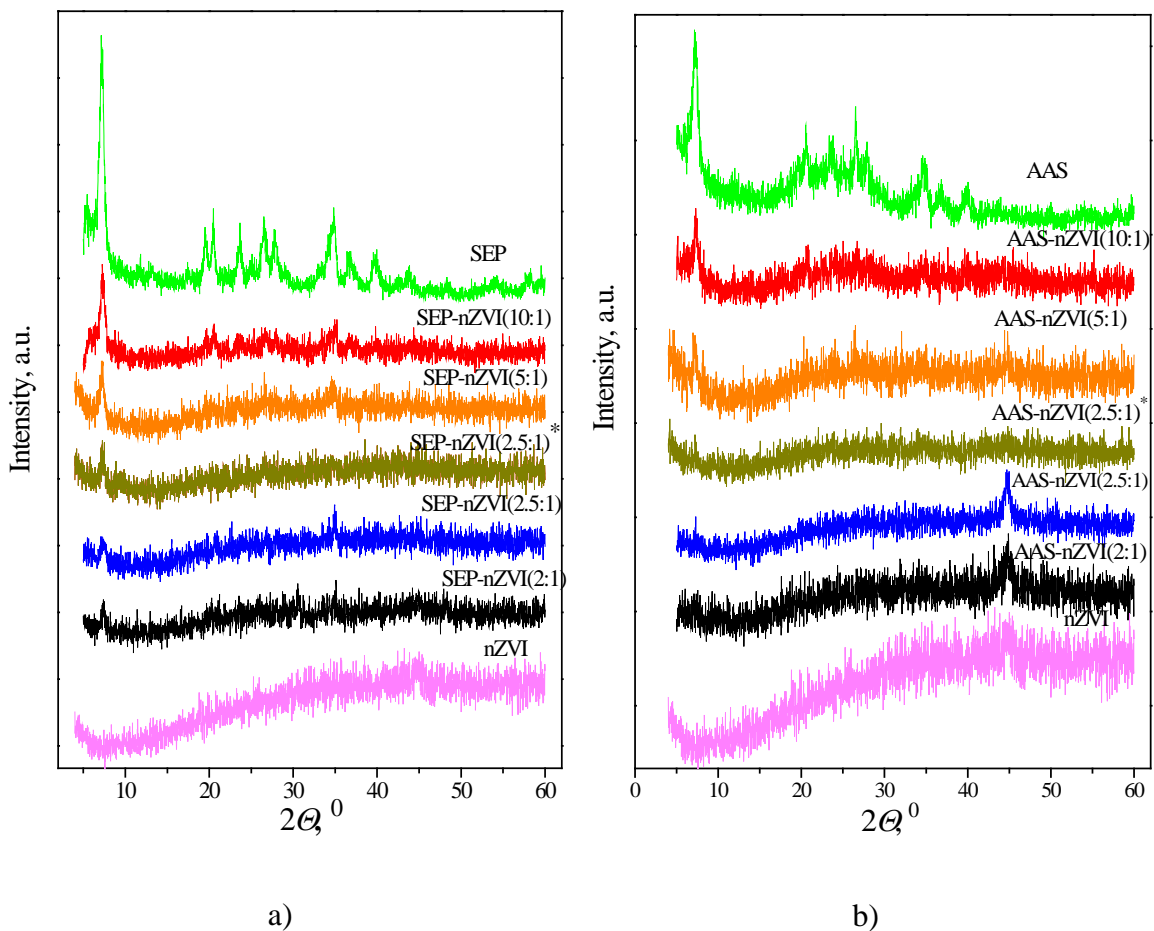
Fig. 6.1. XRD patterns of the pure compounds and composites with: a) sepiolite, b) acid-activated sepiolite.

6.1.2. FTIR spectroscopy

The FTIR spectra of the SEP/AAS-nZVI composites (Fig. 6.2) are similar and display the characteristic absorption bands of sepiolite (Table 6.1) and nZVI.
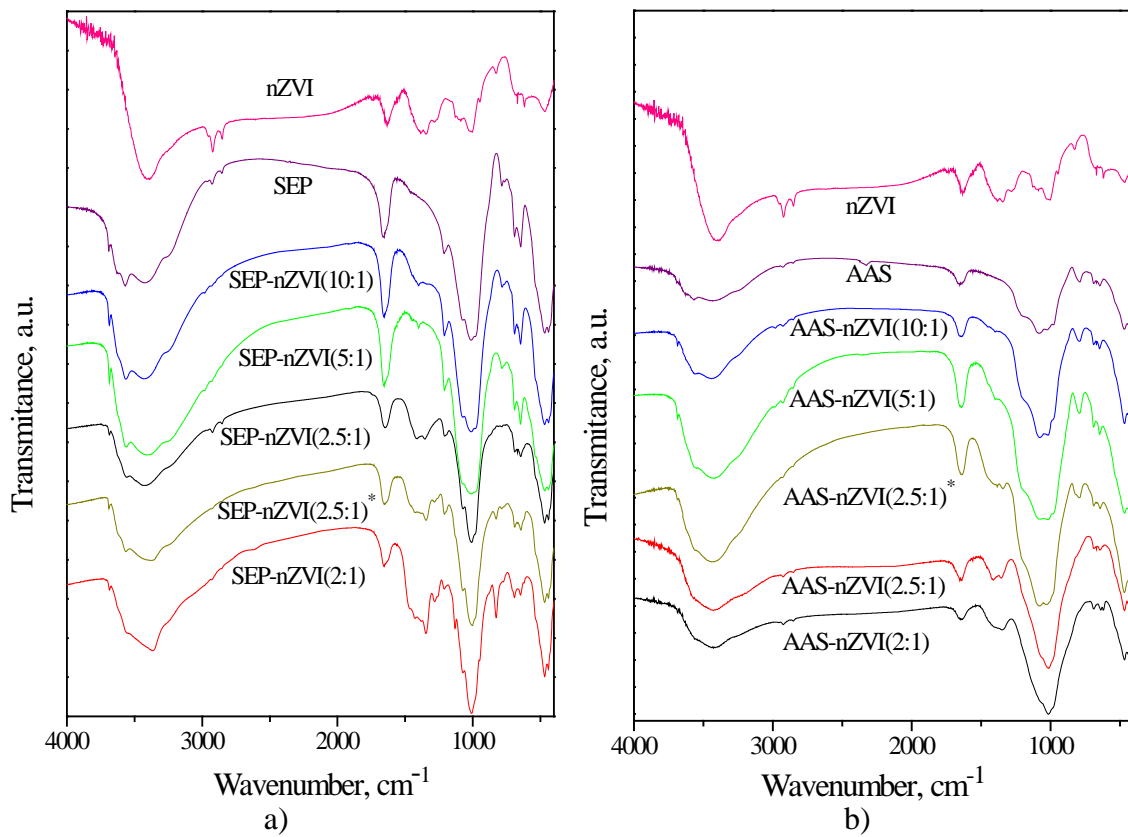
Fig. 6.2. FTIR spectra of the pure compounds and composites with: a) sepiolite, b) acid-activated sepiolite.

Table 6.1. Characteristics bands of sepiolite [11]

Band position (cm^{-1})	Assignments
3690	stretching vibrations of OH group attached to the octahedral Mg^{2+} ion
3568	stretching vibrations of OH group from coordinated water
3420	stretching vibrations of OH group from zeolitic and adsorbed water
1671	bending vibrations of OH group from coordinated, zeolitic and adsorbed water
1016	stretching vibrations of Si-O in the Si-O-Si groups of the tetrahedral sheet
690	bending vibration of OH group attached to the octahedral Mg^{2+} ion
460	Si-O-Si bending vibrations
437	Si–O–Mg bending vibration

The broad band in the FTIR spectra of the composites in the 1200–400 cm^{-1} range encompasses bonds characteristic of silicate structure of sepiolite and the bands characteristic for the nZVI. The bands characteristic for the nZVI correspond to Fe-O vibration, indicating a partial surface oxidation of nZVI. The broad absorption band at ~ 1390 cm^{-1}, absent in the spectrum of sepiolite, could be also correlated with the presence of oxidation products [141], as the intensity of this band increased as the nZVI quantity in the composites increased. The intensity of this band was lower in the spectra of the AAS-composites, which could be an indicator of a smaller quantity of iron oxides in the AAS-NZVI than in the SEP-nZVI composites. However, the band at ~ 1390 cm^{-1} could also be assigned to the borate species produced during the synthesis and can not be used with certainty as a confirmation of the presence of iron oxides in the composites.

Besides bands characteristic for the nZVI and sepiolite structures, all spectra show bands at ~2920 and ~2850 cm^{-1}, indicating the presence of C-H bonds [47, 142]. In the case of nZVI, these peaks can be assigned to ethanol used during synthesis, while in the case of SEP to the organic impurities. The intensities of the peaks are lower in spectra of AAS, owing to the removal of organic impurities during acid activation. The intensities of these peaks in the composites vary depending on the SEP/AAS:nZVI ratio.

6.1.3. SEM and TEM analysis

Scanning electron micrographs (SEM) of the pure compounds and the SEP/AAS-nZVI composites are shown in Figs. 6.3 – 6.6.

The SEM micrographs of the SEP and AAS (Figs. 6.3a and 6.3b, respectively) show that sepiolite particles exhibit a characteristic fibrous morphology, but they are rarely isolated and form aggregates of close packet fibers, as usual. Acid-activation did not cause de-aggregation and disintegration of the fibers bundles into smaller entities (Fig. 6.3b), but fibers were shorter. The SEM micrograph of the nZVI (Fig. 6.3c) shows highly aggregated spherical particles, with sizes between 100 and 200 nm, which form necklace-like aggregates. This type of aggregation is attributed to magnetic interactions between the Fe^0 particles [143]. As already stated, aggregation causes a decrease in the

specific surface area and the reactivity of nZVI, which explains why nZVI is usually immobilized on different support materials.

a)

b)

c)
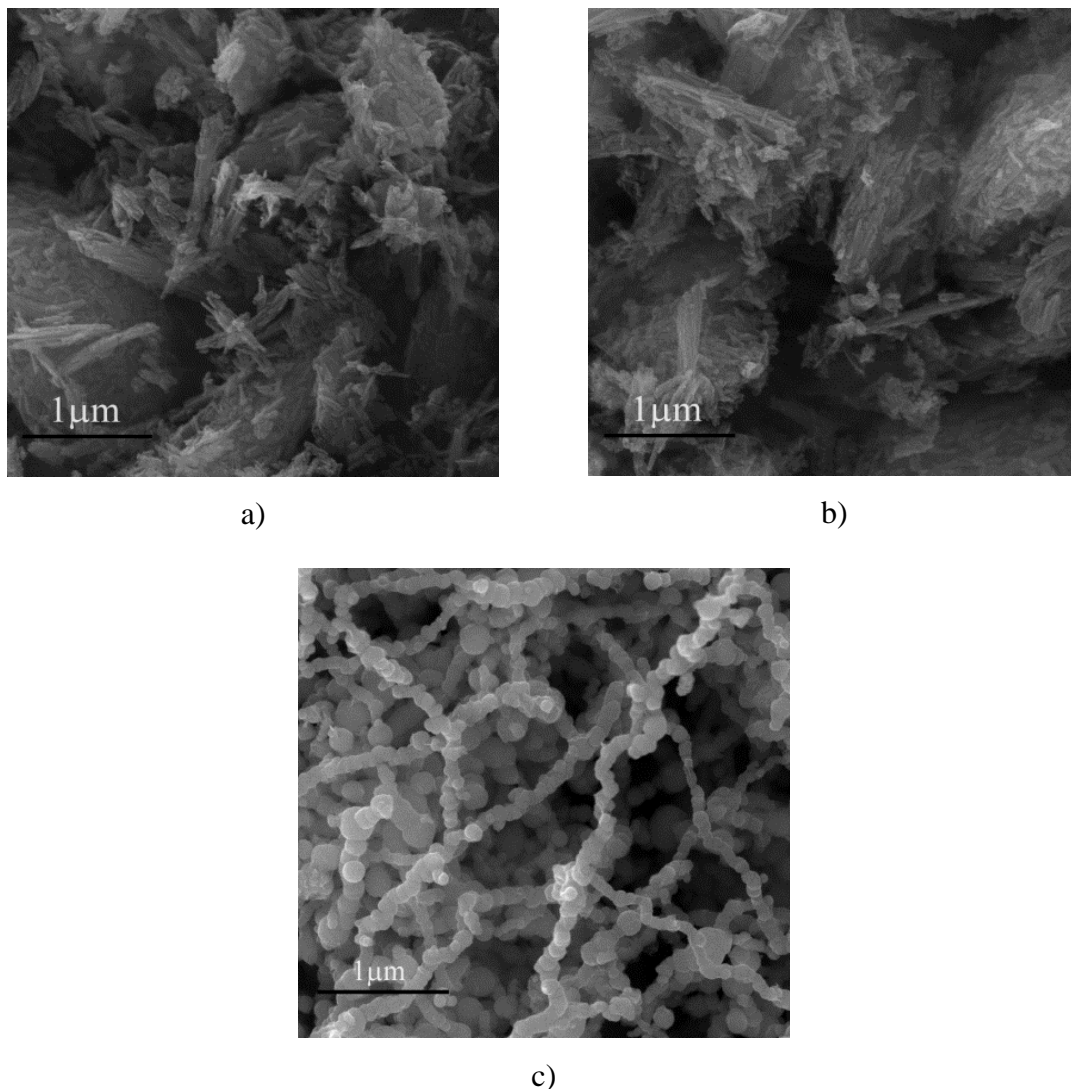
Fig. 6.3. SEM micrograph of: a) SEP, b) AAS, c) nZVI.

When using SEP as the support, with the ultrasound treatment of the SEP suspension during 10 min (Fig. 6.4), the nZVI particles were uniformly distributed throughout the sepiolite matrix in the composites without noticeable aggregation, except in the sample SEP–nZVI(2:1) with the highest content of nZVI (Fig. 6.4d). Obviously, in order to reach a good dispersibility of nZVI particles, the SEP/nZVI mass ratio

should not be lower than 2.5:1. The size of nZVI particles in the SEP–nZVI composites was mainly smaller than 100 nm, i.e. smaller than of pure nZVI (Fig. 6.3c). It could be noticed that, in comparison to pure sepiolite, the fibers in the composites were more separated, as a result of application of an ultrasound probe during the synthesis of the composites.

a) SEP–nZVI(10:1) b) SEP–nZVI(5:1)

c) SEP–nZVI(2.5:1) d) SEP–nZVI(2:1)
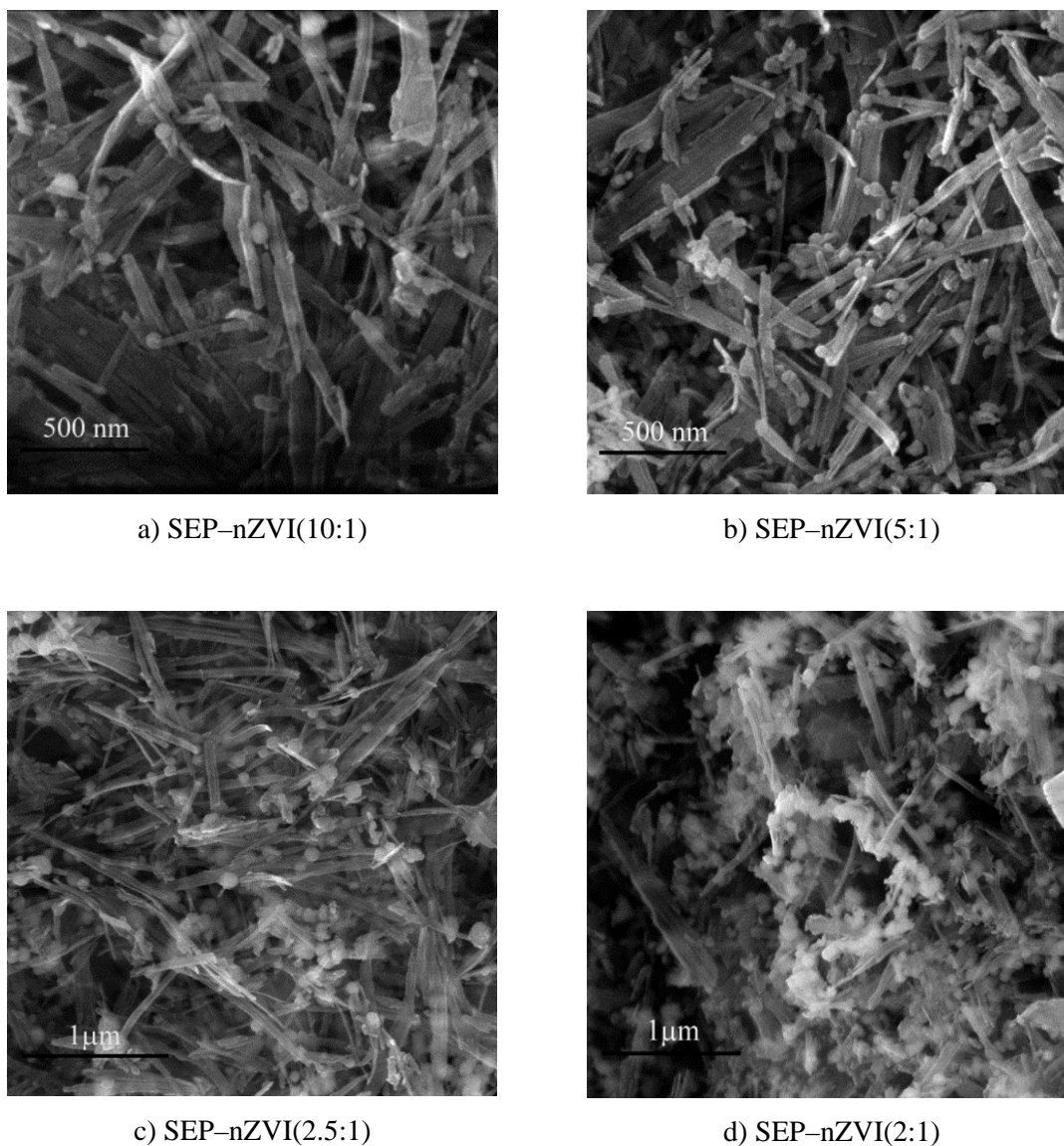
Fig. 6.4. SEM micrographs of the SEP-nZVI composites.

Contrary to expectations, the dispersibility of nZVI was not increased by using AAS as the support (Fig. 6.5). Obviously, the fiber bundles of AAS (Fig. 6.3b) could

not have been destroyed by ultrasound treatment, indicating stronger interfibers bonds than in SEP. Relatively good dispersibility of nZVI on AAS was achieved only with the highest AAS/nZVI ratio (sample AAS–nZVI(10:1)). With decreasing AAS/nZVI ratio, the nZVI particles started to aggregate and at the ratios 2.5:1 and 2:1 (Fig. 6.5c and d), the aggregates were similar to those of pure nZVI.

a) AAS–nZVI(10:1)

b) AAS–nZVI(5:1)

c) AAS–nZVI(2.5:1)

d) AAS–nZVI(2:1)
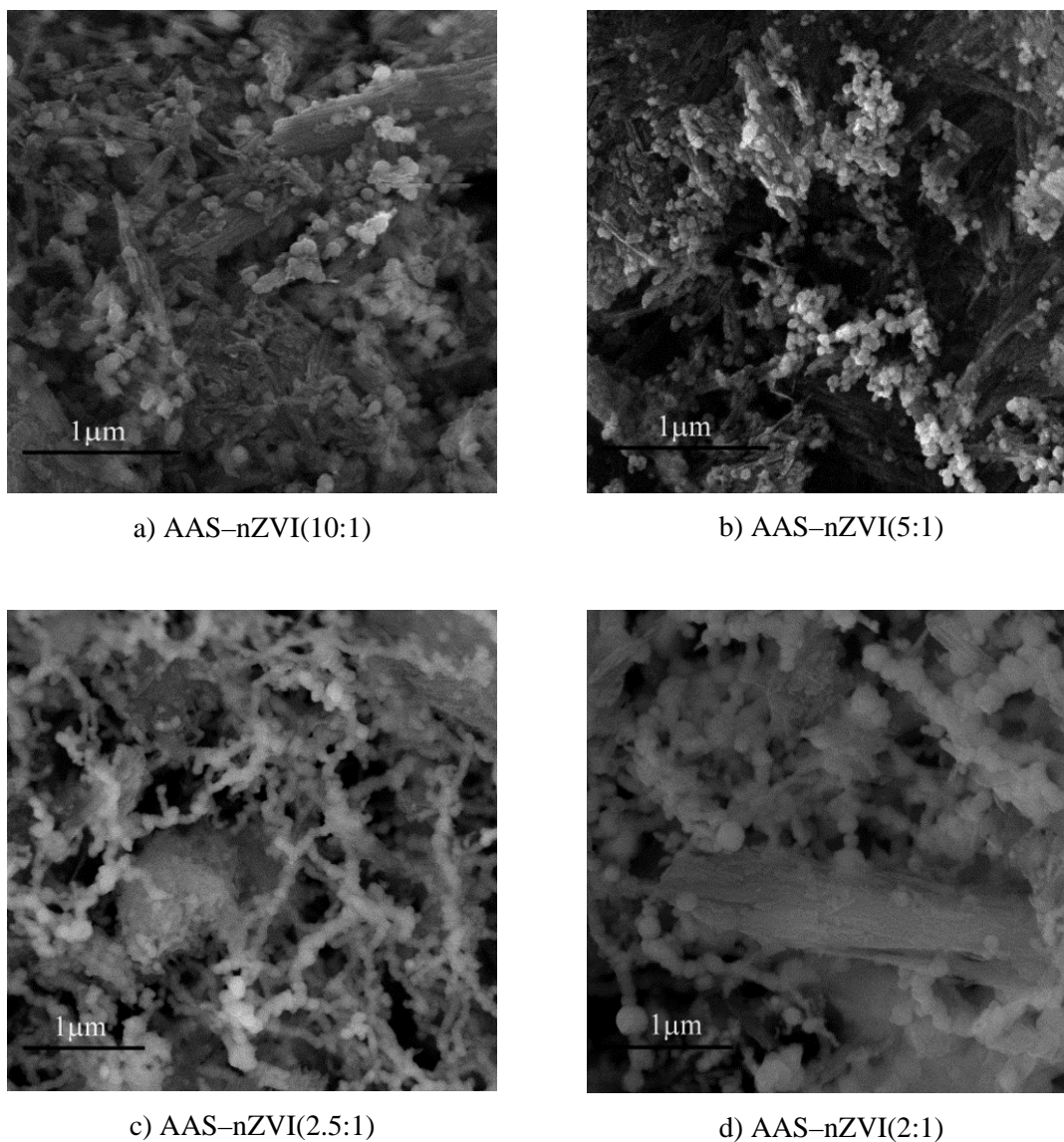
Fig. 6.5. SEM micrographs of the AAS-nZVI composites.

Prolonged ultrasound treatment of the support suspension did not have positive effect on the SEP-based composite properties (Fig. 6.6a and c). It seems that the treatment caused shortening of sepiolite fibers and their re-aggregation. On the other

hand, in the case of the AAS-nZVI(2.5:1)* sample (Fig. 6.6b and d), nZVI particles were slightly better dispersed than in the AAS–nZVI(2.5:1), although sepiolite fibers still formed strong bundles and the nZVI dispersivity was insufficiently good.
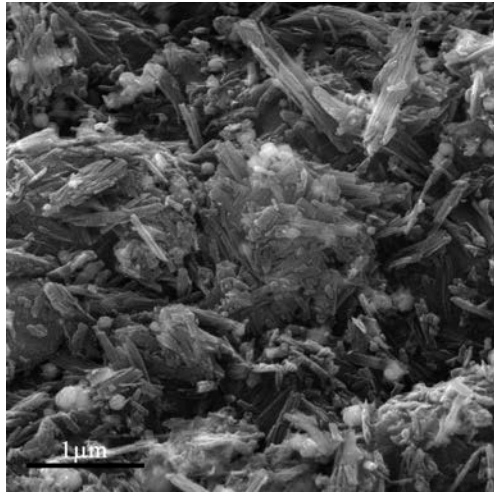
a) SEP–nZVI(2.5:1)*
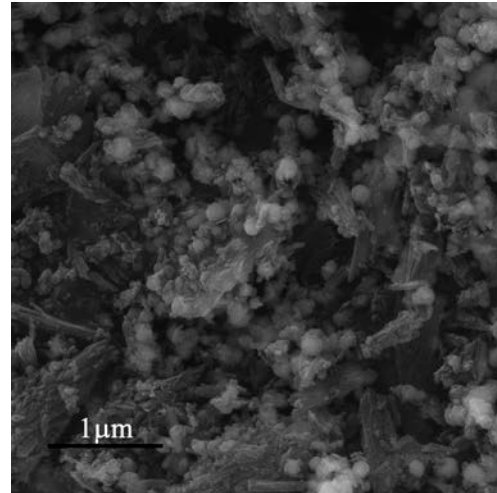
b) AAS-nZVI(2.5:1)*
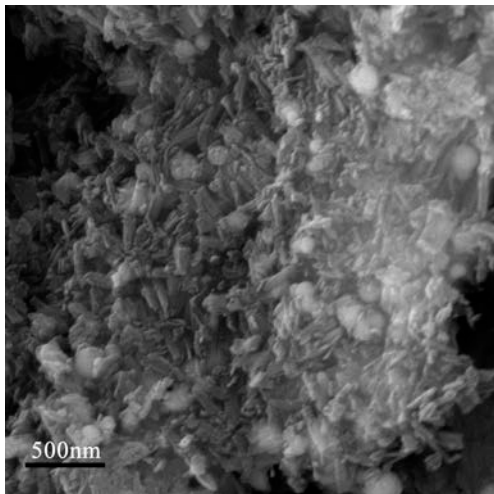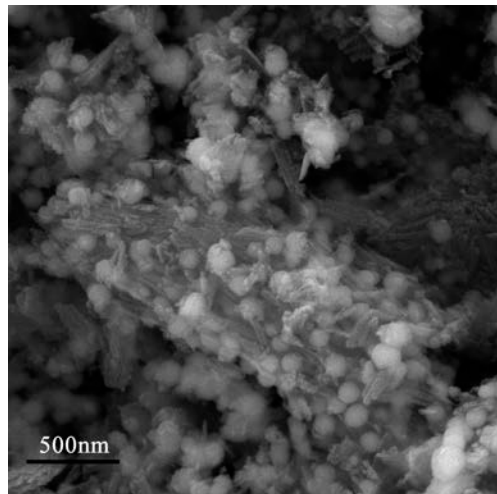
c) SEP–nZVI(2.5:1)*

d) AAS-nZVI(2.5:1)*

Fig. 6.6. SEM micrographs of the samples: (a, c) SEP–nZVI(2.5:1)* and (b, d) AAS-nZVI(2.5:1)*, at different magnifications

Transmission electron microscopy of the samples SEP-nZVI(2.5:1) and AAS-nZVI(2.5:1) (Fig. 6.7) confirmed that the natural sepiolite provided much better dispersibility of nZVI (Fig. 6.7a) than acid-activated sepiolite, where the nZVI particles

were highly aggregated (Fig. 6.7b), mostly apart from the sepiolite particles. The nZVI particles in SEP-nZVI(2.5:1) were spherical and smaller than 100 nm, as already determined by SEM microscopy.

a) SEP-nZVI(2.5:1)   b) AAS-nZVI(2.5:1)
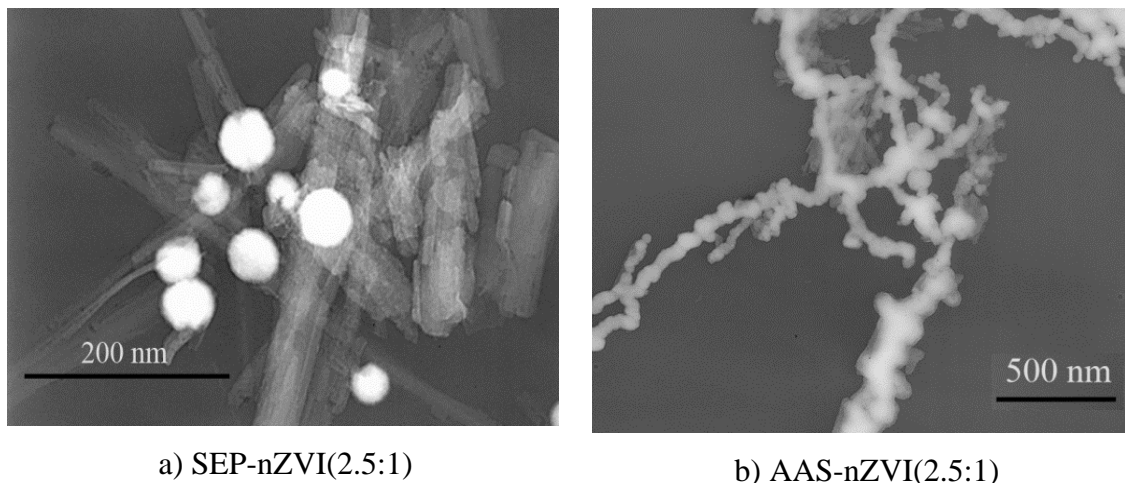
Fig. 6.7. TEM micrographs of the samples: (a) SEP-nZVI(2.5:1) and (b) AAS-nZVI(2.5:1).

6.1.4. Textural properties

The N_2 adsorption–desorption isotherms and mesopore size distributions of nZVI, SEP, AAS and the composites SEP–nZVI and AAS–nZVI are shown in Figs. 6.8 – 6.10. The measured BET surface area, the volumes of the mesopores and micropores, the overall pore volume and D_{max} – the mesopore size at which the distribution of the pore size distribution achieves its maximum and $D_{average}$ – the average mesopore diameter are given in Table 6.2.

The shape of nitrogen isotherms for all the samples is of Type IIb, indicating that materials contain both mesopores, which are responsible for the hysteresis, and macropores, responsible for the absence of a plateau at high p/p_0 values. A plateau at high p/p_0 values is characteristic for Type IV isotherms [136].
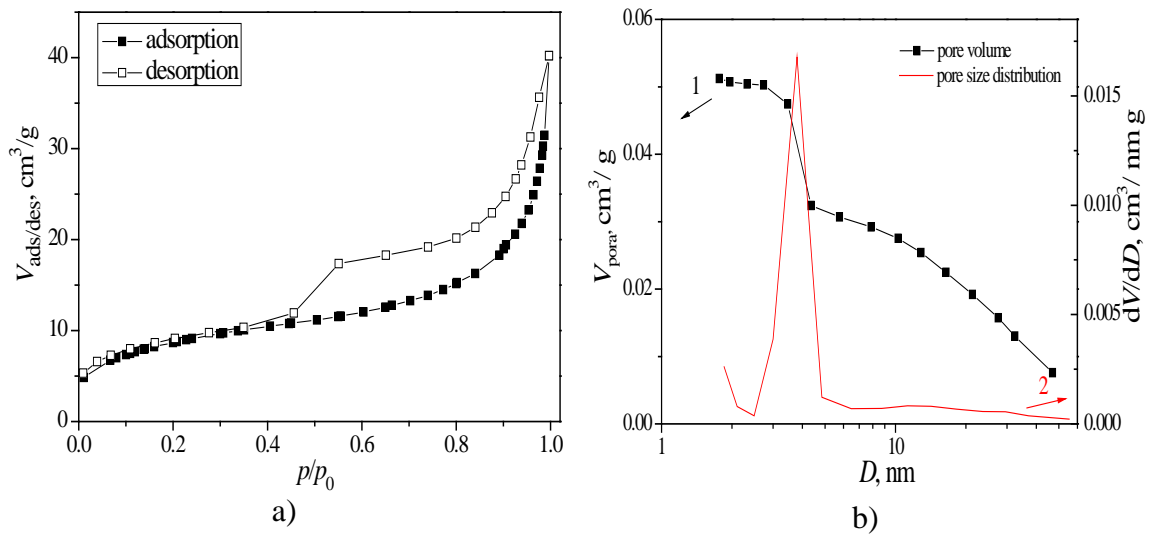
Fig. 6.8. Nitrogen adsorption/desorption isotherms (a), mesopore volume (1) and mesopore size distribution (2) (b) of the pure nZVI.
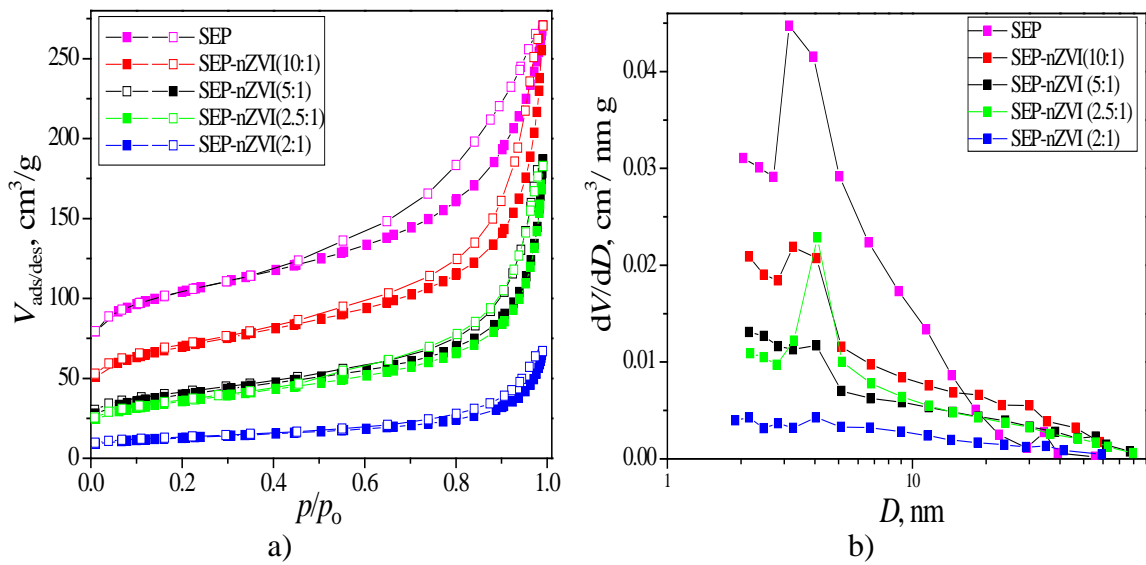
Fig. 6.9. Nitrogen adsorption/desorption isotherms (a) and mesopore size distributions (b) of SEP-nZVI samples.
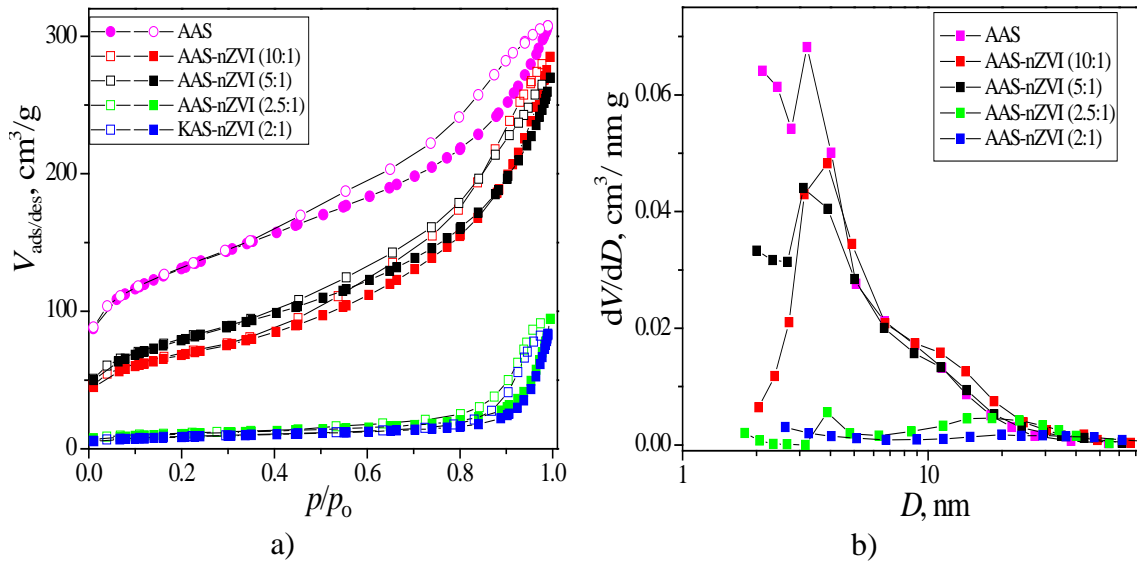
Fig. 6.10. Nitrogen adsorption/desorption isotherms (a) and mesopore size distributions (b) of AAS-nZVI samples.
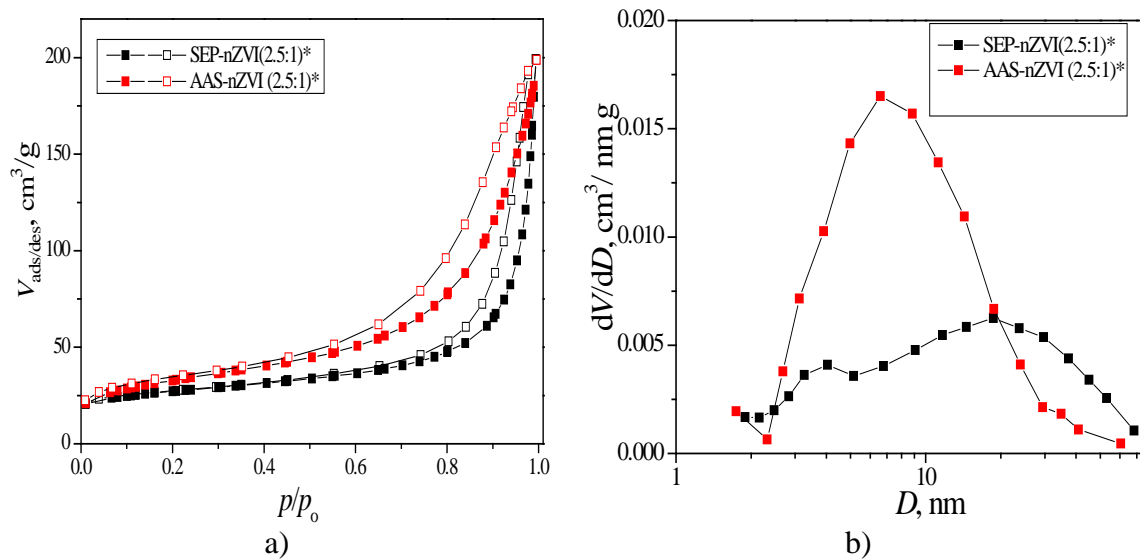
Fig. 6.11. Nitrogen adsorption/desorption isotherms (a) and mesopore size distributions (b) of SEP-nZVI(2.5:1)[*] and AAS-nZVI(2.5:1)[*].

Table 6.2. The textural properties of the pure compounds and the composites

Sample	S_{BET}, m^2/g	V_{total}, cm^3/g	$V_{mesopore}$, cm^3/g	$V_{micropore}$, cm^3/g	D_{max}, nm	$D_{average}$, nm
SEP	**359.9**	**0.410**	**0.343**	**0.139**	**3.2**	**6.7**
nZVI	**30.1**	**0.055**	**0.051**	**0.010**	**3.8**	**7.1**
SEP-nZVI(10:1)	228.4	0.406	0.369	0.089	3.2	9.4
SEP-nZVI(5:1)	132.0	0.279	0.261	0.050	4.1	10.6
SEP-nZVI(2.5:1)	120.5	0.273	0.268	0.043	4.1	9.8
SEP-nZVI(2:1)	42.6	0.099	0.095	0.016	4.0	10.5
AAS	**461.6**	**0.472**	**0.368**	**0.161**	**3.2**	**4.8**
AAS-nZVI(10:1)	231.4	0.433	0.423	0.079	3.7	7.2
AAS-nZVI(5:1)	273.0	0.409	0.391	0.091	3.1	5.9
AAS-nZVI(2.5:1)	36.3	0.141	0.139	0.013	3.9/ 18.1	15.9
AAS-nZVI(2:1)	29.3	0.127	0.125	0.010	19.8	18.2
SEP-nZVI(2.5:1)*	87.9	0.296	0.284	0.035	3.90/ 18.6	18.2
AAS-nZVI(2.5:1)*	111.2	0.299	0.292	0.039	6.6	10.2

The sharp maximum centered at 3.8 nm observed on the pore size distribution of nZVI, indicated that nZVI had a significant volume of small mesopores, which were much smaller than the pores which can be formed between the nZVI particles sizes 100–200 nm (Fig. 6.3c). According to the literature, oxide layer on nZVI surface is responsible for higher specific surface area of nZVI than it could be expected according to the particle size, so higher specific surface area and porosity of pure nZVI sample is explained by oxidiation during the synthesis and drying [90, 95].

The volumes of both micro- and mesopores of nZVI were much smaller than those of SEP/AAS, and hence, the specific surface area of nZVI was much lower than those of SEP/AAS. Thus, S_{BET} and the porosity of the composites decreased as the quantity of nZVI in the composite increased (Table 6.2). In the case of the SEP/nZVI composites, S_{BET} and the porosity decreased gradually up to the SEP/nZVI mass ratio = 2.5:1, and then suddenly decrease for the sample with the SEP/nZVI mass ratio = 2:1.

Similarly, a drastic decrease of S_{BET} and the porosity for AAS–nZVI composites occurred when the AAS/nZVI mass ratio was smaller than 5:1 (samples AAS–nZVI(2.5:1) and AAS–nZVI(2:1)). These results correlate well with the results of the SEM analysis: the samples with a high degree of nZVI agglomeration (Fig. 6.4d, 6.5c and d) have a very low specific surface area and both micro and mesoporosity. The very low micropore volumes of these samples (SEP–nZVI(2:1), AAS–nZVI(2.5:1) and AAS–nZVI(2:1)) could be explained not only by nZVI aggregation, but also by the closing of the sepiolite channels on nZVI loading.

The textural characteristics of the samples SEP-nZVI(2.5:1)* and AAS-nZVI(2.5:1)* are also in an accordance with the SEM results: the nZVI dispersibility in the sample AAS-nZVI(2.5:1)* (Fig. 6.6b and d) is higher than in sample AAS-nZVI(2.5:1) (Fig. 6.5c), which caused higher specific surface area, higher pore volume and narrower pore size distribution. Similarly, higher aggregation of the sepiolite fibers in the sample SEP-nZVI(2.5:1)* (Fig. 6.6a and c) than in sample SEP-nZVI(2.5:1) (6.5c) caused lower specific surface area and wider pore size distribution. In addition, the higer specific surface area of SEP-nZVI(2.5:1) in comparison to SEP-nZVI(2.5:1)* may be because of higher content of Fe(II)/Fe(III) oxide/oxyhidroxide, as a result of oxidation of SEP–nZVI(2.5:1) during synthesis. Probably, prolonged ultrasound treatment removed the oxygen from the system more efficiently and oxidation of the sample SEP-nZVI(2.5:1)* was prevented.

The mesopore size distributions for samples SEP-nZVI(2.5:1)* and AAS-nZVI(2.5:1)* show the shift of D_{max} from the ≈ 4.0 for samples SEP-nZVI(2.5:1) and AAS-nZVI(2.5:1) to higer values (Table 6.2). Although presence of pores ≈ 4.0 nm is observed on the SEP-nZVI(2.5:1)* mesopore size distribution, larger D_{max} and $D_{average}$ in comparison to SEP-nZVI(2.5:1) indicate presence of larger pores as a result of the blocking micropores and small mesopores due to attachment of nZVI particles on the sepiolite fibres.

6.1.5. Thermal analysis

Thermal behavior of the SEP- and AAS-based composites was compared according to DTA and TGA results of the samples SEP-nZVI(2.5:1) and AAS-nZVI(2.5:1). To analyze deeply the thermal behavior of the composites, DTA and TGA were performed in air and N_2, and the results are given in Fig. 6.12.
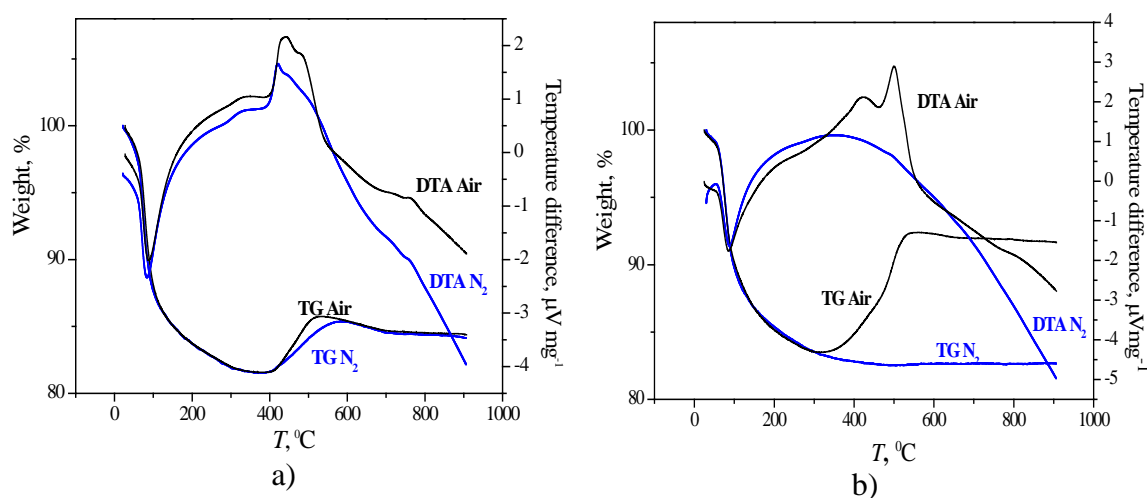
Fig. 6.12. DTA and TGA of the samples: a) SEP-nZVI(2.5:1) and b) AAS-nZVI(2.5:1)

The endothermic peak centered at about 100 °C, present in all the DTA curves, is attributed to the removal of physically bound water and ethanol used in the synthesis. The TG curves for both samples show the same weight loss until ≈300 ºC under both atmospheres, corresponding to the removal of ethanol and adsorbed water, as well as zeolitic water and some quantity of water bound in the sepiolite matrix. In the temperature region from ≈350 °C to ≈600 °C, where two exothermal peaks were registered in both DTA curves recorded in air, the TGA curves show weight increases, implying the oxidation of nZVI. The presence of the two exothermal peaks could be explained by a two-stage oxidation process, probably from Fe(0) to Fe(II) and from Fe(II) to Fe(III). Additionally, it is possible that the first peak is a result of surface oxidation, while the second is due to bulk oxidation [144]. A slow weight loss after ≈550 °C in the case of sample SEP–nZVI(2.5:1) indicates the removal of constitutional

water from sepiolite and its transformation into enstatite ($MgSiO_3$), which was proved by the appearance of an exothermal peak at about 760 °C [11]. This peak was not visible for the sample AAS–nZVI(2.5:1), because the amount of Mg^{2+} ions in AAS is lower than in SEP due to the acid-activation.

The TG curve of AAS–nZVI(2.5:1) recorded in N_2 shows no weight increase and the DTA curve shows no exothermal peaks in the region ≈350 – 600 °C, which confirms that nZVI oxidation occurred in air at these temperatures. However, when the sample SEP–nZVI(2.5:1) was analyzed in N_2, a broad exothermal peak appeared in the DTA curve and the TG curve showed a weight increase, similar to that during analysis in air. It could be supposed that oxygen molecules were present in the channels of the sepiolite structure, and during heating in N_2 atmosphere were displaced with nitrogen, causing oxidation of nZVI attached to the sepiolite fibers. This did not occur when the sample AAS–nZVI(2.5:1) was analyzed in N_2, probably because the channel structure was highly destroyed during the acid-activation of sepiolite and oxygen was not trapped inside.

The weight increase of SEP–nZVI(2.5:1) due to nZVI oxidation in air is lower than that of AAS–nZVI(2.5:1) (Fig. 6.12). This could be explained by the lower content of nZVI, i.e. higher content of Fe(II)/Fe(III) oxide, due to the greater oxidation of SEP–nZVI(2.5:1) during synthesis owing to the presence of oxygen molecules in the sepiolite channels.

6.1.6. Point of zero charge

The point of zero charge (pH_{pzc}) is an important parameter characterizing solids used as adsorbents. The pH_{pzc} represents the solution pH value at which the net surface charge of the solid equals zero. The surface is positively charged at $pH<pH_{pzc}$ and negatively charged at $pH>pH_{pzc}$.

The values of pH_{pzc} of the samples are presented in Table 6.3. The position of the plateau on the pH_f on pH_i dependences for all the samples was independent of the NaCl concentration, indicating that there was no specific adsorption of Na^+ and Cl^- onto the samples surface, i.e. that NaCl was an indifferent electrolyte [11]. As an example,

the dependences of pH_f on pH_i for the samples SEP–nZVI(2.5:1) and AAS–nZVI(2.5:1) are presented in Fig. 6.13. It is also obvious that the samples have a high buffer capacity, which means that over a wide range of pH_i values, the pH_f values were constant and equal to the pH_{pzc}. It should be mentioned that the buffer capacity depends also on the solid/liquid ratio: the capacity decreases, i.e. the plateau narrows, when the ratio decreases.

Table 6.3. pH_{pzc} of the pure compounds and the composites

Sample	pH_{pzc}
nZVI	8.9 ± 0.1
SEP	7.4 ± 0.1
SEP-nZVI(10:1)	8.9 ± 0.1
SEP-nZVI(5:1)	9.0 ± 0.1
SEP-nZVI(2.5:1)	9.2 ± 0.1
SEP-nZVI(2.5:1)*	9.3 ± 0.1
SEP-nZVI(2:1)	9.5 ± 0.1
AAS	6.9 ± 0.1
AAS-nZVI(10:1)	9.3 ± 0.1
AAS-nZVI(5:1)	9.3 ± 0.1
AAS-nZVI(2.5:1)	9.4 ± 0.1
AAS-nZVI(2.5:1)*	9.2 ± 0.1
AAS-nZVI(2:1)	9.5 ± 0.1
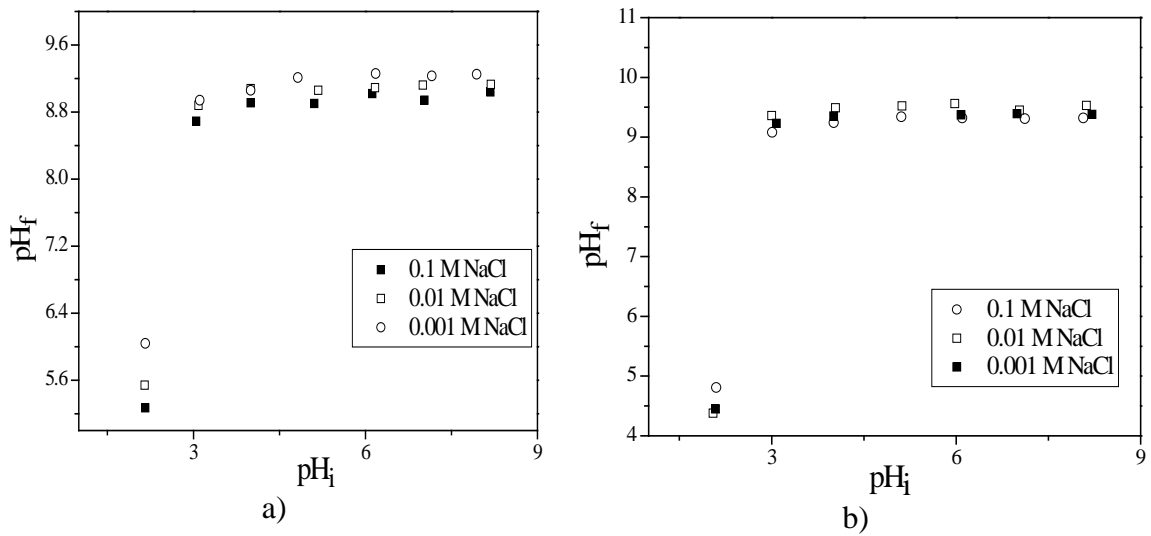
Fig. 6.13. pH_f *vs* pH_i after 24 h equilibration of 0.02 g of: a) SEP-nZVI(2.5:1) and b) AAS-nZVI(2.5:1), with 20 cm^3 of NaCl solution of different concentrations

The point of zero charge of the pure nZVI was slightly higher than the pH_{pzc} values reported in the literature for zero-valent iron (7.7–8.4) [145, 146, 147], but lies in the wide range of values reported for pure iron-oxides (4.5–9.5) [148, 149]. The higher value of pH_{pzc} for the nZVI obtained in this work could be explained by the specific adsorption of sulfate anions from $FeSO_4$ used in the synthesis. It is well known [11, 150] that specific adsorption of anions shifts the point of zero charge towards higher pH values. The pH_{pzc} of the composites were even higher, but slightly, than that of pure nZVI, and increased slightly with increasing quantity of nZVI. These results support the assumption that specific adsorption of sulfate anions influences the values of the pH_{pzc}.

6.1.7. Comparative analysis of the results of the composites characterizations

The presented results (paragraphs 6.1.1-6.1.6.) showed that properties of the nZVI/sepiolite composites are influenced by the sepiolite/nZVI mass ratio, acid activation of sepiolite and duration of sepiolite suspension treatment by ultrasound probe. When nZVI-based composites are synthesized, the content of nZVI should be as large as possible, whereby the particles should be non-aggregated and homogeneously

dispersed on the support surface. To address this issue, a support should have not only a high specific surface area, but also appropriate porosity to provide large available surface for the attachment of nZVI particles. The specific surface area of sepiolite is relatively high, due to the small, fibrous particles and the presence of micro-channels in the structure [11]. However, nZVI particles (sizes of tens of nm) cannot reach the interior of these narrow channels (0.37×1.06 nm) and can be attached only at the outer surface of the particles. Since acid activation increases the specific surface area and pore size of sepiolite [11, 53, 61, 151], it was supposed that the dispersibility of the nZVI particles could be improved by using an acid-activated sepiolite as the support. The composites were synthesized with both sepiolites, untreated and acid-activated, at different support/nZVI ratios in order to determine the optimal content of nZVI, *i.e.* the content at which non-aggregated particles are uniformly dispersed at the sepiolite surface.

Generally, sepiolite fibers are highly aggregated, forming bundles (Fig. 6.3a). SEM analysis showed that acid activation did not provide de-aggregation and formation of individual fibers or smaller entities (Fig. 6.3b), although some researchers have suggested using acid treatment as the de-aggregation method [52, 57-61]. In order to separate the fibers and provide high surface area for the deposition of nZVI particles, ultra-sonication of SEP and AAS suspension, before iron salt addition, was applied in the composites synthesis. The treatment was lasted 10 or 30 min, to study the influence of duration of the ultrasonication on the composites properties. According to the SEM micrographs of the composites prepared by applying 10 min-ultrasound treatment (Fig. 6.4), it is obvious that natural sepiolite was efficiently de-aggregated, while the bundles of acid-activated sepiolite (Fig. 6.5) were stable and resistant to the effect of the ultrasound probe. Obviously, acid activation caused an increase in the specific surface area (Table 6.2) due to extraction of structural magnesium [11], but it resulted in the formation of new Si–OH groups on the fibers surface and stronger interfiber bonds. Therefore, untreated sepiolite is a better support for nZVI and good dispersibility was achieved at SEP/nZVI mass ratios ≥ 2.5:1. On the other hand, nZVI particles were well-dispersed on the AAS surface only at mass ratios AAS/nZVI = 10:1. The results of the SEM analysis are in good correlation with the results of the determination of the textural parameters: the samples with high degree of agglomeration of nZVI particles have a low

specific surface area and both micro- and meso-porosity similar to the values for pure nZVI.

Prolonged ultrasound treatment had negative effect on the morphological and textural properties of SEP-based composite (Fig. 6.6 and Table 6.2), because the sepiolite fibers in the sample obtained with 30 min-ultrasound treatment were shorter and more aggregated. Obviously, during the first 10 minutes of the treatment, the sepiolite fibers were separated (Fig. 6.4), but further treatment caused fibers breaking and the aggregation of so-obtained short fibers. On the other hand, it seems that prolonged ultrasound treatment increased to a small extent de-aggregation of shorter AAS fibers, which provided slightly better dispersibility of nZVI in the composite (Fig. 6.6) than in the sample obtained with 10 min-ultrasound treatment (Fig. 6.5).

The presence of Fe^0 in the composites was confirmed by both XRD and DTA/TGA. It was shown, according to a weight increase (due to Fe^0 oxidation) during TGA in air, that AAS-based composites contain higher quantity of Fe^0 than the SEP-based composite. It indicates higher content of iron-oxides the SEP/nZVI composites, as a result of oxidation during the synthesis. More intensive oxidation of nZVI during synthesis with SEP as a support is explained by the presence of oxygen molecules in the sepiolite channels, which could not be efficiently removed during nitrogen purging before addition of $NaBH_4$ to the suspension of sepiolite with Fe^{2+} ions. nZVI oxidation during DTA/TGA of the SEP–nZVI composite in nitrogen confirmed the strong capture of oxygen in the sepiolite structure, unlike the AAS, which fibers are shorter and oxygen coud be easily removed from the chanels. Different quantity of Fe^0 in SEP- and AAS-based composites explains differences in the intensities of the XRD peak characteristic for zero-valent iron (Fig. 6.1): the intensity of the peak is lower for the SEP-based composites, due to higher oxidation and, consequently, the Fe^0 crystalites were smaller. The presence of crystalline iron-oxide phases was not confirmed by XRD analysis, which indicates the presence of amorphous oxides.

The results of the characterization of the composites showed that better nZVI dispersibility was achieved with SEP as the support, but a lower degree of oxidation during the synthesis was achieved using AAS. The high pHpzc value of all the composites indicated the high basicity of surface resulting from the presence of basic Fe–OH groups. The high buffer capacity indicated the large number of functional

groups that interact with H^+/OH^- ions and that could also be available for the interaction with ions from solution.

6.2. X-Ray photoelectron spectroscopy (XPS)

X-Ray photoelectron spectroscopy (XPS) was used to investigate the composition and chemical state of the sample with the best nZVI dispersibility (SEP–nZVI(2.5:1)) and the same sample loaded with Cd^{2+} ions (SEP–nZVI(2.5:1)/Cd), on the surface and after ion sputtering for 20 min. It was estimated that a depth of about 40 nm beneath the original surface was reached after 20 min of ion sputtering.

The XPS wide-scan survey of the samples SEP–nZVI(2.5:1) and SEP–nZVI(2.5:1)/Cd are shown in Fig. 6.14.
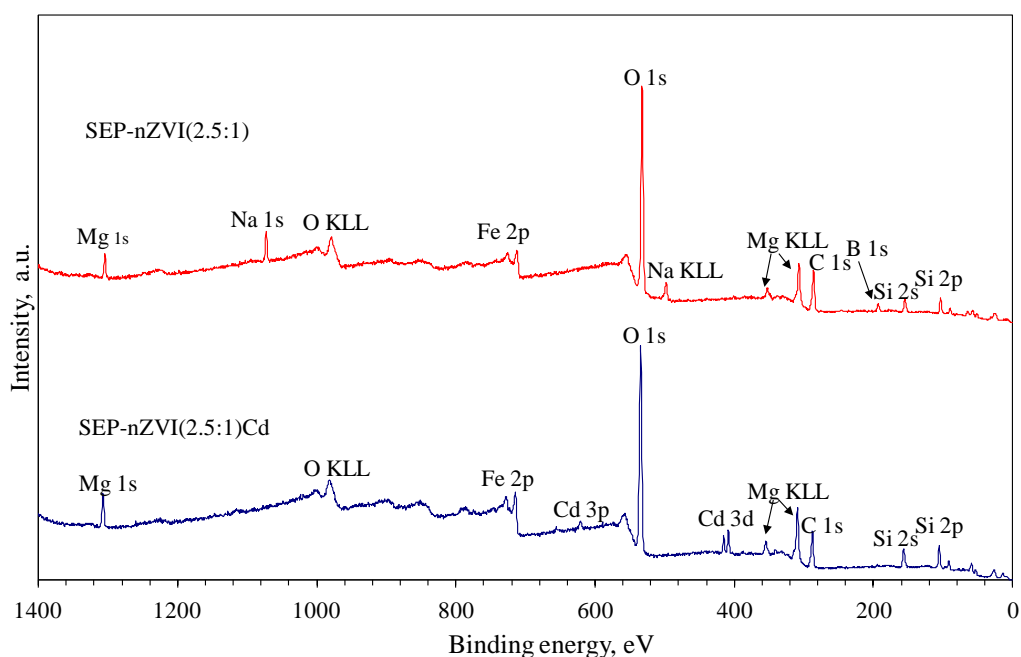
Fig. 6.14. XPS wide-scan survey of the samples SEP-nZVI(2.5:1) and SEP-nZVI(2.5:1)/Cd.

In addition to Fe, Si, Mg and O, originating from nZVI and sepiolite, B, Na and C were also present on the surface of the sample SEP–nZVI(2.5:1). The presence of B and Na could be explained by incomplete washing of the sample, as there were no signals of these elements in XPS spectra of the sample SEP–nZVI(2.5:1)/Cd. Similar

results were obtained after sputtering: signals for Na and B were detected in the spectra of the sample SEP–nZVI(2.5:1) (Figs. 6.15), but not in the spectra of sample SEP–nZVI(2.5:1)/Cd. Obviously, the compounds containing Na and B were rinsed out during equilibration of the sample with the Cd^{2+} solution. The intensities of the B 1s and Na 1s peaks in the spectra before and after sputtering are similar, indicating the same content of the elements at the surface and in sub-surface region. Bearing in mind these results, the FTIR absorption band at ≈1390 cm^{-1} (Fig. 6.2) indicates more likely the presence of borate species than the presence of products of nZVI oxidation.
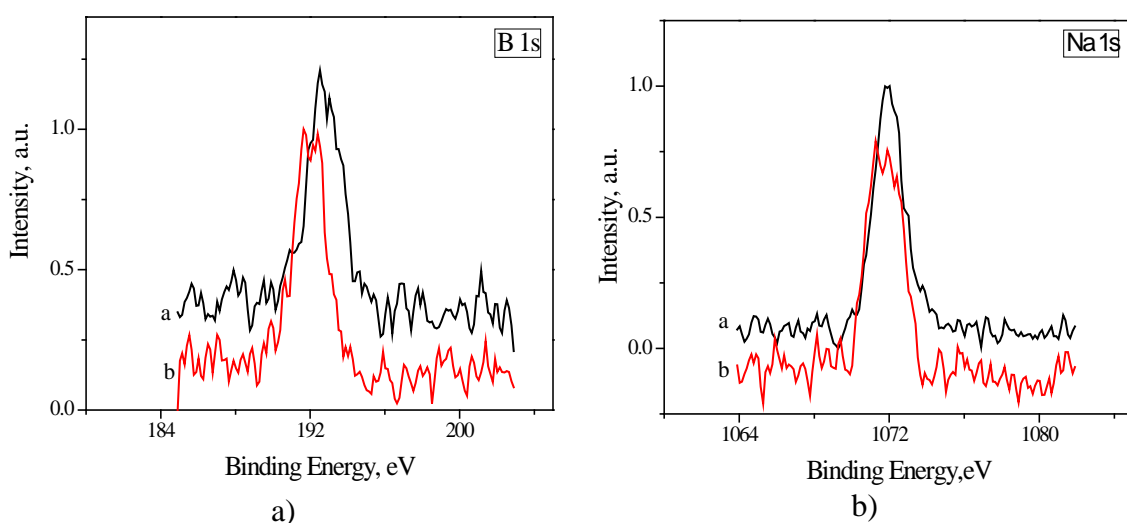
Fig. 6.15. High-resolution XPS (HR-XPS) spectra in the B 1s and Na 1s region of the sample SEP-nZVI(2.5:1) before (a) and after sputtering (b).

On the other hand, carbon was present on the surface of both samples. The XPS C 1s peak was fitted into three components (Fig. 6.16): peak 1 at 284.8 eV (C–C and C–H bonds), peak 2 at 286.4 eV (C–O bonds) and peak 3 at 287.9 eV (C=O bonds) [152]. The presence of C–C, C–H and C–O bonds could be related to the presence of ethanol, used in the synthesis, or some organic impurities in the sepiolite, while the C=O bonds originated from CO_2 adsorbed from the atmosphere. The content of carbon in sample SEP–nZVI(2.5:1)/Cd was only slightly lower (23.2 at. %) than in the pristine sample (25.1 at. %); therefore it is more likely that carbon in both samples originated from CO_2 and organic impurities in the sepiolite, which could not be rinsed out during equilibration of the sample with Cd^{2+} solution. The XPS depth profiles of the samples (the depth profile of sample SEP–nZVI(2.5:1)/Cd is presented in Fig. 6.17) showed that

the concentration of carbon decreased suddenly with depth and even at 5 nm below the surface, the carbon concentration was below 5 at. %. After 20 min sputtering, at a depth of 40 nm, the concentration of carbon in both samples was about 2 at. %, indicating that compounds containing carbon were located mainly on the surface. The intensity of the peak 3 of the XPS C 1s peak of both samples after sputtering (Fig. 6.16) was very low, indicating very low content of CO_2, which means that the subsurface region was analyzed after sputtering.
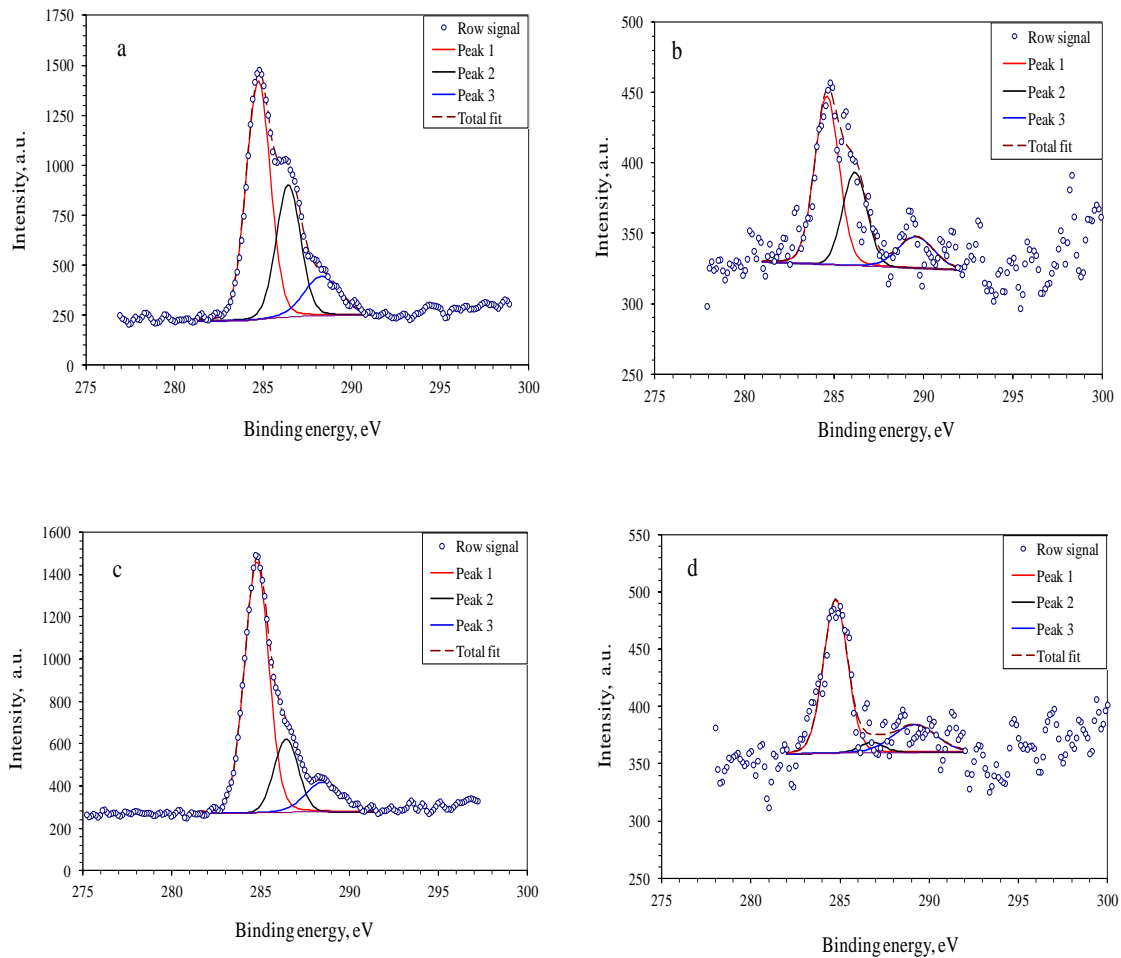
Fig. 6.16. C 1s spectra fitted with three peaks for: a) sample SEP-nZVI(2.5:1) before sputtering, b) sample SEP-nZVI(2.5:1) after sputtering, c) sample SEP-nZVI(2.5:1)/Cd before sputtering and d) sample SEP-nZVI(2.5:1)/Cd after sputtering.

The XPS depth profile (Fig. 6.17) shows that cadmium was present not only at the surface, but also through the entire analyzed depth (insert in Fig. 6.17), whereby its

concentration was higher on the surface than in the subsurface region, where the Cd distribution was uniform.
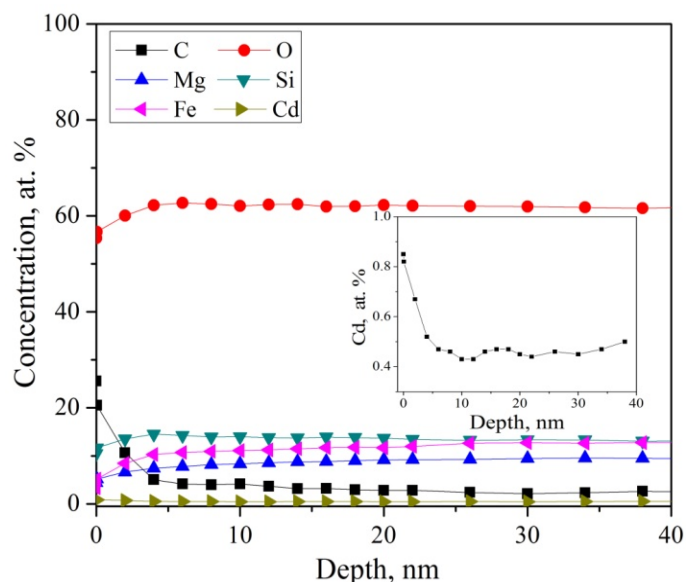
Fig. 6.17. Depth profile of the sample SEP-nZVI/Cd; inset shows the dependence of Cd on the depth.

The XPS O 1s spectra were also fitted with three components (Fig. 6.18) at binding energies of 530.6 eV (peak 1, lattice oxygen, O^{2-}), 532.0 eV (peak 3, hydroxyl groups, OH^-) and 533.0 eV (peak 2, bound and adsorbed water, OH_2) [152].

At the surface of the sample SEP–nZVI(2.5:1), the OH and OH_2 species dominate over O^{2-} (Fig. 6.18a). Such high content of OH groups results from high content of Si–OH groups in sepiolite and probably due to the presence of Fe–OH groups on the surface of nZVI, while OH_2 is present in sepiolite as bound to Mg in the structure and zeolitic water [11], as well as adsorbed water. After Cd^{2+} adsorption, the relative contributions of the oxygen groups were changed (Fig. 6.18b), which could be an indication of Cd^{2+} adsorption. A lower contribution of OH_2 in the surface O 1s spectrum of the sample SEP–nZVI(2.5:1)/Cd in comparison to the sample SEP–nZVI(2.5:1) indicate the exchange of Mg^{2+} with Cd^{2+}, while the higher contribution of O^{2-} could suggest the replacement of H^+ by Cd^{2+} in OH groups, i.e., the inner-sphere complex formation. Similar changes were observed after sputtering: the relative contribution of

O^{2-} was higher, while the contribution of OH_2 was lower after Cd^{2+} adsorption (Figs. 6.18c and 6.18d).
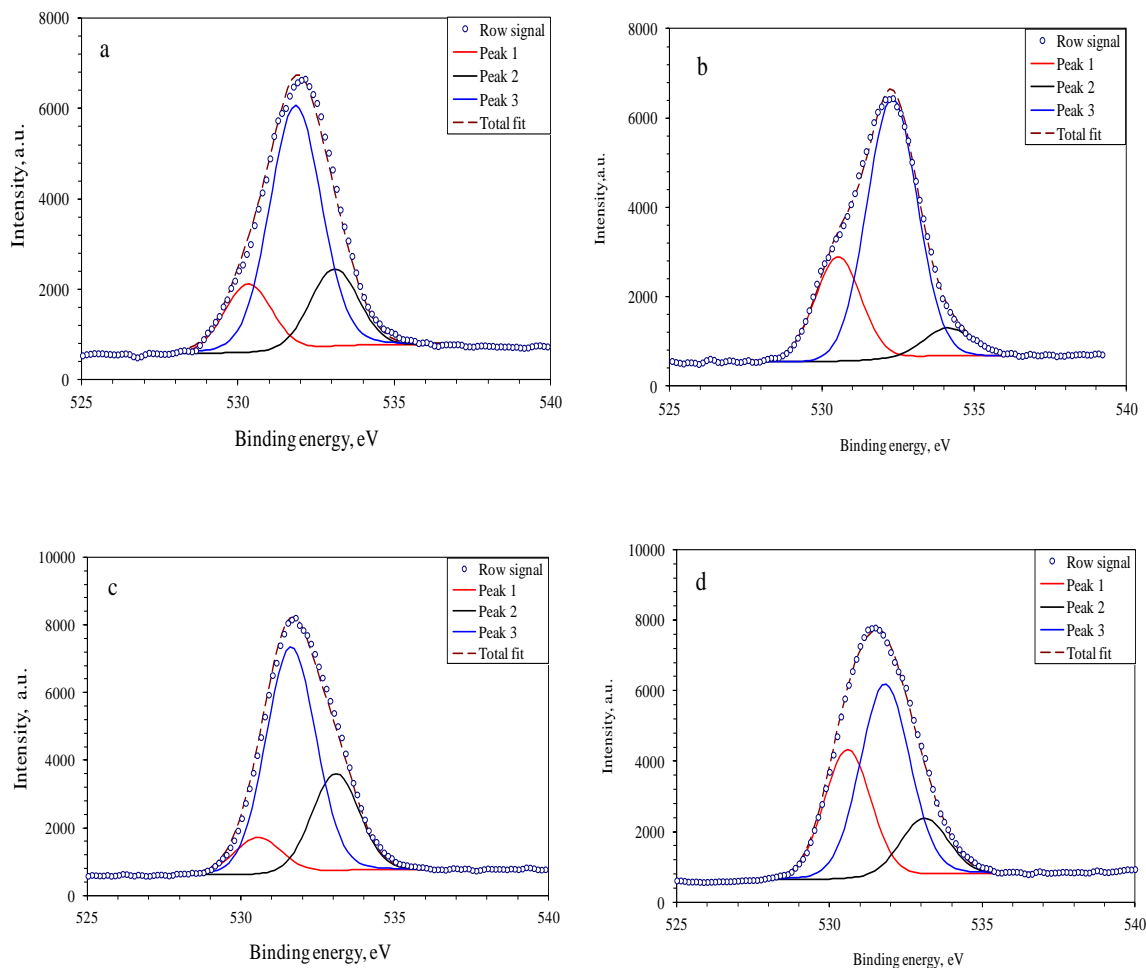
Fig. 6.18. XPS spectra O 1s fitted with three peaks: a) sample SEP-nZVI(2.5:1) before sputtering, b) sample SEP-nZVI(2.5:1)/Cd before sputtering, c) sample SEP-nZVI(2.5:1) after sputtering and d) sample SEP-nZVI(2.5:1)/Cd after sputtering.

The XPS Fe 2p spectra of the samples before and after sputtering are shown in Fig. 6.19.
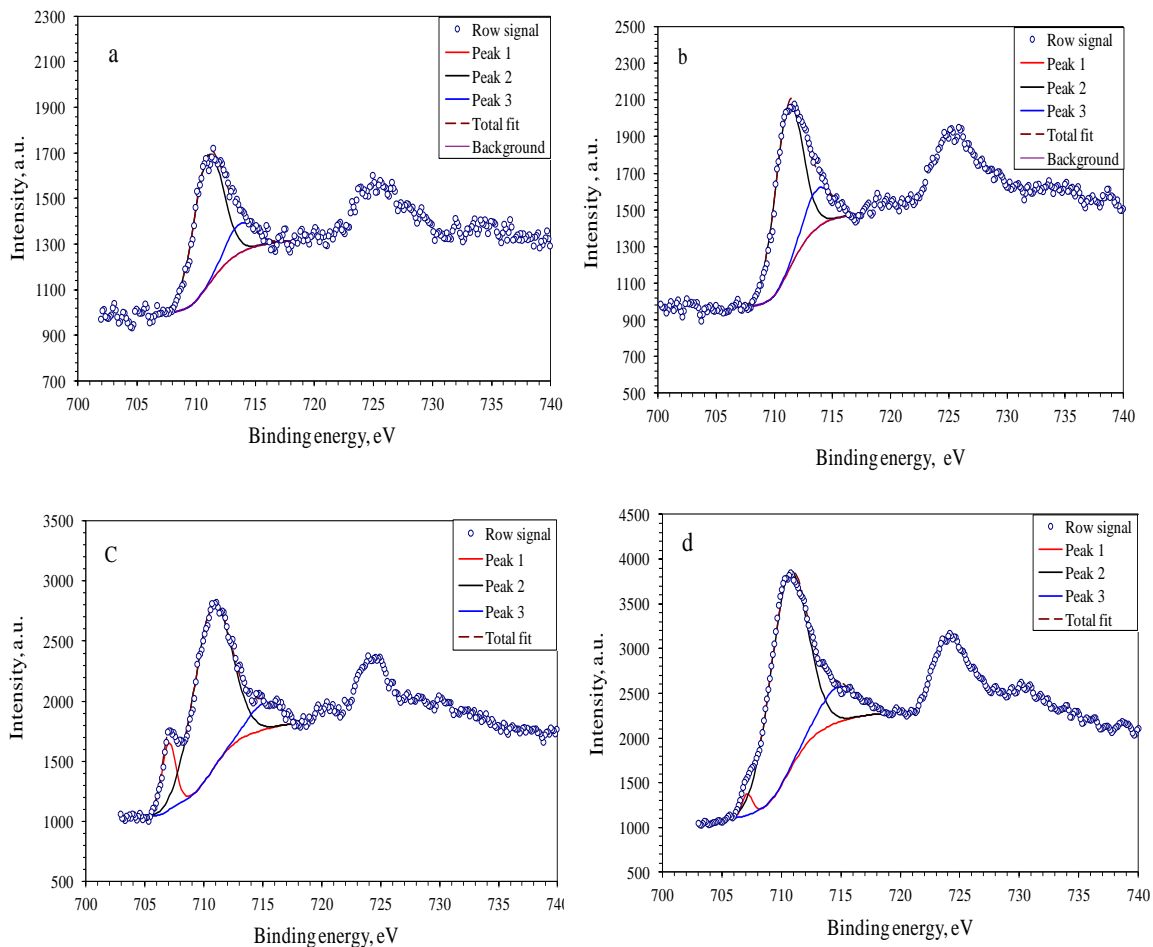
Fig. 6.19. Fe 2p spectra fitted with three peaks for: a) sample SEP-nZVI(2.5:1) before sputtering, b) sample SEP-nZVI(2.5:1)/Cd before sputtering, c) sample SEP-nZVI(2.5:1) after sputtering and d) sample SEP-nZVI(2.5:1)/Cd after sputtering.

In general, the Fe 2p spectrum consists of Fe $2p_{3/2}$ and $2p_{1/2}$ doublet peaks separated by 13.6 eV. The Fe $2p_{3/2}$ peaks from all samples were fitted with three components: a peak 1 at ≈707.0 eV characteristic for Fe^0, a peak 2 at ≈711.0 eV characteristic for Fe–OH/Fe-oxide species and a peak 3 at 713.5 – 715.0 eV [152]. The later peak is a plasmon or satellite peak related to the main Fe $2p_{3/2}$ peak at 711 eV hydro–(oxide) species and is an effect of rearrangement of core electrons after emission of primary photoelectrons. This plasmon peak is an indication of the presence of Fe-hydro-oxide species. The Fe 2p spectra obtained at the surface of SEP–nZVI(2.5:1) before and after Cd^{2+} adsorption (Figs. 6.19a and b) were composed of oxidized iron

81

species, mainly of FeOOH. No metallic iron was present according to the absence of a peak at about 707 eV, which is characteristic for Fe^0.

In the subsurface region of both samples, zero-valent iron Fe^0 was present, as seen from the peak at 707 eV in Fe 2p spectra obtained at a depth of about 40 nm (Figs. 6.19c and d). The relative intensity of zero-valent iron is higher in the SEP–nZVI(2.5:1) than in the SEP–nZVI(2.5:1)/Cd sample: the Fe^0 content decreased after Cd^{2+} adsorption from 13 at. % to 5 at. % (with respect to total amount of Fe). The decrease of Fe^0 content after Cd^{2+} adsorption is a result of iron oxidation by Cd^{2+} or by oxygen, present in the Cd^{2+} solution. Considering the comparable standard electrode potentials between Fe^{2+}/Fe^0 ($E^0 = -0.41$ V) and Cd^{2+}/Cd^0 ($E^0 = -0.40$ V)[153, 154], the likelihood of Cd^{2+} being reduced to Cd^0 on nZVI is low.

The Cd 3d high-resolution spectra of the sample SEP–nZVI(2.5:1)/Cd before and after sputtering are shown in Fig. 6.20. The positions of the $3d_{5/2}$ and $3d_{3/2}$ peaks are at 405.5 eV and 412.2 eV, respectively, characteristic for both Cd(II) and Cd(0) oxidation states [152]. Therefore, according to the HRXPS spectra in the Cd 3d region, it was not possible to determine whether Cd(0) really existed in the sample.
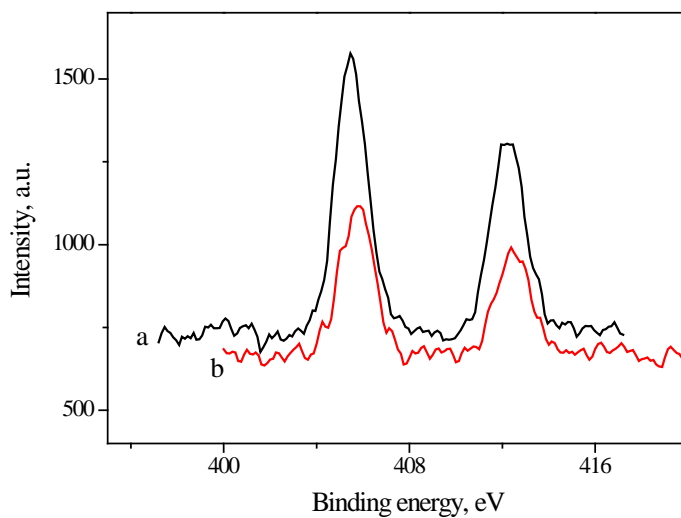
Fig. 6.20. HRXPS spectra in the Cd 3d region of the sample SEP-nZVI(2.5:1)/Cd before (a) and after sputtering (b).

XPS analysis showed that the Fe^0 content in the nZVI composite decreased after Cd^{2+} adsorption due to oxidation during adsorption, but it was not possible to determine

if the oxidation agent was Cd^{2+} or oxygen, present in the Cd^{2+} solution. In addition, it was shown that Cd was present not only at the surface of the adsorbent, but also in the subsurface region. It has been shown [155] that, regardless of which specific mechanisms are involved, heavy metals removal by zero-valent iron is determined by their interactions with the products of Fe^0 oxidation. Oxidized species are always present on the nZVI surface, as shown by XPS analysis, and hence cadmium can form complexes with the Fe–OH groups on the surface. In the case of the SEP–nZVI(2.5:1) composite, the formation of surface complexes with Si–OH groups of sepiolite is also a mechanism of Cd^{2+} removal, as well as ion-exchange with Mg^{2+} ions from the sepiolite structure [11]. The presence of cadmium in the subsurface region of the sample is explained by the porosity of the oxide layer on the surface of nZVI particles, which allows the ions to penetrate the subsurface region. The analysis of the textural properties of pure nZVI (Fig. 6.8) shows the presence of pores sizes (~ 4 nm) of which allows hydrated Cd^{2+} ions (sizes of about 0.4 nm) to enter. Passing through the pores, Cd^{2+} ions can form complexes with the functional groups at the wall of the pores and also reach the core of the nZVI particles. As already stated, it is unlikely that Cd^{2+} would be reduced by Fe^0 in the core. More likely, Fe^0 is oxidized by the oxygen present in the solution and Cd^{2+} ions are co-precipitated with the in-situ formed iron-oxide species and/or form complexes with the newly formed Fe–OH groups.

6.3. Adsorption experiments

6.3.1. Cd^{2+} adsorption

6.3.1.1. Adsorption at different solid/liquid ratios

The adsorption of Cd^{2+} ions were investigated at pH_i = 7.0 ± 0.1 at different solid/liquid (S/L) ratios in order to optimize the conditions of adsorption process, *i.e.* to avoid precipitation of $Cd(OH)_2$. During equilibration of a solution of Cd^{2+} ions with an adsorbent, the pH value changes and the final value generally depends on pH_{pzc} of the adsorbent, solid/liquid ratio, mechanisms of adsorption (when cations form inner-sphere

complexes, solution pH value decreases in comparison to the value in a solution of inert electrolyte) [11], etc. According to the results of the pH_{pzc} determination (Fig. 6.13, as an example), upon the equilibration of the adsorbents with solutions of NaCl as inert electrolyte, the values of pH_f were between 8.9 and 9.5, depending on the type of the sample, over a wide range of pH_i values, at $S/L = 0.02$ g/20 cm^3. At these pH values, the precipitation of $Cd(OH)_2$ should start at relatively low Cd^{2+} concentrations (according to the value of the solubility product constant of $Cd(OH)_2$, the precipitation starts at the concentration of about 10–15 mg/dm^3 for pH = 9 and even lower at higher pH values). When the adsorption experiments were performed at $S/L = 0.02$ g/20 cm^3 and $c_i = 130$ mg/dm^3, the pH_f values in all cases were lower than pH_{pzc}, indicating specific adsorption of Cd^{2+}, i.e. formation of inner-sphere complexes. However, in some cases, the pH_f was near 9. In order to avoid $Cd(OH)_2$ precipitation with certainty, the experiments were then conducted at a lower S/L ratio (0.02/100 cm^3) and at lower Cd^{2+} concentration (34.0 mg/dm^3). The results are shown in Table 6.4.

Table 6.4. Adsorption capacity, q_e, and pH_f for the adsorption of Cd^{2+} onto the composites and pure compounds from a solution of concentration $c_i = 34.0$ mg/dm^3 at $pH_i = 7.0 \pm 0.1$, for $S/L = 0.02$ g/100 cm^3 [156]

Sample	pH_f	q_e (mg/g)
SEP	6.2	25.5
AAS	6.0	18.7
nZVI	8.6	164.9
SEP-nZVI(10:1)	6.8	54.8
SEP-nZVI(5:1)	6.9	72.7
SEP-nZVI(2.5:1)	7.3	111.4
SEP-nZVI(2:1)	7.6	121.9
AAS-nZVI(10:1)	6.7	55.5
AAS-nZVI(5:1)	6.8	60.8
AAS-nZVI(2.5:1)	7.2	123.2
AAS-nZVI(2:1)	7.2	123.3

As seen from Table 6.4, the adsorption capacity of AAS was lower than that of SEP due to the removal of structural magnesium during acid activation, as was shown previously [11], while the capacity of nZVI was much higher than those of both SEP and ASEP. Therefore, the adsorption capacities of the composites increased as the quantity of nZVI increased, regardless of the decrease in the specific surface area (Table 6.2). Except for nZVI, final pH values were far below 9, and increased as the quantity of nZVI in the composites increased. As was mentioned previously, the pH_f depends on the interactions of the surface functional groups with H^+/OH^- and Cd^{2+} ions. The formation of inner-sphere complexes of Cd^{2+} with surface functional groups causes a decrease in the solution pH and the decrease is proportional to the quantity of adsorbed Cd^{2+} ions [11]. However, compared to SEP and AAS, a smaller decrease was found in the case of nZVI, which had the highest adsorption capacity. This indicates a much higher number of surface functional groups, which can bind both H^+ and Cd^{2+} ions, resulting in the increased adsorption capacity of nZVI.

The adsorption capacity of AAS–nZVI(2:1) was practically the same as that of AAS–nZVI(2.5:1), regardless of the higher nZVI quantity, probably due to high aggregation of nZVI particles in AAS–nZVI(2:1). Unlike the AAS-based samples, the adsorption capacity of the SEP–nZVI composites increased continually with increasing quantity of nZVI, owing to better dispersibility of the nZVI particles in SEP–nZVI than in AAS–nZVI. However, despite the better nZVI dispersibility, the adsorption capacities of the composites SEP–nZVI were not higher than those of the AAS–nZVI composites.

In order to compare the maximal adsorption capacity of the composites, the adsorption isotherms were determined for the samples with ratio SEP/AAS:nZVI = 2.5:1 and compared with the adsorption isotherms for the pure compounds. To avoid $Cd(OH)_2$ precipitation, the experiments were performed at ratio S/L=0.02g/100 cm^3.

6.3.1.2. Adsorption isotherms

The adsorption isotherms for SEP–nZVI(2.5:1) and AAS–nZVI(2.5:1) and for the pure compounds are presented in Fig. 6.21. In addition, to analyze the influence of

prolonged ultrasound treatment on the Cd^{2+} adsorption, the adsorption isotherms for SEP–nZVI(2.5:1)* and AAS–nZVI(2.5:1)* were also determined and shown in Fig. 6.21. In all cases, the final pH was below 8.5, $i.e.$ $Cd(OH)_2$ was not precipitated. The adsorption results were analyzed by the Langmuir [16], Freundlich [18] and Sips isotherm models [19]. The isotherms parameters and the related correlation coefficients are given in Table 6.5.
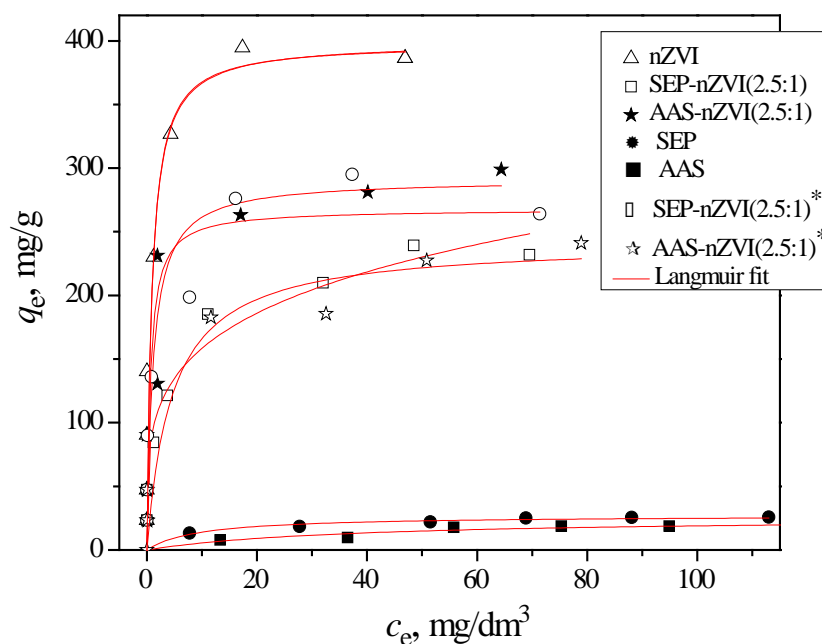
Fig. 6.21. Adsorption isotherms for pure compounds and samples SEP:nZVI(2.5:1) SEP–nZVI(2.5:1)*, AAS:nZVI(2.5:1) and AAS–nZVI(2.5:1)* at $pH_i = 7.0 \pm 0.1$ and S/L=0.02 g/100 cm^3.

The adsorption isotherms confirmed much higher adsorption capacity of nZVI for Cd^{2+} ions compared to SEP and AAS, while the capacities of composites lied between the capacities of the pure compounds. In addition, the capacity of AAS–nZVI(2.5:1) was higher than that of SEP–nZVI(2.5:1) but, in both cases, the values were significantly higher than expected for a simple mixture of nZVI and SEP/AAS at the mass ratio 2.5:1 (for 71 mas. % of SEP/AAS and 29 mas. % of nZVI, the adsorption capacity would be approximately 0.71·25 mg/g + 0.29·400 mg/g ≈133 mg/g, where 25 mg/g is the capacity of SEP and 400 mg/g capacity of nZVI, Table 6.5.). This indicates

that the presence of SEP or AAS improved the dispersion of nZVI, i.e. decreased agglomeration in comparison to pure nZVI, providing higher adsorption capacity. Despite the fact that the dispersion of nZVI in SEP–nZVI(2.5:1) is higher than in AAS–nZVI(2.5:1), its adsorption capacity is lower than that of AAS–nZVI(2.5:1). The reason could be higher oxidation of SEP–nZVI(2.5:1) during the synthesis, as was evidenced by thermal analysis (Fig. 6.12). According to the literature, the adsorption capacities of iron oxides and hydroxides are much lower [157, 158, 159, 160] than that of nZVI [118, 161, 162, 163], although the capacities of the nZVI samples differ significantly among themselves due to both different conditions during the adsorption experiments and different properties of the nZVI samples, mainly particle size and oxidation/aggregation degree.

To compare the adsorption capacity of sepiolite/nZVI and sepiolite/iron(III)-oxyhydroxide composites, the adsorption isotherm for the Fe(III)-sepiolite, synthesized previously [12] with a ratio SEP/Fe = 3.5:1, was determined at the same initial pH value (Fig. 6.22). The Langmuir, Freundlich and Sips models fit curves are presented with the experimental data in Fig. 6.22.
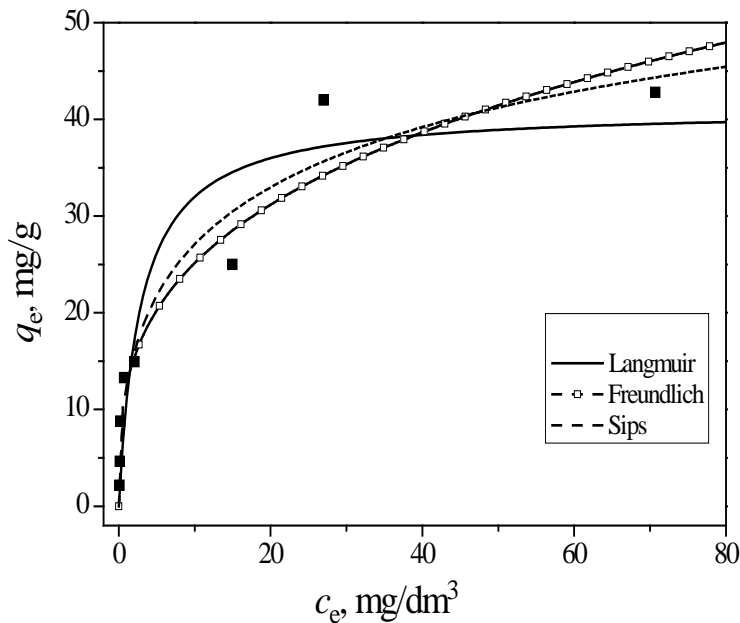
Fig.6.22. The adsorption isotherm for Cd^{2+} ions onto Fe(III)-sepiolite at 25 ºC and initial pH = 7.0 ± 0.1 [164].

Obviously, the adsorption capacity of the sepiolite/iron(III)-oxyhydroxide is much lower than that of nZVI-based composites. Thus, in order to obtain a SEP/AAS–

nZVI composite with high adsorption capacity, it is necessary to prevent both aggregation and oxidation during the synthesis. On the other hand, according to XPS analysis, oxidation during adsorption is beneficial for cadmium removal. Moreover, in recent investigations [155], strong oxidation agents were used with zero-valent iron (ZVI) in order to accelerate the oxidation during adsorption. It was shown that the combination of zero-valent iron and oxidation agent was a very efficient way for the removal of some heavy metals from water through multiple mechanisms, including adsorption and co-precipitation.

Prolonged ultrasound treatment of the support suspension provided higher adsorption capacity for the SEP-based composite (sample SEP–nZVI(2.5:1)*), despite worse textural and microstructure properties in comparison to sample SEP–nZVI(2.5:1). On the other hand, the maximum Cd^{2+} uptake capacity of AAS-nZVI composite decreased with the ultrasound treatment prolongation. Having in mind that the prolonged treatment caused the shortening of sepiolite fibers (Fig. 6.6), it can be supposed that removal of oxygen from the sepiolite channels was more efficient and the nZVI oxidation during synthesis was less pronounced. In that way, the adsorption capacity was higher, regardless of lower dispersibility and lower specific surface area. In the case of sample AAS–nZVI(2.5:1)*, the dispersibility and specific surface area are higher than of sample AAS–nZVI(2.5:1), but nZVI crystals are smaller, according to XRD analysis (Fig. 6.1), which probably caused higher oxidation during synthesis and consequently lower adsorption capacity.

The results presented in Table 6.5 show that all three models applied fit the adsorption equilibrium data well. It is well known that the Langmuir model assumes monolayer adsorption at specific homogeneous sites and formation of strong, usually chemical bonds [16], while the Freundlich model describes adsorption, possibly multilayer, on a heterogeneous surface consisting of non-identical and energetically non-uniform sites [18]. The Sips model combines the Freundlich and Langmuir ones, assuming heterogeneous adsorption at lower concentration as it predicts the Freundlich model and formation of monolayer at higher concentration, as in the case of the Langmuir model [19]. Based on good fiting of the results with all three models, formation of strong bonds between Cd^{2+} and adsorbents sites of different energy is assumed, until a monolayer was formed.

Table 6.5. Langmuir, Freundlich and Sips isotherms constants for the adsorption of Cd^{2+} onto the composites and pure compounds at $pH_i = 7.0 \pm 0.1$ (q_m (mg/g), K_L (dm^3/mg), K_f ($mg^{(1-1/n)}$ $dm^{3/n}$/g), K_a (dm^3/mg)$^{n}_{s}$))

		nZVI	AAS-nZVI(2.5:1)	SEP-nZVI(2.5:1)	AAS-nZVI(2.5:1)[*]	SEP-nZVI(2.5:1)[*]	SEP	AAS	Fe(III)-sepiolite
Langmuir	q_m	399.3	291.2	240.4	242.0	267.8	27.2	26.0	41.1
	K_L	1.12	0.87	0.32	0.22	1.58	0.11	0.03	0.35
	R^2	0.997	0.936	0.981	0.928	0.899	0.983	0.932	0.888
Freundlich	K_f	255.7	127.0	92.7	116.7	148.1	8.4	2.8	12.3
	$1/n$	0.12	0.22	0.23	0.16	0.17	0.24	0.42	0.31
	R^2	0.964	0.866	0.978	0.937	0.926	0.985	0.917	0.938
Sips	q_m	397.6	302.0	286.3	224.2	357.4	36.3	25.5	79.3
	K_a	1.12	0.85	0.35	0.01	0.72	0.18	0.03	0.18
	n_s	1.04	0.81	0.62	0.16	0.41	0.55	1.03	0.46
	R^2	0.996	0.928	0.990	0.784	0.905	0.987	0.916	0.948

6.3.1.3. Effect of contact time

The effect of the contact time on the amount of Cd^{2+} adsorbed onto SEP-nZVI(2.5:1) and AAS-nZVI(2.5:1) is shown in Fig. 6.23. It can be seen that the removal of Cd^{2+} ions by adsorption onto SEP-nZVI(2.5:1) and AAS-nZVI(2.5:1) was comprised of three steps: rapid adsorption in the first 0.5 h, then slightly decreased adsorption, followed by its slow increase after 2 h, until the equilibrium was reached. The high number of active sites available at the beginning of adsorption explains the initial fast Cd^{2+} uptake at the composites surface. However, some rapidly adsorbed ions were desorbed in the next step. After that, a slow increase of the amount of adsorbed Cd^{2+} ions was observed, since the most of adsorption sites were occupied and Cd^{2+} concentration in the solutions was decreased; thus, the adsorption became less efficient.
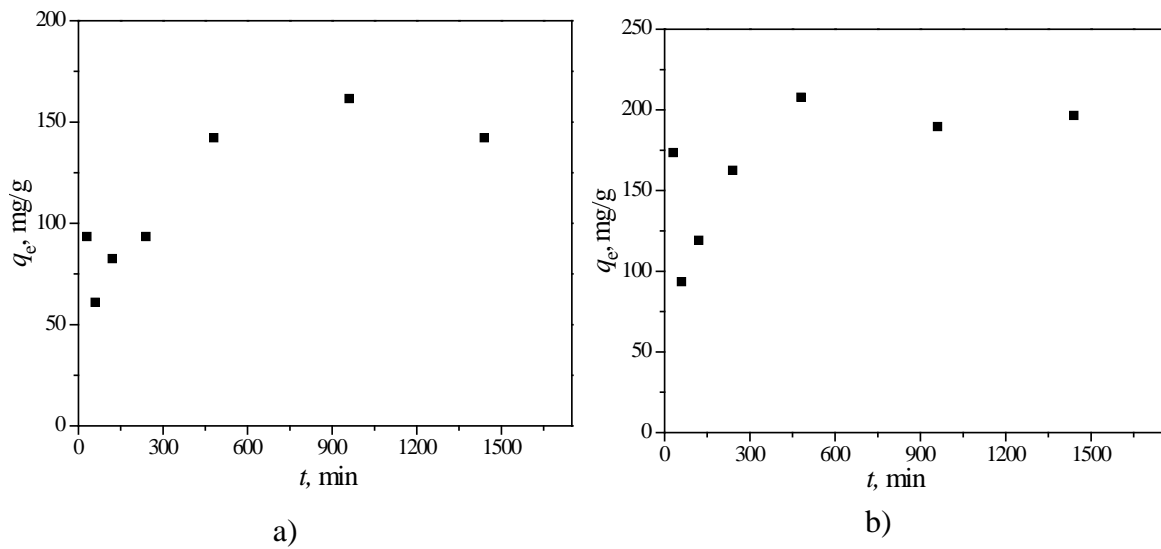
Fig. 6.23. The effect of contact time on Cd^{2+} adsorption onto: a) SEP-nZVI(2.5:1) and b) AAS-nZVI(2.5:1), at 25°C and initial pH of 7 ± 0.1 ($c_i(Cd^{2+})$ = 100 mg/dm^3; S/L = 0.02 g/100 cm^3).

In order to obtain more information about the mechanism of adsorption and the potential rate-controlling steps, the two most widely applied kinetic models were used to fit the experimental data: the pseudo-first order and the pseudo-second order kinetic models (Eqs. 2.9 and 2.16). The obtained parameters for the adsorption kinetics are given in Table 6.6, while the pseudo-second order model fits are shown in Fig. 6.24.

Table 6.6. Kinetic parameters for Cd^{2+} adsorption onto SEP-nZVI(2.5:1) and AAS-nZVI(2.5:1)

Adsorbent	Pseudo-first order			Pseudo-second order			
	k_1, 1/min	q_e, mg/g	R^2	k_2, g/mg·min	q_e, mg/g	R^2	h, mg/g·min
SEP-nZVI(2.5:1)	0.000967	53.0	0.586	0.0000386	161.0	0.958	1.00
AAS-nZVI(2.5:1)	0.002276	63.9	0.565	0.0001091	202.4	0.985	4.47

a)   b)
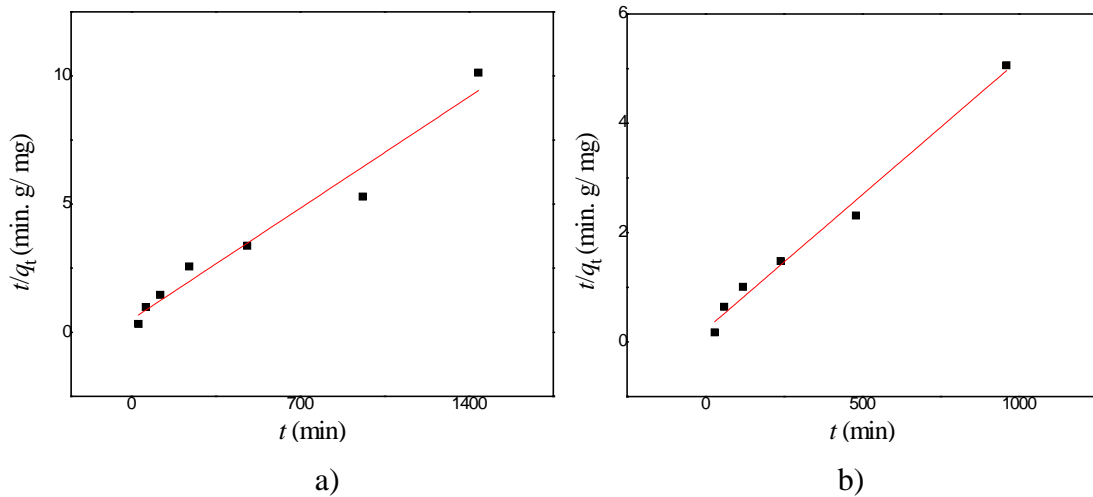
Fig. 6.24. Linear fitting of the kinetic data for Cd^{2+} adsorption onto: a) SEP-nZVI(2.5:1) and AAS-nZVI(2.5:1) by the pseudo-second order kinetic model.

According to obtained kinetic parameters (Table 6.6) it is clear that the pseudo-second order model fits the experimental data better than the pseudo-first order model, since the q_e values estimated by this model are in good agreement with the experimental results and that the values of the correlation coefficients are close to 1. The fact that the pseudo-second order model gave better agreement with the experimental data is not surprising, since this seems to be a generally prevalent observation in heavy metal adsorption studies [165]. Further, this suggests that the rate-limiting step in heavy metal adsorption is chemisorption, which involves valence forces through the sharing or exchange of electrons between adsorbent and adsorbate, complexation, coordination and/or chelation, rather than physisorption [165]. As the correlation coefficients values for the pseudo-second order model are high (Table 6.6), it can be stated that the adsorption of Cd^{2+} onto SEP-nZVI and AAS-nZVI occurs through chemisorptions, as it already concluded according to adsorption modeling (formation of strong bonds with the adsorbent sites) and final pH values (formation of inner-sphere complexes).

Kinetic analysis confirmed that adsorption capacity of AAS-nZVI was higher than of SEP-nZVI, as shown by adsorption isotherms (Fig. 6.21). In addition, according to the values of rate constants, the rate of adsorption onto AAS-nZVI was higher, as well as initial adsorption rate.

6.3.1.4. Effect of temperature

The effect of temperature on the Cd^{2+} adsorption onto samples SEP-nZVI(2.5:1), SEP-nZVI(2.5:1)*, AAS-nZVI(2.5:1) and AAS-nZVI(2.5:1)* is illustrated in Fig. 6.25, where the adsorption isotherms at 25, 40 and 50 °C are presented.
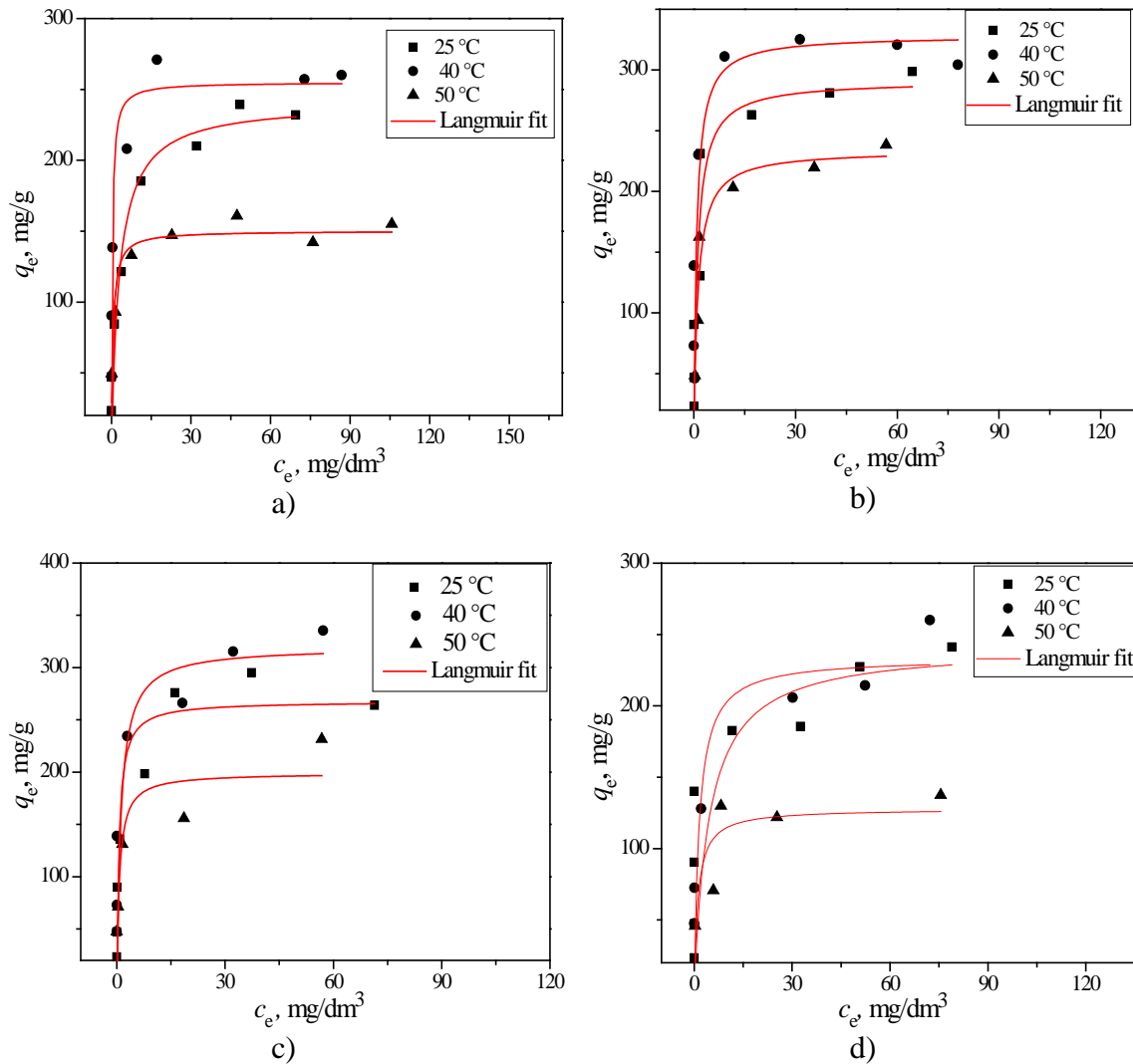
Fig. 6.25. Adsorption isotherms for Cd^{2+} ions at different temperature onto: a) SEP-nZVI(2.5:1), b) AAS-nZVI(2.5:1), c) SEP-nZVI(2.5:1)* and d) AAS-nZVI(2.5:1)* at pH= 7.0 ± 0.1.

It is known that the adsorption capacity of an adsorbent increases with the temperature increase if the adsorption process is endothermic and vice versa, the capacity decreases with the temperature if the process is exothermic. According to Fig. 6.24, Cd^{2+} adsorption on all investigated adsorbents increased with the temperature increasing from 25 to 40 °C and than decreased with further increase of temperature up to 50 °C. Such unusual behavior can be explained taking into account that several factors possibly affect the temperature-dependence of sorption reactions. First, Cd^{2+} ions are well-hydrated in aqua solutions and, in order to be adsorbed onto an adsorbent,

the ions have to denude of their hydration sheath [166], which is an endothermic process. On the other hand, the adsorption of dehydrated ions is exothermic process. Overall enthalpy change of the ions adsorption depends on the values of dehydration end adsorption enthalpy. As the adsorption of Cd^{2+} ions increased from 25 to 40 °C, it can be supposed that the enthalpy of dehydration was higher than the enthalpy of adsorption. But, with the further temperature increase, the Cd^{2+} adsorption decreased, which indicates an exothermic process. The results suggest that endothermicity of the dehydration process decrease with the temperature, while the enthalpy of adsorption increased, so the overall process of adsorption became exothermal, which caused the decreasing of the adsorption capacity. In addition, some authors stated that physical damage to the adsorbent could occur at high temperature, reducing its adsorption capacity. Decreasing of adsorption capacity with the temperature increasing can be also attributed to the increased solubility of the metal ions in the solution which favored the migration of metal ions from the adsorbent to the liquid phase [167]. Further, aqueous speciation of the adsorbate solutes is temperature dependent, which will in turn affect adsorption process. Moreover, an increase in temperature causes a decrease in the point of zero charge, which changes the surface charge of adsorbent at constant pH value [168] and, consequently, its adsorption capacity. Taking into account all the mentioned possible influences of the temperature on the capacity of adsorbent, the observed dependence of Cd^{2+} adsorption on temperature is not unexpected. Because of such temperature dependence of Cd^{2+} adsorption, thermodynamic parameters of the Cd^{2+} adsorption could not have been determined.

The Langmuir, Freundlich and Sips isotherms parameternd the coefficients of correlation are presented in Tables 6.7-6.9. Obviously, none of the three models fits the results of the adsorption on higher temperatures well.

Table 6.7. Langmuir isotherm constants and coefficient of correlation for the adsorption of Cd^{2+} onto the composites, at different temperatures

Adsorbent	T, °C	K_L, dm^3/mg	q_m, mg/g	R^2
SEP-nZVI(2.5:1)	25	0.32	240.4	0.981
	40	3.12	255.0	0.703
	50	1.68	150.2	0.892
AAS-nZVI(2.5:1)	25	0.87	291.2	0.936
	40	1.17	328.3	0.664
	50	0.81	233.9	0.932
SEP-nZVI(2.5:1)*	25	1.58	267.8	0.899
	40	0.87	319.6	0.572
	50	1.34	199.3	0.696
AAS-nZVI(2.5:1)*	25	0.22	242.0	0.928
	40	0.654	233.7	0.738
	50	0.871	127.9	0.589

Table 6.8. Freundlich isotherm constants and coefficient of correlation for the adsorption of Cd^{2+} onto the composites, at different temperatures

Adsorbent	T, °C	K_f, dm^3/mg	$1/n$	R^2
SEP-nZVI(2.5:1)	25	92.7	0.23	0.978
	40	173.1	0.10	0.703
	50	88.4	0.13	0.892
AAS-nZVI(2.5:1)	25	127.0	0.22	0.866
	40	172.7	0.16	0.472
	50	107.4	0.21	0.808
SEP-nZVI(2.5:1)*	25	148.1	0.17	0.926
	40	189.6	0.13	0.589
	50	100.2	0.20	0.784
AAS-nZVI(2.5:1)*	25	116.7	0.16	0.937
	40	111.4	0.18	0.904
	50	66.3	0.18	0.664

Table 6.9. Sips isotherm constants and coefficient of correlation for the adsorption of Cd^{2+} onto the composites, at different temperatures

Adsorbent	T, °C	q_m, mg/g	K_a	n_S	R^2
SEP-nZVI(2.5:1)	25	286.3	0.35	0.62	0.990
	40	269.1	194.6	124.8	0.467
	50	164.4	1.20	0.57	0.955
AAS-nZVI(2.5:1)	25	302.0	0.85	0.81	0.928
	40	275.9	0.63	5.53	0.503
	50	230.0	0.82	1.13	0.911
SEP-nZVI(2.5:1)[*]	25	357.4	0.72	0.41	0.905
	40	238.9	0.02	74.69	0.201
	50	187.6	0.003	0.20	0.677
AAS-nZVI(2.5:1)[*]	25	224.2	0.01	0.16	0.784
	40	100.4	235.3	39.61	0.234
	50	171.3	0.56	0.47	0.573

6.3.2. Cr(VI) adsorption

The adsorption of Cr(IV) ions were investigated at $pH_i = 2.0 \pm 0.1$ and 3.0 ± 0.1 at different initial concentration in order to determine the adsorption isotherms for the composites and to compare their maximal adsorption capacity.

Solution pH is an important parameter that influences the adsorption because it determines both the surface charge of the adsorbent and existing form of Cr(VI). Regardless of different forms, Cr(VI) is always present as anion: $HCrO_4^-$ is the main species at low concentrations at pH 2–4, CrO_4^{2-} becomes dominant species at $pH \geq 7$, whereas $Cr_2O_7^{2-}$ and $HCr_2O_7^-$ exist only in solutions of high concentration.

It was shown that the removal of Cr(VI) by various adsorbents is highly dependent on the solution pH [47, 67, 102, 121, 128, 133, 134]. Generally, the efficiency of Cr (VI) removal decreases with the increase in pH. One of the reasons is the increasing of negative charge on the adsorbent surface and, thus, stronger repulsive

forces between Cr(VI) anions and negatively charged surface. When pH decreases, more H^+ ions are present in solution and degree of protonation of the surface functional groups of the adsorbent increases, which is favorable for the adsorption of negatively charged ions. In addition, in the case of nZVI and the nZVI-based composites, acid condition favors the reduction of Cr(VI) to Cr(III) by nZVI:

$$Cr_2O_7^{2-} + 2Fe + 14H^+ \rightarrow 2Cr^{3+} + 2Fe^{3+} + 7H_2O \tag{6.1}$$
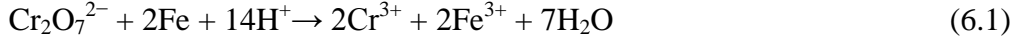
It is believed that the removal of Cr(VI) involves instantaneous adsorption of Cr(VI) on the nZVI surface, where the electron transfer takes place. With the oxidation of nZVI to Fe^{3+}, Cr(VI) is reduced to Cr^{3+}, followed by the subsequent precipitation of mixed Cr and Fe hydroxides [78] (Eqs. 4.11. - 4.14).

At higher pH values, Cr(III) and Fe(III) hydroxides are undoubtedly developed, forming passivation layer which hindered Cr(VI) access to the nZVI surface and inhibited further decomposition of surface iron. At lower pH values, high concentration of H^+ causes corrosion of nZVI particles, additionally due to nZVI reaction with dissolved oxygen and with water itself (Eqs. 4.6-4.8). This would renew the fresh reactive sites and improve electron transfer from nZVI to Cr(VI), leading to a significant increase in the reduction of Cr(VI) to Cr(III) [135]. It should be noted that, although lower pH values could regenerate the reactive sites in nZVI particles, this would also decrease the lifespan of nZVI particles in longer periods.

Taking into account foregoing analysis and the fact that the commercial method for the removal of Cr(VI) from water is its reduction in acid conditions and $Cr(OH)_3$ precipitation in basic conditions [169], the Cr(VI) adsorption onto nZVI composites was analyzed in this work in acid conditions, at $pH_i = 2.0 \pm 0.1$ and 3.0 ± 0.1. The dependences of the adsorbed amount of Cr(VI), q_e, on the Cr(VI) equilibrium concentration, c_e, are shown in Figs. 6.26 and 6.27. Final pH values were in the region 2.5-3 for $pH_i = 2.0$ and for $pH_i = 3.0$ in the region 6.5-9. As the Cr(VI) concentration increased, final pH decreased.
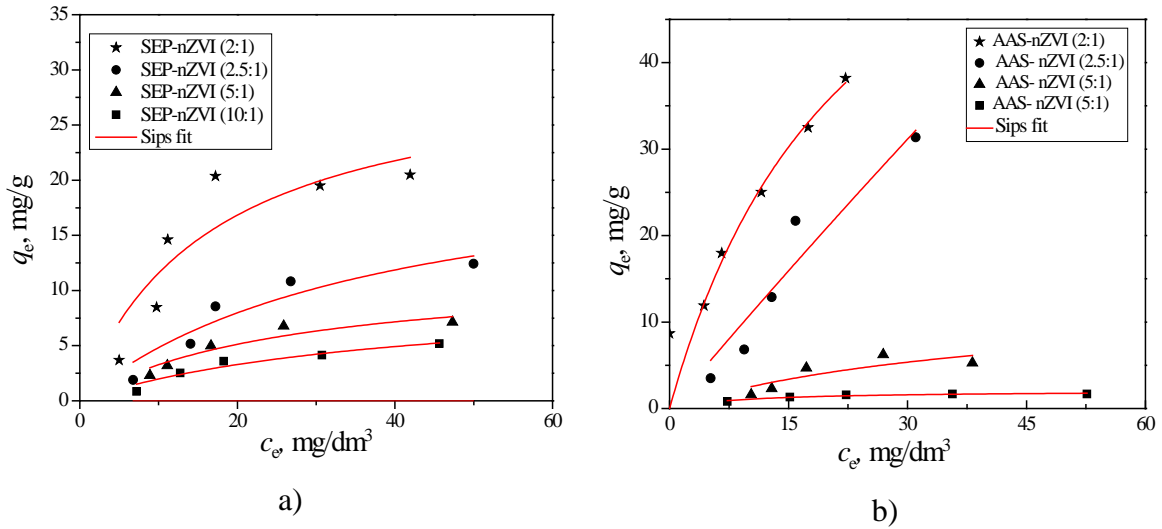
Fig. 6.26. Adsorption isotherm for Cr(VI) ions onto SEP-nZVI (a) and AAS-nZVI (b) composites at $pH_i = 2.0 \pm 0.1$.
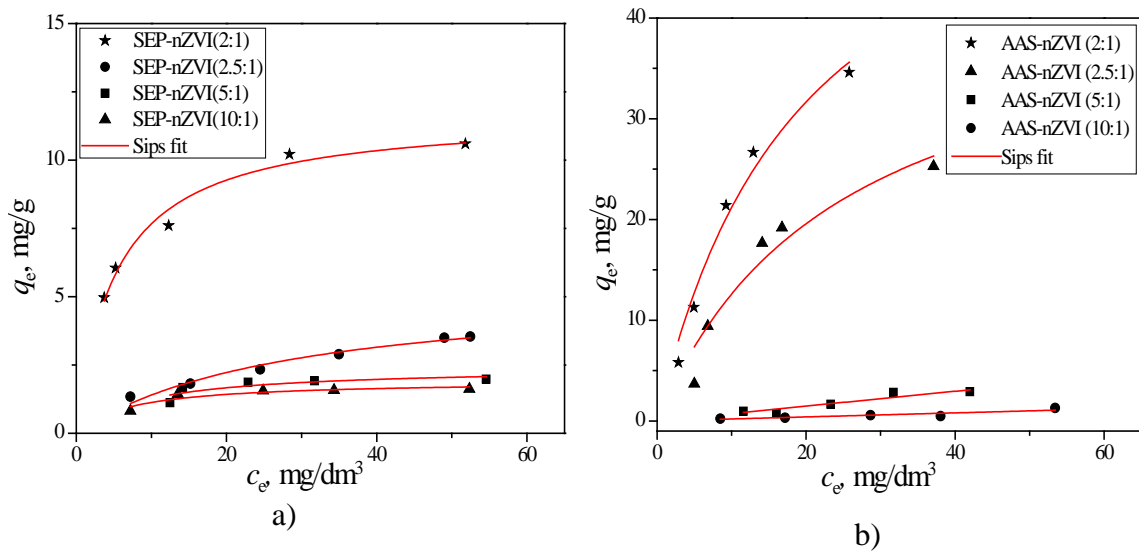
Fig. 6.27. Adsorption isotherm for Cr(VI) ions onto SEP-nZVI (a) and AAS-nZVI (b) composites at $pH_i = 3.0 \pm 0.1$.

As seen from Figs. 6.26 and 6.27, the adsorption capacity increased as the quantity of nZVI in the composite increased. According to the literature [47], adsorption capacities of the sepiolite and acid-activated sepiolites for Cr(VI) were negligible, even at low initial pH values, due to negatively charged surfaces in a wide range of pH values. Therefore, the content of nZVI was the factor that determined the adsorption capacity of the composites.

The adsorption capacities of AAS–nZVI composites were higher than of SEP-nZVI, as it is the case in Cd^{2+} adsorption. Obviously, degree of nZVI oxidation during synthesis is the factor that determines the adsorption capacity more than nZVI particles dispersivity.

Adsorption capacities of the composites were higher at $pH_i = 2.0 \pm 0.1$ than at $pH_i = 3.0 \pm 0.1$, as it was expected according to the literature. During the equilibration of the adsorbents with Cr(VI) solutions, pH value changed owing to different processes: interactions of H^+/OH^- ions with the surface functional groups (as in the case of equilibration with inert electrolyte during pH_{PZC} determination), interactions of Cr(VI) anions with the surface functional groups, Cr(VI) reduction to Cr^{3+} and its interaction with the surface functional groups, precipitation of $Cr(OH)_3$ and $Fe(OH)_3$ etc. Final pH values (pH_f) were higher than pH_i, mainly owing to high consumption of H^+ ions in the interaction with the adsorbent surface (high buffer capacity of adsorbents). Reasonably, final pH values were lower for $pH_i = 2.0 \pm 0.1$ than for $pH_i = 3.0 \pm 0.1$. Having in mind this pH increase which occured regardless the presence or absence of Cr(VI), it was difficult to detect the pH changes due to Cr(VI) interactions with the adsorbent and/or H^+/OH^- ions from the solution. Some conclusions can be drawn, however, from the pH changes recorded with the increase of Cr(VI) concentration during adsorption isotherms determination. Namely, pH decreased with the Cr(VI) concentration increasing, indicating higher releasing of H^+ ions into solution than the consumption/binding of the ions to the surface, i.e. higher consumption of OH^- ions. This H^+ releasing or OH^- consumption suggests specific adsorption of Cr^{3+} ions (inner-sphere complexes) or formation of $Cr(OH)_3$ and $Fe(OH)_3$. Accordingly, it can be concluded that the mechanism of Cr(VI) removal by SEP/AAS-nZVI composites involves Cr(VI) reduction and adsorption of Cr^{3+} or $Cr(OH)_3$ precipitation. In addition, electrostatic interactions between protonated surface and Cr(VI) anions is possible, especially at lower pH values.

The parameters of isotherm models are shown in Tables 6.10 and 6.11 for the samples with high adsorption capacity. By comparing the correlation coefficients, it was found that the equilibrium data was best described by Sips isotherm model.

Table 6.10. Langmuir, Freundlich and Sips isotherms constants for the adsorption of Cr(VI) onto the composites of SEP and AAS at $pH_i = 2.0 \pm 0.1(q_m$ (mg/g), K_L (dm^3/mg), K_f (mg$^{(1-1/n)}$ dm$^{3/n}$/g), K_a (dm^3/mg)^n_s))

		SEP-nZVI(2.5:1)	SEP-nZVI(2:1)	AAS-nZVI(2.5:1)	AAS-nZVI(2:1)
Langmuir model	K_L	0.026	0.061	0.002	0.043
	q_m	23.1	30.8	63.5	77.3
	R^2	0.859	0.748	0.897	0.857
Freundlich model	K_f	1.16	3.65	1.00	4.86
	n	0.63	0.49	1.01	0.67
	R^2	0.790	0.645	0.897	0.857
Sips model	q_m	13.0	23.8	44.0	53.9
	K_a	0.076	0.013	0.017	0.032
	n_S	2.66	3.94	3.28	0.833
	R^2	0.956	0.901	0.962	0.811

Table 6.11. Langmuir, Freundlich and Sips isotherms constants for the adsorption of Cr(IV) onto the composites of SEP and AAS at $pH_i = 3.0 \pm 0.1(q_m$ (mg/g), K_L (dm^3/mg), K_f (mg$^{(1-1/n)}$ dm$^{3/n}$/g), K_a (dm^3/mg)^n_s))

		SEP-nZVI(2.5:1)	SEP-nZVI(2:1)	AAS-nZVI(2.5:1)	AAS-nZVI(2:1)
Langmuir model	K_L	0.035	0.192	0.040	0.051
	q_m	5.4	11.7	43.9	62.7
	R^2	0.967	0.972	0.909	0.969
Freundlich model	K_f	0.45	3.79	3.00	4.65
	N	0.52	0.27	0.61	0.64
	R^2	0.995	0.940	0.839	0.922
Sips model	q_m	4.7	13.0	26.7	40.4
	K_a	0.032	0.226	0.009	0.029
	n_S	0.52	0.77	2.05	1.64
	R^2	0.994	0.968	0.974	0.999

6.3.3. Removal of dye C.I. Reactive Orange 16

6.3.3.1. Reductive and oxidative removal

Removal of anionic dye C.I. Reactive Orange 16 by the composites was analyzed in two ways: with addition of H_2O_2 to provide heterogeneous Fenton oxidation and without H_2O_2, when adsorption/reduction processes were dominant. The results obtained in the experiments without H_2O_2 are given in Table 6.12, while those obtained with different H_2O_2 concentrations are given in Table 6.13. In both cases, experiments were performed with the solution of dye concentration 74.0 mg/dm^3, with no pH adjustment (pH$_i$ of the solution was ~ 5.8).

Table 6.12. Results of adsorption of dye onto composites and pure compounds at pH$_i$ = 5.8 and temperature of 25 °C (c_i = 74.0 mg/dm^3, S/L = 0.04 g/20 cm^3)

Sample	pH$_f$	q_e, mg/g
nZVI	9.32	32.47
SEP	7.45	0.74
SEP-nZVI(10:1)	9.24	0.83
SEP-nZVI(5:1)	9.35	0.93
SEP-nZVI(2.5:1)	9.43	22.56
SEP-nZVI(2:1)	9.49	16.14
AAS	7.11	0.46
AAS-nZVI(10:1)	9.32	0.31
AAS-nZVI(5:1)	9.43	0.89
AAS-nZVI(2.5:1)	9.55	18.63
AAS-nZVI(2:1)	9.69	14.22

Similar as for chromates, adsorption capacities of sepiolite and acid-activated sepiolite for the dye were very low, as already shown [170]. Removal capacity of nZVI was much higher, while those of composites lied between the capacity of nZVI and SEP/AAS. As it was observed for chromates, the capacities of the composites with low

quantity of nZVI (ratio 10:1 and 5:1) were very low, comparable to the SEP and AAS capacities.

According to final pH values (Table 6.12), which are close to pH_{PZC}, the surface of the adsorbents is not positively charged and electrostatic interactions between dye anions and surface are not favorable. Therefore, the dye removal involves other mechanisms. According to the literature [170, 171, 172] adsorption followed by reduction is the main mechanism of dye removal. Upon reduction, chromofore structure in dye is degraded, leading to decolorization of dye solution. It is shown that Fe^0 can easily degrade azo structure (-N=N-), but the resulting intermediate organic compounds needs further mineralization into CO_2, H_2O and inorganic ions to achieve complete degradation. On the other hand, the resulting organic compounds can be adsorbed on the oxidized surface of nZVI or support. Therefore, the reductive mechanism implys a close contact between dye molecule and Fe^0, which is not likely in the case of the composites SEP/AAS-nZVI at $pH_i = 5.8$, due to negative charge of the surface. Consequently, the removal efficiency of the composites with low content of nZVI is low – electrons are probably spent on other oxidation agents before they reach dye molecules. The highest efficiency was achieved with the composites at ratio 2.5:1, while further increase of nZVI quantity decreased the removal efficiency. In addition, higher efficiency was achieved with SEP-nZVI(2.5:1) than with AAS-nZVI(2.5:1), contrary to results on Cr(VI) removal. Unlike Cr(VI), dye removal was investigated at relatively high pH_i and final pH values were very high, causing formation of passivation layer. In the case of composites with more aggregated nZVI particles, the passivation layer blocs the nZVI particles in the interior, preventing their reaction with the dye.

Dye removal by heterogeneous Fenton process implies oxidation by reactive $OH^\bullet$ radicals (Eq. 6.2) formed by reaction of hydrogen peroxide with ferrous ions (Eq. 4.10) generated in situ by nZVI corrosion (Eqs. 4.9).

$$OH^\bullet + dye \rightarrow oxidized\ dye + H_2O \tag{6.2}$$

The nZVI surface can reduce the ferric ions formed in the reaction 4.13 down to ferrous ions, and faster recycling of ferric iron at the iron surface occurs through Eq. (6.3):

$$2Fe^{3+} + Fe^0 \rightarrow 3Fe^{2+} \tag{6.3}$$

As a source of OH$^\bullet$ generation, H_2O_2 plays a very important role in Fenton's reaction. The effect of H_2O_2 dosage on the dye removal was examined by varying initial concentration of H_2O_2 (Table 6.13). Another main parameter in Fenton's reaction that catalytically decomposes H_2O_2 to generate OH$^\bullet$ is Fe^{2+}. The concentration of Fe^{2+} depends on the nZVI concentration and the conditions in the system (pH value, oxygen concentration etc.). In the experiments, concentration of the composites was constant, but the content of nZVI in the composites was different, therefore the nZVI concentration of was different (Table 6.13).

Table 6.13. Results of dye removal by the samples nZVI, SEP-nZVI and AAS-nZVI in the presence of different concentration of H_2O_2, at pH_i = 5.8 and temperature of 25 °C (c_i = 74.0 mg/dm^3, S/L = 0.04 g/20 cm^3)

Sample	$c(H_2O_2)$ = 4 mM		$c(H_2O_2)$ = 8 mM		$c(H_2O_2)$ = 12 mM	
	pH_f	q_e, mg/g	pH_f	q_e, mg/g	pH_f	q_e, mg/g
nZVI	9.03	18.49	9.18	13.06	9.19	17.01
SEP-nZVI(10:1)	8.99	2.70	9.28	5.66	8.92	6.22
SEP-nZVI(5:1)	9.07	2.58	9.41	6.16	9.39	6.53
SEP-nZVI(2.5:1)	9.04	2.09	9.39	3.70	9.37	4.93
SEP-nZVI(2:1)	9.14	5.79	9.47	4.01	9.48	5.66
AAS-nZVI(10:1)	9.12	2.65	9.40	4.07	9.40	4.63
AAS-nZVI(5:1)	8.51	0.12	8.78	1.04	9.03	1.10
AAS-nZVI(2.5:1)	9.23	3.39	9.56	5.41	9.53	6.22
AAS-nZVI(2:1)	9.39	3.88	9.72	6.22	9.70	6.84

Following listed results, the efficiency of the nZVI composites is lower than of pure nZVI, and there is no regular dependence of the efficiency on the nZVI quantity in the composite. Increasing of H_2O_2 concentration enhances the dye removal, but not significantly. Namely, in the presence of excess H_2O_2, its scavenging effect towards OH$^\bullet$ radicals is significant, resulting in the formation of less reactive species such as HO$_2^\bullet$[173, 174].

In comparison to reductive mechanism, higher efficiency was achieved with composites with lower quantities (ratio 10:1 and 5:1), while the efficiency of the composites with higher nZVI quantities is significantly lower. In addition, reductive mechanism for nZVI is more efficient than oxidative mechanism, as opposed to the literature [175]. Besides concentration of H_2O_2 and Fe^{2+}, many parameters influence the efficiency of Fenton oxidation process: solution pH, presence of some other organic substances, presence of ions that scavenge the radicals, etc. High pH values (pH_f, Table 6.13) were unfavorable for the Fenton reaction, because of the $Fe(OH)_3$ precipitation, preventing Fe^{2+} regeneration. It is well known that Fenton process is effective at low pH values, generally at pH = 2-4. Taking into account the efficiency of the nZVI and the composites (Table 6.13), it can be concluded that the supports used do not have positive influence on the heterogeneous Fenton process. Most likely, SEP/AAS reacts with H_2O_2, decreasing the quantity of H_2O_2 responsible for generating of $OH^{\bullet}$ radicals in the reaction with Fe^{2+} ions.

6.3.3.2. Effect of temperature on the reductive removal of dye

Reductive removal of dye by the samples which showed the highest efficiency, SEP-nZVI(2.5:1) and AAS-nZVI(2.5:1), was investigated at different temperatures, by determining the dependence of q_e on c_e. The results are presented in Fig. 6.28. Langmuir, Freundlich and Sips isotherms constants are summarized in Table 6.14. In the Fig. 6.28, the Langmuir fit curves, as the best fit, are presented with the experimental data.
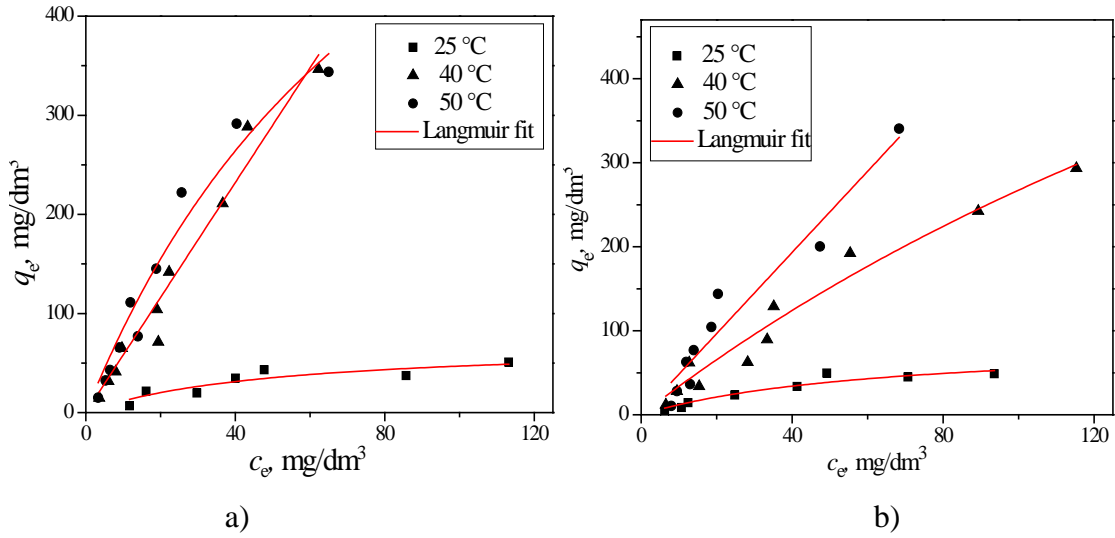
Fig. 6.28. Adsorption isotherms for dye onto: a) SEP-nZVI(2.5:1) and b) AAS-nZVI(2.5:1) at pH= 5 and T = 25, 40, 50 °C.

Table 6.14. Langmuir, Freundlich and Sips isotherms constants correlation coefficients (R^2) for the adsorption of C. I. Reactive Orange 16 onto SEP-nZVI(2.5:1) and AAS-nZVI(2.5:1) at pH_i = 5.0 ± 0.1 and different temperatures ((q_m (mg/g), K_L (dm^3/mg), K_f (mg$^{(1-1/n)}$ dm$^{3/n}$/g), K_a (dm^3/mg)^n_s))

		SEP-nZVI(2.5:1)			AAS-nZVI(2.5:1)		
		T, °C			T, °C		
		25	40	50	25	40	50
Langmuir model	K_L	0.020	0.017	0.011	0.016	0.003	0.001
	q_m	70.3	387.4	395.8	65.4	375.3	384.2
	R^2	0.788	0.965	0.959	0.911	0.961	0.948
Freundlich model	K_f	0.525	5.31	13.63	2.9	4.78	4.70
	$1/n$	4.25	1.02	0.79	0.65	0.87	1.01
	R^2	0.741	0.965	0.938	0.862	0.956	0.934
Sips model	q_m	52.07	67.5	69.24	14.58	58.72	53.35
	K_a	0.005	0.007	0.01	0.054	0.015	30.9
	n_s	1.6	87.4	135.7	66.8	67.2	86.1
	R^2	0.761	0.346	0.267	0.421	0.386	0.438

It is evident that the removal efficiency increased significantly with the temperature increase, and was slightly more intensive for the sample SEP-nZVI(2.5:1) than for AAS-nZVI(2.5:1). Such strong influence of temperature on the removal efficiency should be related to the following issues: (i) rate of reaction (reduction) increases with the temperature, (ii) decrease in the point of zero charge with increasing temperature changes the surface charge of the samples leading to lower final pH values; therefore, passive layer is formed to a lesser extent; (iii) the removal of the passivation layer from the nZVI particles is more intensive at higher temperatures, rendering the nZVI surface more available for the dye and thus resulting in more efficient reduction process. nZVI particles are better dispersed in the sample SEP-nZVI(2.5:1) than in AAS-nZVI(2.5:1), so the surface of nZVI after removal of oxide layer is larger and more available in SEP-based composite.

7. Conclusions

In this investigation, nanoscale zero-valent iron (nZVI) particles were loaded via chemical reduction onto natural (SEP) and partially acid-activated (AAS) sepiolites at different support/nZVI mass ratios (10:1, 5:1, 2.5:1 and 2:1) in order to obtain composites with good nZVI dispersibility and high efficiency for the removal of Cd^{2+}, CrO_4^{2-} and dye C. I. Reactive Orange 16 from water. In the synthesis process, duration of the ultrasonic treatment of the SEP/AAS suspensions was varied (10 and 30 min) to achieve good de-aggregation of the sepiolite fibers to host efficiently nZVI particles.

Morphology analysis by scanning electron microscopy (SEM) showed that good dispersibility without noticeable aggregation of the spherical nZVI particles was achieved with SEP at the SEP:nZVI mass ratios $\geq$ 2.5:1. Despite the higher surface area of AAS, the dispersibility of nZVI particles was lower when AAS was used as the support, because of stronger bonds between the AAS fibers, which could not be broken during synthesis of the composites. The results of SEM analysis were in good correlation with those of the textural parameters determination: the samples with high degree of nZVI agglomeration had low specific surface area and both micro- and meso-porosity, similar to the values for pure nZVI. Prolonged ultrasound treatment improved de-aggregation of AAS, but caused shortening of the fibers in SEP and their re-aggregation.

The presence of Fe^0 in the composites was confirmed by both X-ray diffraction (XRD) and differential-thermal/thermo-gravimetric (DTA/TGA) analyses. The DTA/TGA results in air and nitrogen indicated higher content of iron oxide in the composite with SEP than with AAS, at the same support/nZVI ratio. The iron oxide was formed by Fe^0 oxidation during synthesis. This was explained by the presence of oxygen molecules in the channels of SEP, which were destroyed during acid-activation of sepiolite. Thus, oxygen was not trapped inside the AAS sample.

Based on SEM and DTA/TGA results, nZVI particles were better dispersed when SEP was used as a support, but a lower degree of oxidation during the synthesis was achieved using AAS.

The high values of point of zero charge of all the composites indicate high basicity of surface due to the presence of basic Fe–OH groups, proven by infrared spectroscopy (FTIR).

X-Ray photoelectron spectroscopy (XPS) of the SEP/nZVI composite, ratio 2.5:1, before and after Cd^{2+} adsorption, confirmed that the surface of nZVI was composed of oxidized iron species. Metallic iron was not present on the surface but it was detected after sputtering, at a depth of 40 nm beneath the original surface. The content of Fe^0 decreased after Cd^{2+} adsorption as a result of the oxidation during adsorption process. The XPS depth profile showed that cadmium was present not only at the surface of the composite, but also in the subsurface region, whereas its concentration was higher on the surface.

Regardless of the decrease in the specific surface area, the adsorption capacities of the composites for Cd^{2+} ions increased as the quantity of nZVI increased, due to much higher adsorption capacity of nZVI for Cd^{2+} than that of both SEP and ASEP. The adsorption isotherms confirmed that the presence of SEP and AAS as supports decreased agglomeration of nZVI particles in comparison to pure nZVI, providing higher adsorption capacities of nZVI in the composites than of pure nZVI. Taking into account that the adsorption capacities of the SEP/nZVI composites were higher than that of previously studied sepiolite/iron(III)-oxide composite, it was concluded that the prevention of both aggregation and oxidation during the synthesis was necessary to obtain SEP/AAS–nZVI composite with a high adsorption capacity. On the other hand, oxidation during adsorption was beneficial for cadmium removal. Despite worse textural and microstructural parameters, prolonged ultrasound treatment of the support suspension provided higher adsorption capacity for the SEP-based composite, while the opposite was found in the case of AAS-based composite. Such findings confirmed the positive influence of the nZVI oxidation during the synthesis on the adsorption capacity. Based on modeling of adsorption data, the formation of strong bonds between Cd^{2+} and adsorbents sites of different energy and monolayer formation were supposed.

Adsorption capacity of the composites obtained at support/nZVI ratio = 2.5:1 for Cd^{2+} ions increased with a temperature increase from 25 to 40 ºC, but decreased with further temperature increase to 50 ºC.

The content of nZVI in the composites was a determining factor for efficiency of CrO_4^{2-} removal from water as the capacity of support was negligible. The adsorption capacities of AAS–nZVI composites were higher than of SEP-nZVI, suggesting that the degree of nZVI oxidation during synthesis had stronger influence on adsorption capacity than dispersivity degree of nZVI particles. The suggested possible mechanisms of CrO_4^{2-} removal by the composites comprise CrO_4^{2-} reduction to Cr^{3+}, followed by Cr^{3+} adsorption or $Cr(OH)_3$ and $Fe(OH)_3$ co-precipitation and electrostatic attraction between CrO_4^{2-} and protonated functional groups of the composite.

The efficiency of the composites with small content of nZVI for the removal of anionic dye C. I. Reactive Orange 16 was very low, but it was increased significantly when H_2O_2 was used due to the formation of Fenton reagens. On the other hand, the efficiency of the composites with higher content of nZVI was much higher without H_2O_2, when reductive mechanism was dominant, especially at higher temperatures.

The influence of temperature on the removal of the dye and Cd^{2+} ions indicated that the *in situ* formed oxide layer onto nZVI particles was beneficial for the removal of Cd^{2+}, but the detachment of oxide layer was desirable for the reductive mechanism of the removal.

8. References

[1] Do DD (1998) Adsorption analysis: equilibria and kinetics. Imperial College Press, London.

[2] http://cpe.njit.edu/dlnotes/CHE685/Cls11-1.pdf.

[3] Liu S (2015) Cooperative adsorption on solid surfaces. J Colloid Interface Sci 450: 224–238.

[4] Worch E (2012) Adsorption technology in water treatment. Walter de Gruyter GmbH & Co. KG, Berlin/Boston, Germany.

[5] Galan E (1996) Properties and application of palygorskite-sepiolite clays. Clay Miner 31: 443–453.

[6] Moreno-Castilla C (2004) Adsorption of organic molecules from aqueous solutions on carbon materials. Carbon 42: 83–94.

[7] Sposito G (1989) The chemistry of soils. Oxford Univ. Press, Oxford, England.

[8] Zhou Y-F, Haynes RJ (2010) Sorption of heavy metals by inorganic and organic components of solid wastes: significance to use of wastes as low-cost adsorbents and immobilizing agents. Crit Rev Environ Sci Technol 40: 909–977.

[9] Šljivić M, Smičiklas I, Pejanović S, Plećaš I (2009) Comparative study of Cu^{2+} adsorption on a zeolite, a clay and a diatomite from Serbia. Appl Clay Sci 43: 33–40.

[10] Everett DH (1972) Manual of symbol and terminology for physico–chemical quantities and units, appendix II: definitions, terminology and symbols in colloid and surface chemistry. Pure Appl Chem 31: 577–638.

[11] Lazarević S, Janković-Častvan I, Jovanović D, Milonjić S, Janaćković Đ, Petrović R (2007) Adsorption of Pb^{2+}, Cd^{2+} and Sr^{2+} ions onto natural and acid-activated sepiolites. Appl Clay Sci 37: 47–57.

[12] Lazarević S, Janković-Častvan I, Đokić V, Radovanović Ž, Janaćković Đ, Petrović R (2010) Iron-Modified sepiolite for Ni^{2+} sorption from aqueous solution: an equilibrium, kinetic, and thermodynamic study. J Chem Eng Data 55: 5681–5689.

[13] Appel C, Ma LQ, Rhue RD, Kennelley E (2003) Point of zero charge determination in soils and minerals via traditional methods and detection of electroacoustic mobility. Geoderma 113: 77–93.

[14] Erdem E, Karapinar N, Donat R (2004) The removal of heavy metal cations by natural zeolites. J Colloid Interface Sci 280: 309–314.

[15] http://www.separationprocesses.com/Adsorption/AD_Chp01d.htm.

[16] Langmuir I (1918) The adsorption of gases on plane surfaces of glass, mica and platinum. J Am Chem Soc 40: 1361–1403.

[17] Kuncek I, Sener S (2010) Adsorption of methylene blue onto sonicated sepiolite from aqueous solution. Ultrason Sonochem 17: 250–257.

[18] Freundlich H (1906) Uber die Adsorption in Losungen. Z Phys Chem 57: 385–470.

[19] Sips R (1948) Combined form of Langmuir and Freundlich equations J Chem Phys 16: 490–495.

[20] Gunay A, Arslankaya E, Tosun I (2007) Lead removal from aqueous solution by natural and pretreated clinoptilolite: adsorption equilibrium and kinetics. J Hazard Mater 146: 362–371.

[21] Pérez-Marín AB, Meseguer Zapata V, Ortuño JF, Aguilar M, Sáez J, Lloréns M (2007) Removal of cadmium from aqueous solutions by adsorption onto orange waste. J Hazard Mater 139: 122–131.

[22] Hernández-Montoya V, Pérez-Cruz MA, Mendoza-Castillo DI, Moreno-Virgen MR, Bonilla-Petriciolet A (2013) Competitive adsorption of dyes and heavy metals on zeolitic structures. J Environ Manag 116: 213–221.

[23] Qiu H, Lv L, Pan B-C, Zhang Q-J, Zhang W-M, Zhang Q-X (2009) Critical review in adsorption kinetic models. J Zhejiang Univ Sci A 10: 716-724.

[24] Brigatti MF, Lugli C, Poppi L (2000) Kinetics of heavy metal removal and recovery in sepiolite. Appl Clay Sci 16: 45–57.

[25] Augustine AA, Orike BD, Edidiong AD (2007) Adsorption kinetics and modeling of Cu(II) ion sorption from aqueous solution by mercaptoacetic acid modified Cassava (manihot sculenta cranz) wastes. EJEAFChe 6: 2221–2234.

[26] Anastopoulos I, Kyzas GZ (2016) Are the thermodynamic parameters correctly estimated in liquid-phase adsorption phenomena? J Mol Liq 218: 174–185.

[27] Ghosal PS, Gupta AK (2017) Determination of thermodynamic parameters from Langmuir isotherm constant-revisited. J Mol Liq 225: 137–146.

[28] Liu Y (2006) Some consideration on the Langmuir isotherm equation. Colloids Surf. A 274: 34–36.

[29] Liu Y(2009) Is the free energy change of adsorption correctly calculated?. J Chem Eng Data 54: 1981–1985.

[30] Milonjić SK (2007) A consideration of the correct calculation of thermodynamic parameters of adsorption. J Serb Chem Soc 72: 1363–136.

[31] Bhattacharya AK, Naiya TK, Mandal SN, Das SK (2008) Adsorption, kinetics and equilibrium studies on removal of Cr(VI) from aqueous solutions using different low-cost adsorbents. Chem Eng J 137: 529–541.

[32] Fan H-T, Fan X, Li J, Guo M, Zhang D, Yan F, Sun T (2012) Selective removal of arsenic(V) from aqueous solution using a surfaceion- imprinted amine-functionalized

[33] Galán E, Aparicio P (2015) Natural Mineral Nanotubes: Properties and Applications. Apple Academic Press, Inc., Canada.

[34] García-Romero E, Suárez M (2013) Sepiolite–palygorskite: Textural study and genetic considerations. Appl Clay Sci 86: 129–144.

[35] Suárez M, García-Romero E (2012) Variability of the surface properties of sepiolite. Appl Clay Sci 67–68: 72–82.

[36] Mitrovic M, Dojcinovic M, Vucelic D, Simic D, Martic M (1999) Sepiolite - an important mineral for industry and environment protection. Bull Chem Ttech Maced 18: 101–115.

[37] Brauner K, Preisinger A (1956) Struktur und entstehung des sepioliths. Tschermaks Miner Petz Mitt 6: 120–140.

[38] Singer A, Kirsten WFA, Buhmann C (1992) Occurrence of the sepiolite in the Northern Transvaal, South Africa. S Afr J Geol 95: 165–170.

[39] Nagata HS, Shimoda S, Sudo T (1974) Dehydration of bound water on sepiolite. Clays Clay Miner 23: 285–293.

[40] Serna C, Alrichs JL, Serratos JM (1975) Folding in sepiolite crystals. Clays Clay Miner 23: 452–457

[41] Dandy AJ (1968) Sorption of vapors by sepiolite. J Phys Chem 72: 334–339.

[42] Barrer RM, Mackenzie W (1954) Sorption by attapulgite. J Phys Chem 58: 568–572.

[43] Lazarević S, Jankovic-Častvan I, Radovanovic Z, Potkonjak B, Janaćković Đ, Petrović R (2011) Sorptionof Cu^{2+} and Co^{2+} from aqueous solutions onto sepiolite: an equilibrium, kinetic and thermodynamic study. J Serb Chem Soc 76: 101-112.

[44] Han Z-X, Zhu Z, Wu D-D, Wu J, Liu Y-R (2014) Adsorption kinetics and thermodynamics of acid blue 25 and methylene blue dye solutions on natural sepiolite. Synth React Inorg Metals 44: 140–147.

[45] Rytwo G, Nir S, Margulies L, Casal B, Merino J, Ruiz-Hitzky E, Serratosa JM (1998) Adsorption of monovalent organic cations on sepiolite: experimental results and model calculations. Clays Clay Miner 46: 340–348.

[46] Santos S, Boaventura R (2008) Adsorption modelling of textile dyes by sepiolite. Appl Clay Sci 42: 137–145.

[47] Marjanović V, Lazarević S, Janković-Častvan I, Potkonjak B, Janaćković Đ, Petrović R (2011) Chromium (VI) removal from aqueous solutions using mercaptosilane functionalized sepiolites. J Chem Eng 166: 198–206.

[48] Tumsek F, Avci O (2013) Investigation of kinetics and isotherm models for the acid orange 95 adsorption from aqueous solution onto natural minerals. J Chem Eng Data 58: 551–559.

[49] Ozdemir O, Armagan B, Turan M, Celik MS (2004) Comparison of the adsorption characteristics of azo-reactive dyes on mezoporous minerals. Dyes Pigm 62: 49–60.

[50] Bhattacharyya KG, Gupta SS (2008) Kaolinite and montmorillonite as adsorption for Fe(III), Co(II) and Ni(II) in aqueous medium. Appl Clay Sci 41: 1–9.

[51] Belzunce MJ, Mendioroz S, Haber J (1998) Modification of sepiolite by treatment with fluorides: structural and textural changes. Clays Clay Miner 46: 603–614.

[52] Inukai K, Miyawaki R, Tomura S, Shimosaka K, Irkeç T (1994) Purification of Turkish sepiolite through hydrochloric acid treatment. Appl Clay Sci 12: 119–216.

[53] Chitnis SR, Sharma MM (1997) Industrial applications of acid-treated clays as catalysts. React Funct Polym 32: 93–l15

[54] Sabah E, Turan M, Celik MS (2002) Adsorption mechanism of cationic surfactants onto acid- and heat- activated sepiolites. Water Res 36: 3957–3964.

[55] Vico LI (2003) Acid–base behaviour and Cu^{2+} and Zn^{2+} complexation properties of the sepiolite/water interface. Chem Geol 198: 213–222.

[56] Kara M, Yuzer H, Sabah E, Celik MS (2003) Adsorption of cobalt from aqueous solutions onto sepiolite. Water Res 37: 224–232.

[57] Hernandez LG, Rueda LI, Diaz AR, Anton CC (1986) Preparation of amorphous silica by acid dissolution of sepiolite: kinetic and textural study. J Colloid interface Sci 109: 150–160.

[58] Aznar AJ, Gutierrez E, Diaz P, Alvarez A, Poncelet G (1996) Silica from sepiolite: preparation textual properties and use as support to catalysts. Microporous Mater 6: 105-114.

[59] Balci S (1996) Thermal decomposition of sepiolite and variations in pore structure with and without acid pre-treatment. J Chem Technol Biot 66: 72–78.

[60] Valentine JL, Lopez-Manchado MA, Rodrigues A, Posadas P, Ibarra L (2007) Novel anhydrous unfolded structure by heating of acid pre-treated sepiolite. Appl Clay Sci 36: 245–255.

[61] Franco F, PozoM, Cecilia JA, Benítez-Guerrero M, Pozo E, Martín Rubí J (2014) Microwave assisted acid treatment of sepiolite: the role of composition and crystallinity. Appl Clay Sci 102: 15–27.

[62] Alkan M, Tekin G, Namli H (2005) FTIR and zeta potential measurements of sepiolite treated with some organosilanes. Micropor Mesopor Mater 84: 75–83

[63] Celis R, Hermosín MC, Cornejo J (2000) Heavy metal adsorption by functionalized clays. Environ Sci and Technol 34: 4593–4599.

[64] Özcan AS, Gök Ö (2012) Structural characterization of dodecyltrimethylammonium (DTMA) bromide modified sepiolite and its adsorption isotherm studies. J Mol Struct 1007: 36–44.

[65] Tartaglione G, Tabuani D, Camino G (2008) Thermal and morphological characterisation of organically modified sepiolite. Micropor Mesopor Mat 107: 161–168.

[66] Demirbaş Ö, Alkan M, Doğan M, Turhan Y, Namli H, Turan P (2007) Electrokinetic and adsorption properties of sepiolite modified by 3-aminopropyltriethoxysilane. J Hazard Mater 149: 650–656.

[67] Marjanović V, Lazarević S, Janković-Častvan I, Potkonjak B, Janaćković Đ, Petrović R(2013) Chromium (VI) removal from aqueous solutions onto amine-functionalized natural and acid-activated sepiolites. Appl Clay Sci 80–81: 202–210.

[68] Liang X, Sun G, Wang L, sun Y, sun Y, Qin X (2011) Preparation and characterization of mercapto functionalized sepiolite and their application for sorption of lead and cadmium. J Chem Eng 174: 436–444.

[69] Liang X, Xu Y, Wang L, Lin D, sun Y, Qin X, Wan Q (2013) Sorption of Pb^{2+} on mercapto functionalized sepiolite. Chemosphere 90: 548–555.

[70] Eren E, Gumus H (2011) Characterization of the structural properties and Pb(II) adsorption behavior of iron oxide coated sepiolite. Desalination 273: 276–284.

[71] Doula MK (2007) Synthesis of a clinoptilolite–Fe system with high Cu sorption capacity. Chemosphere 67: 731–740.

[72] Eren E, Gumus H, Ozbay N (2010) Equilibrium and thermodynamic studies of Cu (II) removal by iron oxide modified sepiolite. Desalination 262: 43–49.

[73] Lazarević S, Janković-Častvan I, Potkonjak B, Janaćković Đ, Petrović R (2012) Removal of Co^{2+} ions from aqueous solutions using iron-functionalized sepiolite. Chem Eng Process 55: 40–47.

[74] Ilić N, Lazarević S, Rajaković-Ognjanović V, Rajaković Lj, Janaćković Đ, Petrović R (2014) The sorption of inorganic arsenic on modified sepiolite: the effect of hydrated iron(III) oxide. J Serb Chem Soc 79: 815–828 .

[75] Yu S, Zhai L, Zhong S, Qiu Y, Cheng L, Ren X (2016) Synthesis and structural characterization of magnetite/sepiolite composite and its sorptive properties for Co(II) and Cd(II). J Taiwan Inst Chem Eng 59: 221–228.

[76] Ahribesh A, Lazarević S, Janković-Častvan I, Jokić B, Spasojević V, Radetić T, Janaćković Đ, Petrović R (2017) Influence of the synthesis parameters on the properties of the sepiolite-based magnetic adsorbents. Powder Technol 305: 260–269.

[77] Lu H-J, Wang J-K, S Ferguson S, Wang T, Bao Y, Hao H-X (2016) Mechanism, synthesis and modification of nano zerovalent iron in water treatment. Nanoscale 8: 9962–9975.

[78] Fua F, Dionysiou DD, Liu H (2014) The use of zero-valent iron for groundwater remediation and wastewater treatment: A review. J Hazard Mater 267: 194–205.

[79] Ezzatahmadi N, Ayoko GA, Millar GJ, Speight R, Yan C, Li J, Li S, Zhu J, Xi Y (2017) Clay-supported nanoscale zero-valent iron composite materials for the remediation of contaminated aqueous solutions: A review. Chem Eng J 312: 336–350.

[80] Li S, Yan W, Zhang W (2009) Solvent-free production of nanoscale zero-valent iron (nZVI) with precision milling. Green Chem 11: 1618–1626.

[81] Jamei MR, Khosravi MR, Anvaripour B (2013) Investigation of ultrasonic effect on synthesis of nano zero valent iron particles and comparison with conventional method. J Chem Eng 8: 767–774.

[82] Jamei MR, Khosravi MR, Anvaripour B (2014) A novel ultrasound assisted method in synthesis of NZVI particles, Ultrason Sonochem 21: 226–233.

[83] Liao C-J, Chung T-L, Chen W-L, Kuo SL (2007) Treatment of pentachlorophenol-contaminated soil using nano-scale zero-valent iron with hydrogen peroxide. J Mol Catal A Chem 265: 189–194.

[84] Theron J, Walker JA, Cloete TE (2008) Nanotechnology and Water Treatment: Applications and Emerging Opportunities. Crit Rev Microbiol 34: 43–69.

[85] Hwang YH, Kim DG, Ahn YT, Moon CM, Shin HS (2010) Fate of nitrogen species in nitrate reduction by nanoscale zero valent iron and characterization of the reaction kinetics. Water Sci Technol 61: 705–712.

[86] Todaka Y, Tsuchiya K, Umemoto M, Sasaki M, Imai D (2003) Growth of Fe_3O_4 whiskers from solid solution nanoparticles of Fe–Cu and Fe–Ag systems produced by DC plasma jet method. Mater Sci Eng A 340: 114–122.

[87] Zhang Y, Xu J-L, Xu H-J, Yuan Z-H, Guo Y (2010) Cellulase deactivation based kinetic modeling of enzymatic hydrolysis of steam-exploded wheat straw. Bioresour Technol 101: 8261–8266.

[88] Wang C-B, Zhang W-X (1997) Synthesizing Nanoscale Iron Particles for Rapid and Complete Dechlorination of TCE and PCBs. Environ Sci Technol 31: 2154–2156.

[89] He F, Zhao D (2005) Preparation and Characterization of a New Class of Starch-Stabilized Bimetallic Nanoparticles for Degradation of Chlorinated Hydrocarbons in Water. Environ Sci Technol 39: 3314–3320.

[90] Woo H, Park J, Lee S, Lee S (2014) Effects of washing solution and drying condition on reactivity of nano-scale zero valent irons (nZVIs) synthesized by borohydride reduction. Chemosphere 97: 146–152.

[91] Nurmi JT, Sarathy V, Tratnyek PG, Baer DR, Amonette JE, Karkamkar A (2010) Recovery of iron/iron oxide nanoparticles from solution: comparison of methods and their effects. J Nanopart Res 13: 1937–1952.

[92] WanYaacob WZ, Kamaruzaman N, Samsudin AR (2012) Development of nano-zero valent iron for the remediation of contaminated water. Chem Eng Trans 28: 25–30.

[93] Jozwiak WK, Kaczmarek E, Maniecki TP, Ignaczak W, Maniukiewicz W (2007) Reduction behavior of iron oxides in hydrogen and carbon monoxide atmospheres. Appl Catal A-Gen 326: 17–27.

[94] Chen S-S, Hsu H-D, Li C-W (2004) A new method to produce nanoscale iron for nitrate removal. J Nanopart Res 6:639–647.

[95] Crane RA, Scott TB (2012) Nanoscale zero-valent iron: future prospects for an emerging water treatment technology. J Hazard Mater 211–212: 112–125.

[96] Yoo BY, Hernandez SC, Koo B, Rheem Y, Myung NV (2007) Electrochemically fabricated zero-valent iron, iron–nickel, and iron–palladium nanowires for environmental remediation applications. Water Sci Technol 55: 149–156.

[97] Machado S, Grosso JP, Nouws HPA, Albergaria JT, Delerue-Matos C (2014) Utilization of food industry wastes for the production of zero-valent iron nanoparticles. Sci Total Environ 496: 233–240.

[98] Machado S, Pinto SL, Grosso JP, Nouws HPA, Albergaria JT, Delerue-Matos C(2013) Green production of zero-valent iron nanoparticles using tree leaf extracts. Sci Total Environ 445–446: 1–8.

[99] Reddy AVB, Yusop Z, Jaafar J, Reddy YVM, Aris AB, Majid ZA, Talib J, Madhavi G (2016) Recent progress on Fe-based nanoparticles: Synthesis, properties, characterization and environmental applications. JECE 4: 3537–3553.

[100] Wang T, Jin X, Chen Z, Megharaj M, Naidu R (2014) Green synthesis of Fe nanoparticles using eucalyptus leaf extracts for treatment of eutrophic wastewater. Sci Total Environ 466–467: 210–213.

[101] Machado S, Stawin'ski W, Slonina P, Pinto AR, Grosso JP, Nouws HPA, Albergaria JT, Delerue-Matos C (2013) Application of green zero-valent iron nanoparticles to the remediation of soils contaminated with ibuprofen. Sci Total Environ 461–462: 323–329.

[102] Mystrioti C, Sparis D, Papasiopi N, Xenidis A, Dermatas D, Chrysochoou M (2015) Assessment of polyphenol coated nano zero valent iron for hexavalent chromium removal from contaminated waters. B Environ Contam Tox 94: 302–307.

[103] Huang L, Weng X, Chen Z, Megharaj M, Naidu R (2014) Green synthesis of iron nanoparticles by various tea extracts: comparative study of the reactivity, Spectrochim. Acta Part A Mol. Biomol. Spectrosc. 130: 295–301.

[104] Tosco T, Papini MP, Viggi CC, Sethi R (2014) Nanoscale zerovalent iron particles for groundwater remediation: a review. J Clean Prod 77: 10–21.

[105] O'Carroll D, Sleep B, Krol M, Boparai H, Kocur C (2013) Nanoscale zero valent iron and bimetallic particles for contaminated site remediation. Adv. Water Resour 51: 104–122.

[106] Li X-Q, Elliot DW, Zhang W-X (2006) Zero-valent iron nanoparticles for abatement of environmental pollutants: materials and engineering aspects Crit Rev Solid State, 31: 111–122.

[107] Sun Y-P, Li X-Q, Cao J, Zhang W-X, Paul Wang H (2006) Characterization of zero-valent iron nanoparticles. Adv Colloid Interface Sci 120: 47–56.

[108] Tiraferri A, Chen KL, Sethi R, Elimelech M (2008) Reduced aggregation and sedimentation of zero-valent iron nanoparticles in the presence of guar gum. J Colloid Interface Sci 324: 71-79.

[109] Liu Y, Lowry GV (2006) Effect of particle age (Fe^0 content) and solution pH on NZVI reactivity: H$_2$ evolution and TCE dechlorination, Environ Sci Technol 40: 6085–90.

[110] Yan W, Lien H-L, Koel, BE, Zhang, W-X (2013) Iron nanoparticles for environmental clean-up: recent developments and future outlook. Environ Sci: Processes Impacts 15: 63–77.

[111] Laumann S, Micic V, Lowry GV, Hofmann T (2013) Carbonate minerals in porous media decrease mobility of polyacrylic acid modified zero-valent iron nano-particles used for groundwater remediation. Environ Pollut 179: 53-60.

[112] Christian P, Kammer F, Baalousha M, Hofmann T (2008) Nanoparticles: structure,properties, preparation and behaviour in environmental media. Ecotoxicology 17: 326-343.

[113] https://cfpub.epa.gov/ncer_abstracts/index.cfm/fuseaction/display.highlight/abstract/2365/report/F.

[114] Stefaniuk M, Oleszczuk P, Ok YS (2016) Review on nano zero valent iron (nZVI): from synthesis to environmental applications. Chem Eng J 287: 618–632.

[115] Guan X, Sun Y, Qin H , Li J, Lo IMC, He D, Dong H (2015) The limitations of applying zero-valent iron technology in contaminants sequestration and the corresponding countermeasures: The development in zero-valent iron technology in the last two decades (1994–2014). Water Res 75: 224–248.

[116] Hug SJ, Leupin O (2003) Iron-catalyzed oxidation of arsenic(III) by oxygen and by hydrogen peroxide: pH-dependent formation of oxidants in the Fenton reaction. Environ Sci Technol 37: 2734–2742.

[117] Lee C, Kim JY, Lee WI, Nelson KL, Yoon J, Sedlak DL(2008) Bactericidal effect of zerovalent iron nanoparticles on Escherichia coli. Environ Sci Technol 42: 4927–4933.

[118] Zhang Y, Li Y, Dai C, Zhou X, Zhang W (2014) Sequestration of Cd(II) with nanoscale zero-valent iron (nZVI): characterization and test in a two-stage system. Chem Eng J 244: 218–226.

[119] Choi H, Al-Abed SR, Agarwal S, Dionysiou DD (2008) Synthesis of reactive nano-Fe/Pd bimetallic system-impregnated activated carbon for the simultaneous adsorption and dechlorination of PCBs. Chem Mater 20: 3649–3655.

[120] Lee S, Lee K, Rhee S, Park J (2007) Development of a new zerovalent iron zeolite material to reduce nitrate without ammonium release. J Environ Eng 133: 6–12.

[121] Ponder SM, Darab JG, Mallouk TE (2000) Remediation of Cr(VI) and Pb(II) aqueous solutions using supported, nanoscale zero-valent iron. Environ Sci Technol 34: 2564–2569.

[122] Zhu B-W, Lim T-T, Feng J (2006) Reductive dechlorination of 1,2,4-trichlorobenzene with palladized nanoscale Fe^0 particles supported on chitosan and silica. Chemosphere 65: 1137–1145.

[123] Huang QG, Shi XY, Pinto RA, Petersen EJ, Weber WJ (2008) Tunable synthesis and immobilization of zero-valent iron nanoparticles for environmental application. Environ Sci Technol 42: 8884–8889.

[124] Zhang X, Lin S, Lu X-Q, Chen Z-L (2010) Removal of Pb(II) from water using synthesized kaolin supported nanoscale zero-valent iron. Chem Eng J 163: 243–248.

[125] He F, Zhao D, Liu J, Roberts CB (2007) Stabilization of Fe-Pd nanoparticles with sodium carboxymethyl cellulose for enhanced transport and dechlorination of trichloroethylene in soil and groundwater. Ind Eng Chem Res 46: 29–34.

[126] Li L, Hu J, Shi X, Fan M, Luo J, Wei X (2016) Nanoscale zero-valent metals: a review of synthesis, characterization, and applications to environmental remediation. Environ Sci Pollut Res 23: 17880–17900.

[127] Bhowmick S, Chakraborty S, Mondal P, Van Renterghem W, Van den Berghe S, Roman-Ross G, Chatterjee D, Iglesias M (2014) Montmorillonite-supported nanoscale zero-valent iron for removal of arsenic from aqueous solution: Kinetics and mechanism. J Chem Eng 243: 14–23.

[128] Shi L-N, Zhang X, Chen Z-L(2011) Removal of Chromium (VI) from wastewater using bentonite-supported nanoscale zero-valent iron. Water Res 45: 886–892.

[129] Zhang X, Lin S, Chen Z, Megharaj M, Naidu R (2011) Kaolinite supported nanoscale zero-valent iron for removal of Pb^{2+} from aqueous solution: reactivity, characterization and mechanism.Water Res 45:3481–3488.

[130] Üzüm Ç, Shahwan T, Eroğlu AE, Hallam KR, Scott TB, Lieberwirth I (2009) Synthesis and characterization of kaolinite-supported zerovalent iron nanoparticles and their application for the removal of aqueous Cu^{2+} and Co^{2+} ions. Appl Clay Sci 43:172–181

[131] Kim SA, Kamala-Kannan S, Lee K-J, Park Y-J, Shea PJ, Lee W -H, Kim H-M, Oh B-T (2013) Removal of Pb(II) from aqueous solution by a zeolite–nanoscale zero-valent iron composite. J Chem Eng 217: 54–60.

[132] Frost RL, Xi Y, He H (2010) Synthesis, characterization of palygorskite supported zero-valent iron and its application for methylene blue adsorption. J Colloid Interf Sci 341: 153–161.

[133] Esfahani AR, Hojati S, Azimi A, Farzadian M, Khataee A (2015) Enhanced hexavalent chromium removal from aqueous solution using a sepiolite-stabilized zero-valent iron nanocomposite: impact of operational parameters and artificial neural network modeling. J Taiwan Inst Chem Eng 49: 172–182.

[134] Fu R, Yang Y, Xu Z, Zhang X, Guo X, Bi D (2015) The removal of chromium (VI) and lead (II) from groundwater using sepiolite-supported nanoscale zero-valent iron (S-NZVI). Chemosphere 138: 726–734.

[135] Greenlee LF, Torrey JD, Amaro RL, Shaw JM (2012) Kinetics of zero valent iron nanoparticle oxidation in oxygenated water. Environ Sci Technol 46: 12913–12920.

[136] Rouquerol F, Rouquerol J, Sing K (1999) Adsorption by powders and porous solids. Academic Press, London.

[137] Barrett EP, Joyner LG, Halenda PP (1951) The determination of pore volume and area distributions in porous substances. I. Computations from nitrogen isotherms. J Am Chem Soc 73: 373–380.

[138] Lippens BC, de Boer JH (1965) Studies on pore systems in catalysts: V. The t method. J Catalysis 4: 319–323.

[139] Milonjić SK, Ruvarac AL, Šušić MV (1975) The heat of immersion of natural magnetite in aqueous solutions. Thermochim Acta 11: 261–266.

[140] Hono K, Ping DH, Ohnuma M, Onodera H (1999) Cu clustering and Si parti t ioning in the early crystal l i zation stage of an $Fe_{73.5}Si_{13.5}B_9Nb_3Cu_1$ amorphous alloy. Acta Mater 47: 997–1006.

[141] Zha S, Cheng Y, Gao Y, Chen Z, Megharaj M, Naidu R (2014) Nanoscale zero-valent iron as a catalyst for heterogeneous Fenton oxidation of amoxicillin. Chem Eng J 255: 141–148.

[142] Frost RL, Mendelovici E (2006) Modification of fibrous silicates surfaces with organic derivatives: an infrared spectroscopic study. J Colloid Interf Sci 294: 47–52.

[143] Li X, Zhang M, Liu Y, Li X, Liu Y, Hua R, He C (2013) Removal of U(VI) in aqueous solution by nanoscale zero-valent iron (nZVI).Water Qual Expo Health 5: 31–40.

[144] Földvári M (2011) Handbook of thermogravimetric system of minerals and its use in geological practice. Geological Institute of Hungary, Budapest.

[145] Arancibia-Miranda N, Baltazar SE, García A, Muñoz-Lira D, Sepúlveda P, Rubio MA, Altbir D (2016) Nanoscale zero valent supported by zeolite and montmorillonite: template effect of the removal of lead ion from an aqueous solution. J Hazard Mater 301: 371–380.

[146] Su Y, Adeleye AS, Huang Y, Sun X, Dai C, Zhou X, Zhang Y, Keller AA (2014) Simultaneous removal of cadmium and nitrate in aqueous media by nanoscale zerovalent iron (nZVI) and Au doped nZVI particles. Water Res 63: 102–111.

[147] Wen Z, Zhang Y, Dai C (2014) Removal of phosphate from aqueous solution using nanoscale zerovalent iron (nZVI). Colloid Surface A 457: 433–440.

[148] Kosmulski M (2009) Compilation of PZC and IEP of sparingly soluble metal oxides and hydroxides from literature. Adv Colloid Interf Sci 152: 14–25.

[149] Kosmulski M (2011) The pH-dependent surface charging and points of zero charge V. Update. J Colloid Interface Sci 353: 1–15.

[150] Babić BM, Milonjić SK, PolovinaMJ, Čupić S, Kaludjerović BV (2002) Adsorption of zinc, cadmium and mercury ions from aqueous solutions on an activated carbon cloth. Carbon 40: 1109–1115.

[151] Radojević M, Jović V, Karaulić D, Vitorović D (2002) Study of sepiolite from Goleš (Kosovo, Yugoslavia). II. Acid activation. J Serb Chem Soc 67: 499–506.

[152] Moulder JF, StickleWF, Sobol PE, Bomben KD (1995) Handbook of Xray photoelectron spectroscopy. Physical Electronics Inc., Eden Prairie, Minesota.

[153] Huang P, Ye Z, Xie W, Chen Q, Li J, Xu Z, Yao M (2013) Rapid magnetic removal of aqueous heavy metals and their relevant mechanisms using nanoscale zero valent iron (nZVI) particles. Water Res 47: 4050–4058.

[154] ChenW, Zhang J, Zhang X,Wang W, Li Y (2016) Investigation of heavy metal (Cu, Pb, Cd, and Cr) stabilization in river sediment by nanozero- valent iron/activated carbon composite. Environ Sci Pollut Res 23: 1460–1470.

[155] Guo X, Yang Z, Dong H, Guan X, Ren Q, Lv X, Jin X (2016) Simple combination of oxidants with zero-valent-iron (ZVI) achieved very rapid and highly efficient removal of heavy metals from water. Water Res 88: 671–680.

[156] Habish AJ, Lazarević S, Janković-Častvan I, Jokić B, Kovač J, Janaćković Đ, Petrović R (2017) Nanoscale zerovalent iron (nZVI) supported by natural and acid-activated sepiolites: the effect of the nZVI/support ratio on the composite properties and Cd^{2+} adsorption. Environ Sci Pollut Res 24: 628–643.

[157] Rao KS, Mohapatra M, Anand S, Venkateswarlu P (2010) Review on cadmium removal from aqueous solutions. Int J Eng Sci Tech 2: 81–103.

[158] Granados-Correa F, Corral-Capulin NG, Olguín MT, Acosta-León CE (2011) Comparison of the Cd(II) adsorption processes between boehmite (γ-AlOOH) and goethite (α-FeOOH). Chem Eng J 171: 1027–1034.

[159] Chowdhury SR, Yanful EK (2013) Kinetics of cadmium(II) uptake by mixed maghemite-magnetite nanoparticles. J Environ Manag 129: 642–651.

[160] Zhang C, Yu Z, Zeng G, Huang B, Dong H, Huang J, Yang Z, Wei J, Hu L, Zhang Q (2016) Phase transformation of crystalline iron oxides and their adsorption abilities for Pb and Cd. Chem Eng J 284: 247–259.

[161] Boparai HK, Joseph M, O'Carroll DM (2011) Kinetics and thermodynamics of cadmiumion removal by adsorption onto nano zero valent iron particles. J Hazard Mater 186: 458–465.

[162] Su Y, Adeleye AS, Keller AA, Huang Y, Dai C, Zhou X, Zhang Y (2015) Magnetic sulfide-modified nanoscale zerovalent iron (S-nZVI) for dissolved metal ion removal. Water Res 74: 47–57.

[163] Li J, Chen C, Zhu K, Wang X (2016a) Nanoscale zero valent iron particles modified on reduced graphene oxides using a plasma technique for Cd(II) removal. J Taiwan Inst Chem Eng 59: 389–394.

[164] Habish AJ, Lazarević S, Janković-Častvan I, Potkonjak B, Janaćković Đ, Petrović R (2015) The effect of salinity on the sorption of cadmium ions from aqueous medium on Fe(III)-sepiolite. Chem Ind Chem Eng Q 21: 295–303.

[165] Lesmana SO, Febriana N, Soetaredjo FE, Sunarso J, Ismadji S (2009) Studies on potential applications of biomass for the separation of heavy metals from water and wastewater. Biochem Eng J 44: 19–41.

[166] Mihajlović M, Lazarević S, Janković-Častvan I, Kovač J, Jokić B, Janaćković Đ, Petrović R (2015) Kinetics, thermodynamics, and structural investigations on the removal of Pb^{2+}, Cd^{2+}, and Zn^{2+} from multicomponent solutions onto natural and Fe(III)-modified zeolites. Clean Techn Environ Policy 17: 407–419.

[167] Malamisa S, Katsoua E (2013) A review on zinc and nickel adsorption on natural and modified zeolite, bentonite and vermiculite: Examination of process. J Hazard Mater 252– 253: 428–461.

[168] Toth J (2002) Adsorption theory, modeling and analysis. Marcel Dekker Inc., New York, Basel.

[169] Soliemanzadeh A, Fekri M (2017) The application of green tea extract to prepare bentonite-supported nanoscale zero-valent iron and its performance on removal of Cr(VI): Effect of relative parameters and soil experiments. Micropor Mesopor Mat 239: 60-69.

[170] Radusinović M (2012) The adsorption of anionic dyes from aqueous solutions of the functionalized sepiolite. Diploma thesis, Faculty of Technology and Metallurgy, University of Belgrade, Belgrade.

[171] Wang X, Wang P, Ma J, Liu H, Ning P (2015) Synthesis, characterization, and reactivity of cellulose modified nanozero-valent iron for dye discoloration. Appl Surf Sci 345: 57–66.

[172] Fana J, Guo Y, Wang J, Fan M (2009) Rapid decolorization of azo dye methyl orange in aqueous solution by nanoscale zerovalent iron particles. J Hazard Mater 166: 904–910.

[173] Luo S, Qin P, Shao J, Peng L, Zeng Q, Gu J-D (2013) Synthesis of reactive nanoscale zero valent iron using rectorite supports and its application for Orange II removal. Chem Eng J 223: 1–7.

[174] Sun S-P, Li C-J, Sun J-H, Shi S-H, Fan M-H, Qi Zhou. Decolorization of an azo dye Orange G in aqueous solution by Fenton oxidation process: Effect of system parameters and kinetic study. J Hazard Mater 161 (2009) 1052–1057.

[175] Kerkez D, Tomašević D, Kozma G, Bečelić-Tomin M, Prica M, Rončević S, Kukovecz A, Dalmacija B, Kónya Z (2014) Three different clay-supported nanoscale zero-valent iron materials for industrial azo dye degradation: A comparative study. J Taiwan Inst Chem Eng 45: 2451–2461.

Curriculum Vitae

Date of birth: 29.05.1975.

Place of birth: Alkums, Libya.

1982-1987: Primary school: "Al-Harati Central School", Alkums, Libya.

1988-1990: Elementary school: "Al-Harati Central School", Alkums, Libya.

1991-1993: High school: "Al-Majd", Alkoms, Libya.

1994-1998: Bachelor study: University of Elmergib (AlKhums, Libya), Faculty of Engineering, Chemical engineering.

1999-2009: Worked as a teaching assistant at the University of Elmergib, Faculty of Engineering, Chemical engineering.

2010-2012: Master study: University of Belgrade, Faculty of Technology and Metallurgy, Belgrade, Serbia. Master thesis: "The sorption of cadmium ions from the natural sea water and aqueous solutions on modified sepiolite".

2013-2017: PhD study: University of Belgrade, Faculty of Technology and Metallurgy, Belgrade, Serbia.

Published papers:

[1] Habish AJ, Lazarević S, Janković-Častvan I, Jokić B, Kovač J, Janaćković Đ, Petrović R (2017) Nanoscale zerovalent iron (nZVI) supported by natural and acid-activated sepiolites: the effect of the nZVI/support ratio on the composite properties and Cd^{2+} adsorption. Environ Sci Pollut Res 24: 628–643.

[2] Habish AJ, Lazarević S, Janković-Častvan I, Potkonjak B, Janaćković Đ, Petrović R (2015) The effect of salinity on the sorption of cadmium ions from aqueous medium on Fe(III)-sepiolite. Chem Ind Chem Eng Q 21:295–303.

[3] Habish A J, Lazarević S, Jokić B, Janković-Častvan I, Janaćković Đ, Petrović R: Synthesis and characterization of sepiolite-suported nano zerovalent iron, - Programme and the book of abstracts of the 3rd Conference of the Serbian Society for Ceramic Materials, Beograd, 2015, p. 77.

Прилог 1.

Изјава о ауторству

Потписани-а   **Amal Juma Habish**

Број индекса или пријаве докторске дисертације   **4041/2013**

Изјављујем

да је докторска дисертација под насловом

„Утицај параметара синтезе на својства композитних адсорбената на бази сепиолита и наночестица елементарног гвожђа" (Influence of synthesis parameters on the properties of the composite adsorbents based on sepiolite and nano-zerovalent iron)

- резултат сопственог истраживачког рада,
- да предложена дисертација у целини ни у деловима није била предложена за добијање било које дипломе према студијским програмима других високошколских установа,
- да су резултати коректно наведени и
- да нисам кршио/ла ауторска права и користио интелектуалну својину других лица.

Потпис докторанда

У Београду,   10.04.2017.

Прилог 2.

Изјава о истоветности штампане и електронске верзије докторског рада

Име и презиме аутора ___**Amal Juma Habish**_____

Број индекса или пријаве докторске дисертације ___**4041/2013**_____

Студијски програм ___**Хемијско инжењерство**_____

Наслов рада „**Утицај параметара синтезе на својства композитних адсорбената на бази сепиолита и наночестица елементарног гвожђа**" (**Influence of synthesis parameters on the properties of the composite adsorbents based on sepiolite and nano-zerovalent iron**)

Ментор ___**проф. др Рада Петровић**_____

Потписани ___**Amal Juma Habish**_____

изјављујем да је штампана верзија мог докторског рада истоветна електронској верзији коју сам предао/ла за објављивање на порталу **Дигиталног репозиторијума Универзитета у Београду.**

Дозвољавам да се објаве моји лични подаци везани за добијање академског звања доктора наука, као што су име и презиме, година и место рођења и датум одбране рада.

Ови лични подаци могу се објавити на мрежним страницама дигиталне библиотеке, у електронском каталогу и у публикацијама Универзитета у Београду.

<div align="right">

Потпис докторанда

</div>

У Београду, ___10.04.2017._____

Прилог 3.

Изјава о коришћењу

Овлашћујем Универзитетску библиотеку „Светозар Марковић" да у Дигитални репозиторијум Универзитета у Београду унесе моју докторску дисертацију под насловом:

„Утицај параметара синтезе на својства композитних адсорбената на бази сепиолита и наночестица елементарног гвожђа" (Influence of synthesis parameters on the properties of the composite adsorbents based on sepiolite and nano-zerovalent iron)

која је моје ауторско дело.

Дисертацију са свим прилозима предао/ла сам у електронском формату погодном за трајно архивирање.

Моју докторску дисертацију похрањену у Дигитални репозиторијум Универзитета у Београду могу да користе сви који поштују одредбе садржане у одабраном типу лиценце Креативне заједнице (Creative Commons) за коју сам се одлучио/ла.

1. Ауторство

2. Ауторство - некомерцијално

3. Ауторство – некомерцијално – без прераде

4. Ауторство – некомерцијално – делити под истим условима

5. Ауторство – без прераде

6. Ауторство – делити под истим условима

(Молимо да заокружите само једну од шест понуђених лиценци, кратак опис лиценци дат је на полеђини листа).

Потпис докторанда

У Београду, ___10.04.2017._____

1. Ауторство - Дозвољавате умножавање, дистрибуцију и јавно саопштавање дела, и прераде, ако се наведе име аутора на начин одређен од стране аутора или даваоца лиценце, чак и у комерцијалне сврхе. Ово је најслободнија од свих лиценци.

2. Ауторство – некомерцијално. Дозвољавате умножавање, дистрибуцију и јавно саопштавање дела, и прераде, ако се наведе име аутора на начин одређен од стране аутора или даваоца лиценце. Ова лиценца не дозвољава комерцијалну употребу дела.

3. Ауторство - некомерцијално – без прераде. Дозвољавате умножавање, дистрибуцију и јавно саопштавање дела, без промена, преобликовања или употребе дела у свом делу, ако се наведе име аутора на начин одређен од стране аутора или даваоца лиценце. Ова лиценца не дозвољава комерцијалну употребу дела. У односу на све остале лиценце, овом лиценцом се ограничава највећи обим права коришћења дела.

4. Ауторство - некомерцијално – делити под истим условима. Дозвољавате умножавање, дистрибуцију и јавно саопштавање дела, и прераде, ако се наведе име аутора на начин одређен од стране аутора или даваоца лиценце и ако се прерада дистрибуира под истом или сличном лиценцом. Ова лиценца не дозвољава комерцијалну употребу дела и прерада.

5. Ауторство – без прераде. Дозвољавате умножавање, дистрибуцију и јавно саопштавање дела, без промена, преобликовања или употребе дела у свом делу, ако се наведе име аутора на начин одређен од стране аутора или даваоца лиценце. Ова лиценца дозвољава комерцијалну употребу дела.

6. Ауторство - делити под истим условима. Дозвољавате умножавање, дистрибуцију и јавно саопштавање дела, и прераде, ако се наведе име аутора на начин одређен од стране аутора или даваоца лиценце и ако се прерада дистрибуира под истом или сличном лиценцом. Ова лиценца дозвољава комерцијалну употребу дела и прерада. Слична је софтверским лиценцама, односно лиценцама отвореног кода.